Diffrimoscopy; a Study in Diffraction.

by J. Legendre.

Submitted in partial fulfillment
of the requirements for the degree of
Master of Science.

Department of Physics,
Faculty of Pure and Applied Science,
The University of Ottawa,
Ottawa, Canada.

May, 1966.

Abstract

This project has been concerned with the manner of the formation of diffrimoscopic images. Some of the parameters which directly affect the final images are discussed.

A connection is made between ultra-microscopy and diffrimoscopy and certain practical applications of diffrimoscopy are established. The resolving power of an optical system, for example, is greatly increased with this technique.

The advantages of the diffrimoscopic technique in the fundamental study of diffraction particularly in the "near-field" are investigated. The Fourier transform theory or a modified version thereof is used throughout.

Foreword

Visual observation of diffraction patterns usually presents few problems; however, the recording of these patterns meets with several difficulties because of the nature of photographic emulsions. Diffraction patterns usually have areas which differ in luminosity by several orders of magnitude. The problem then is one of recording the weaker details while retaining good definition in the bright areas. It was found that black and white film was strongly affected by irradiation within the emulsion. In colour films these irradiation effects proved to be much less serious. These films, thus, could accept a certain amount of over-exposing without an accompanying deterioration in image quality. However, the colour rendition of the film is in many cases very poor. Kodak films, for instance, rendered yellow monochromatic light (wavelength 5780 A) as a green, while Ansco films rendered light of the same wavelength as a deep red. In both films blue light (wavelength 4352 A) was not easily photographed although the rendition was good. Midway through the project it was found that Ansco had changed the dyes in their films to give a much improved rendition of yellow light.

The majority of the prints made for this report were reproduced from composite colour slides. The inter-negative method was used throughout. A special enlarger which lowered the contrast present in the original slide was used in both stages of the reproduction. The spectral distribution of the cathode ray tube and the spectral response of the modulating probe used in the enlarger affected the final images although in most cases this was not serious. The prints which are presented in colour in this report were done by a commercial firm and the problems of contrast are clearly evident in these pictures. The laboratory at the N.R.C. is unfortunately not equipped as yet to handle colour enlargements.

The author begs the reader's indulgence if the prints presented in this paper do not always show all the details described. Generally speaking, the black and white prints are of a better overall quality than the colour prints. This is due mainly to the efforts of Mr. M. Bergin and the effectiveness of the LogEtronic enlarger at the National Research Council.

Acknowledgements

I would like to express my thanks to the Physics Department and especially to Dr. J. Robson who permitted the research work to be done at the N.R.C.,who acted as my advisor during the writing of the thesis and who provided encouragement when it was most needed.

I would also like to thank Mr. M. Bergin and Mr. M. Ranger for their invaluable help. I am especially grateful to Miss Y. Armengaud for her help and patience in the typing of this work.

Recognition with thanks must be given to Dr. G. Lansraux for his contribution to the experiments.

These experiments were carried out at the National Research Council. The Council provided all the equipment for this project as well as providing support in the form of two bursaries.

Jacques Legendre,
Physics Department,
University of Ottawa.

Index of Figures.

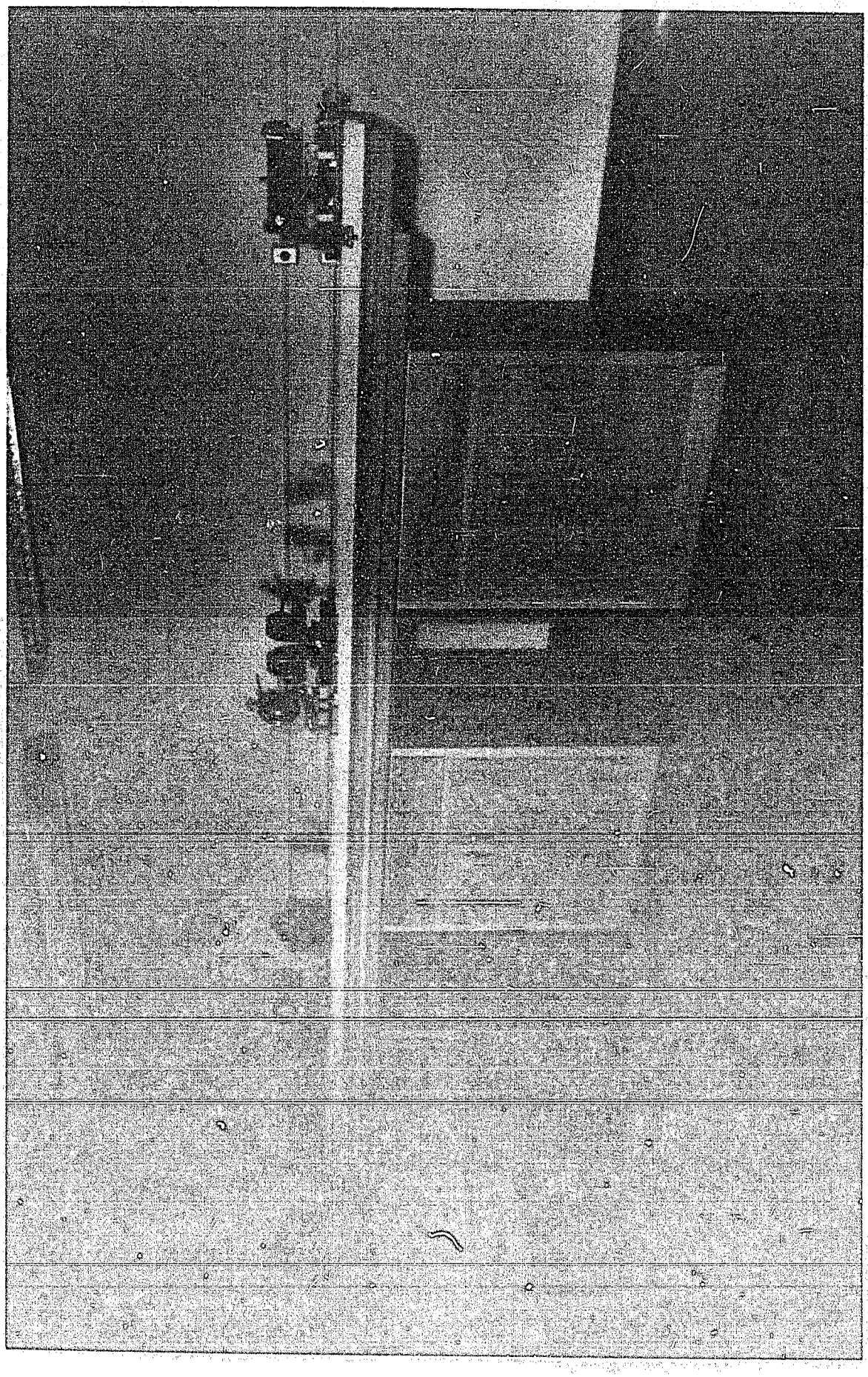

Figure 1 - The optical bench used for studies in diffrimoscopy.

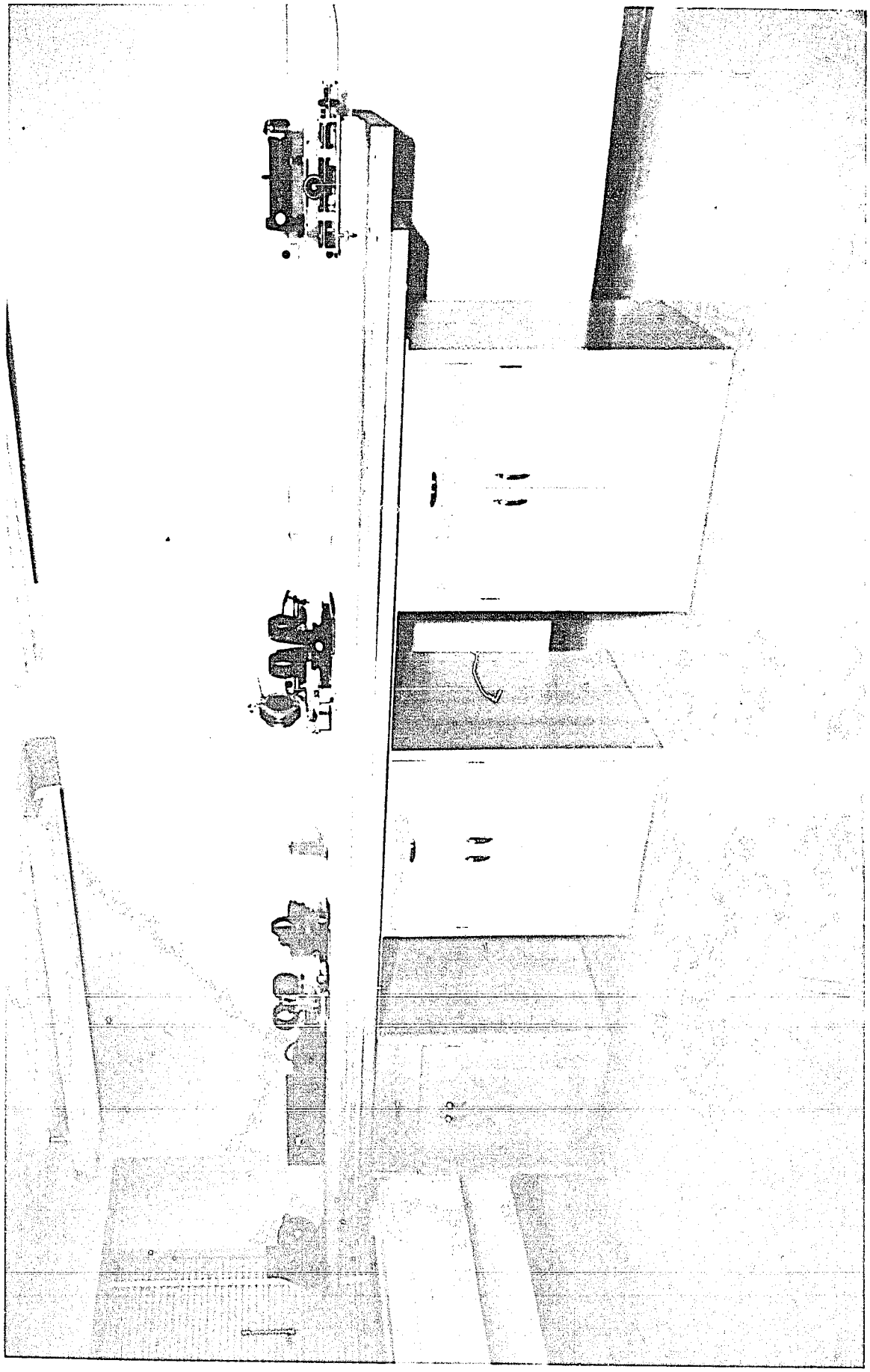

TABLE OF CONTENTS

1 - An Introduction to Diffrimoscopy.

The Origins of Diffrimoscopy.

The word "diffraction" is derived from the Latin "dis", meaning apart or asunder, and "frangere", to break. The term "diffraction of light" signifies a certain breaking up which a beam of light undergoes in passing an obstacle, and also signifies other types of breaking up which are fundamentally related to the one mentioned. The subject of diffraction covers a wide field.

Much work in the study of diffraction has been done outside the realm of visible optics. The important contribution of those working in the microwave region of the spectrum may be cited as an example (e.g. C.L. Andrews*, T.J.F. Pavlasek, G.W. Farnell**). However, in the 300 years since the first paper on diffraction was published by Grimaldi***, the field still lacks a useable theory which would explain all facets of the phenomenon. Moreover, since the advent of the well-known and much-quoted Rayleigh criterion for the resolution limit of optical systems, optics has been faced with a seemingly impassable barrier.

Recently certain authors have found means of surpassing the limit of resolution set by the Rayleigh criterion. The image formed in the focal plane of an objective of a point source is the so-called Airy pattern upon which is based the Rayleigh criterion. The transmission properties of the objective may be altered in such a way as to give a distribution of light in the focal plane which differs from the Airy pattern. An example of this is the amplitude filtering technique developed by Dr. Lansraux****.

---

* Andrews, C.L. Optics of the Electromagnetic Spectrum, (Prentice-Hall) 1960.

** Farnell, G.W., Can. J. Phys. 35, 777, (1957).
Farnell, G.W., Can. J. Phys. 36, 935, (1958).

*** Grimaldi, Francesco Maria, "Physics-Mathesis de Lumine Coloribus et Iride".

**** Lansraux, Guy, Revue d'Optique (aout-sept. 1953, T.32, pp. 475-499).

Another approach has been the technique called in French "strioscopie" and the related phenomenon known for many years as ultramicroscopy. "Strioscopy" has until now been used for little more than showing the diffraction effect. Bouasse, however, did study this phenomenon a little more closely and proposed an explanation of which more will be said later.

In this research project the latter phenomenon has been restudied and been called diffrimoscopy. The reason that a term other than "strioscopie" was chosen was that, in the meantime, this term has become ambiguous. The name "diffrimoscopy" was suggested by Dr. L.E. Howlett and comes from the two words "diffraction" and "image". It designates a new field of optics involving image formation using only diffracted light.

The Diffrimoscopic System.

Figure 1 shows a picture of the optical bench used at the National Research Council for studies in diffrimoscopy. From the left can be seen a point light source, two doublets, an object, a mask holder, two more doublets and finally a microscope with which images are observed and photographed.

Figure 2 is a schematic representation of the diffrimoscopic system. It is exactly the system shown in figure 1. In figure 2 no object is present but the plane where the object is to be inserted is clearly indicated. The source S is simply imaged on to the mask M, which cuts out all of the light. The image plane, therefore, is dark.

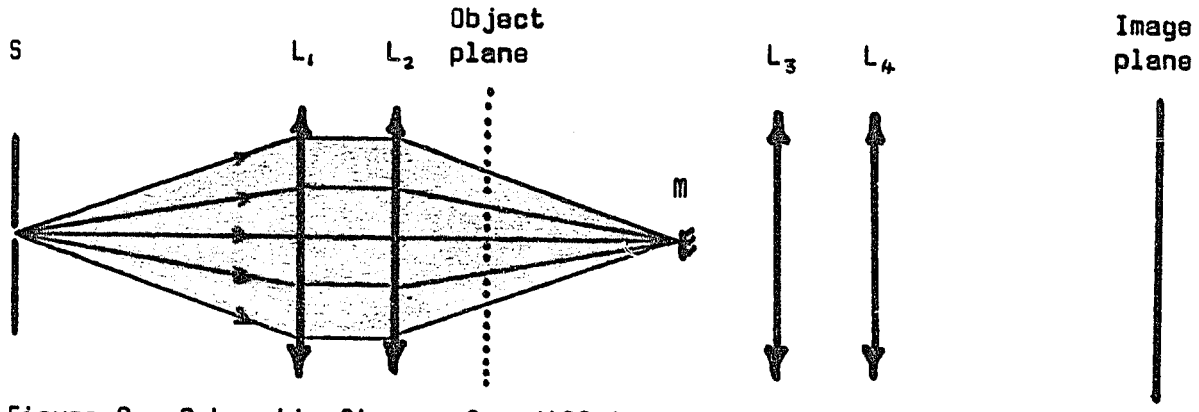

Figure 2: Schematic figure of a diffrimoscopic system - object absent.

Figure 3 shows the effect of inserting an object into the incident beam. The light which misses the object impinges upon the mask and is absorbed.

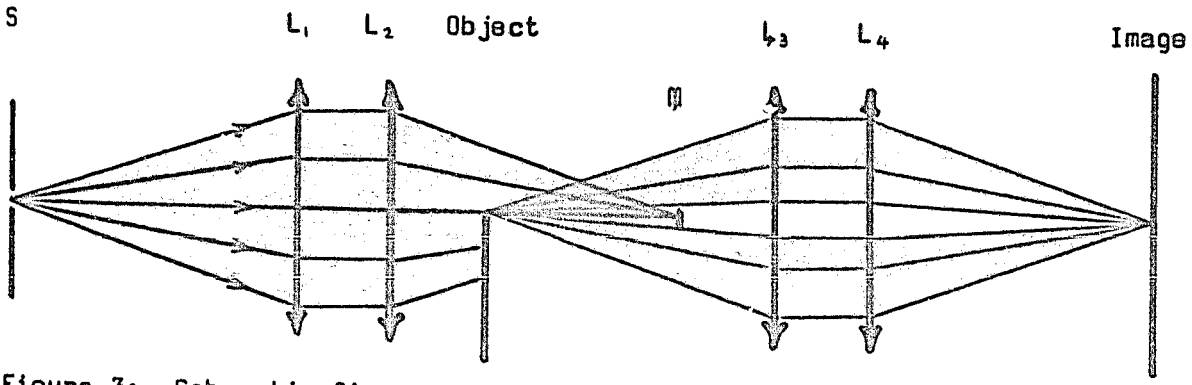

Figure 3: Schematic figure of a diffrimoscopic system with the object placed in a beam of converging light.

The light which strikes the object is simply absorbed or reflected. The light which just "touches" the edge of the object is diffracted and focussed in a diffrimoscopic image.

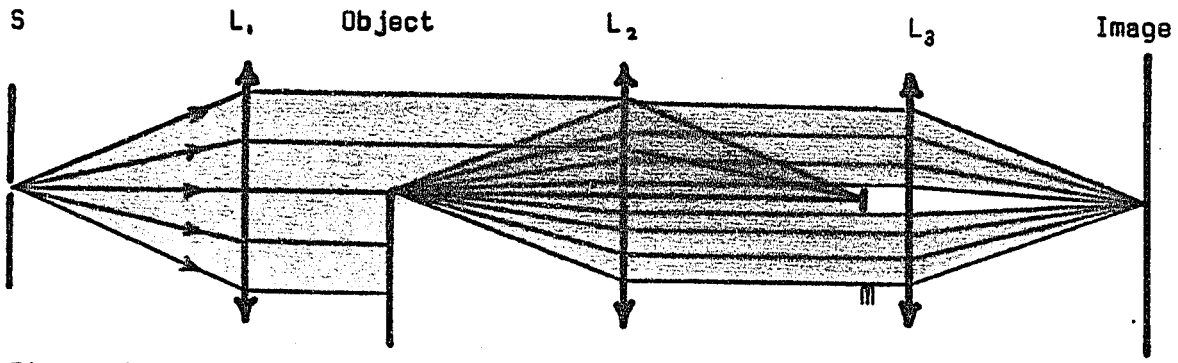

Figure 4: Schematic figure of a diffrimoscopic system with the object placed in a beam of parallel light.

Figure 4 shows another possible diffrimoscopic system. Here the object is located in a beam of parallel light instead of converging light as before. This system has been used to give diffrimoscopic images. Another arrangement (not shown) in which the object is located in a beam of diverging light has also given diffrimoscopic images.

General Characteristics of the Diffrimoscopic Image.

In each of the above mentioned arrangements, the images resemble, at low magnification, a bright line tracing of the object contour on a dark background. It is not surprising that the area within the object profile is dark, but it is most striking that the background which corresponds to the region outside the object, is also dark.

The simplest possible object, a thin opaque plate bounded by a straight edge, will be used in the following discussion. If the diffrimoscopic image is observed accurately with the proper magnification, a very thin black central line appears, as shown in figure 5. It is impossible

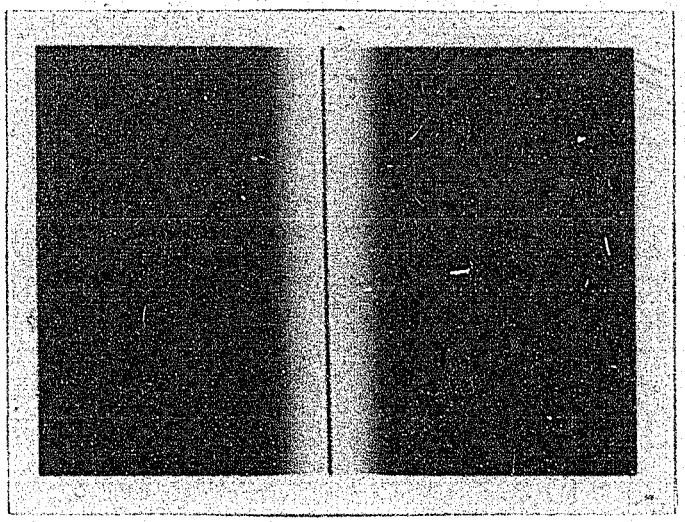

Figure 5 - The diffrimoscopic image of a perfectly smooth straight edge.

to say, from looking at this line image, which side of the line corresponds to the shadow region of the object; that is, it is impossible to say whether the object itself is on the right or on the left of this line. The image is absolutely symmetrical with respect to the central black fringe. This last statement is wholelly true, at present, only for those objects whose diffracting edge has a small radius of curvature. A small amount of asymmetry is present in the case of objects having large radii of curvature. The black fringe, however, is still present and is readily identifiable. For flat objects no such difficulty exists. The central fringe follows exactly the object contour as shown in figure 6. This is the diffrimoscopic image of a thin opaque plate bounded by a somewhat roughened straight edge.

It seems certain that the black central fringe corresponds exactly to the diffracting edge and is not shifted, for instance, into the shadow region behind the object. The experimental evidence for this, however, is still incomplete.

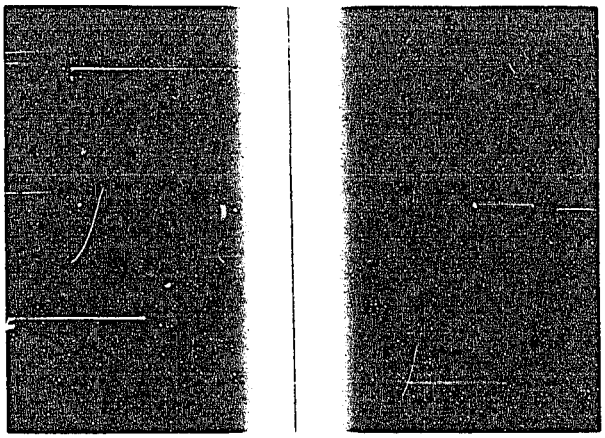

Figure 5 - The diffrimascopic image of a perfectly smooth straight edge.

[illegible] may, from looking at this line image, which side of the line corresp[illegible] to the shadow region of the object; that is, it is impossible to say whether the object itself is on the right or on the left of this line. The image is absolutely symmetrical with respect to the central black fringe. This last statement is strictly true, at present, only for those [illegible] whose diffracting edge has a small radius of curvature. A small [illegible] of asymmetry is present in the case of objects having large radii of curvature. The black fringe, however, is still present and is readily identifiable. For flat objects no such difficulty exists. The central fringe follows exactly the object contour as shown in figure 6. This is the diffrimascopic image of a thin opaque plate bounded by a somewhat [illegible] straight edge.

It seems certain that the black central fringe corresponds exactly to the diffracting edge and is not shifted, for instance, into the [illegible] region behind the object. The experimental evidence for this, however, is still less plain.

Figure 6 - The diffrimoscopic image of a rough edge.

The width of the dark central line is not in itself significant. It depends on the threshold level of the receiver and on the illumination of the light source. The fringe may be made narrower by exposing the photographic film for a longer period of time. Light scattering within the emulsion, however, will eventually make the dark fringe disappear completely. It has been found that colour film is less susceptible to these irradiation effects that is black and white film. Colour film will thus accept a certain amount of over-exposing without degrading the image significantly. This is important when pictures must be taken of diffraction patterns whose illumination over different areas varies by many orders of magnitude.

All measurements made of the width of the fringe, whether by direct visual observation with an ocular or by measurements taken from films, have yielded 5 microns or less. It seems safe to say that, because of the symmetry of the diffraction pattern, the edge can be located at the centre of the dark fringe to within .5 microns. The same system operating in the

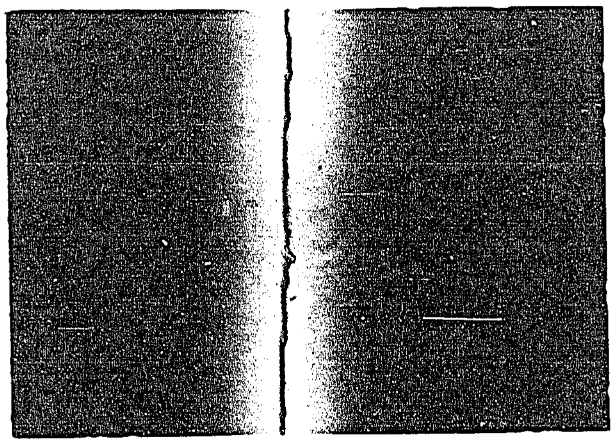

[illegible] 6 - The [illegible] image of a [illegible].

[illegible] not in itself significant. [illegible] and on the illumination [illegible] by exposing the pho- [illegible] scattering within the [illegible] fringe disappear complete- [illegible] to these irra- [illegible] film will thus accept [illegible] the image significantly. [illegible] diffraction patterns whose [illegible] by many orders of magnitude.

[illegible] fringe, whether by direct [illegible] taken from films, have [illegible] because of the sym- [illegible] can be located at the centre of [illegible] operating in the

conventional manner would give, at the edge, a transition zone from light to dark approximately 25 microns wide. Also a change in the illumination provided by the light source or a change in the threshold level of the receiver would result in an apparent shift of the transition zone. The center of a symmetrical pattern would not be affected by such variations. Consequently, there is a net gain in resolution of 50 times over that of the same system used in the conventional manner. A further discussion of the resolution is presented in the appendix. The defects of the edge shown in figure 6 (see page 6) would not be detected in the conventional system.

Some Parameters Affecting the Diffrimoscopic Image.

The diffrimoscopic image is accompanied by a system of broad lateral fringes on either side of the luminous area in the middle of the photograph.

Figure 7 (see page 8) is a composite showing the diffrimoscopic image formed when using white light, blue light (wavelength 4352A), green light (wavelength 5461A) and yellow light (wavelength 5780A). It can be seen that the position of the lateral fringes is dependent on the wavelength of the light utilized. The distance between the central bright zone and the first lateral fringe is largest in the case of the longest wavelength.

The next diagram, figure 8 (see page 9), will require a certain amount of explanation. This figure is a schematic representation of the type of diffrimoscopic system in which the object is inserted in a beam of parallel light (see figure 4 on page 4). The incident light which is not diffracted or stopped by the object itself is focussed by lens L_2 on to a mask M_1 which is here represented as a strip mask. Such a mask may be used since the light which is diffracted by the straight edge lies in a plane which is perpendicular to the edge in the case of a parallel incident beam (the case in which the incident light is convergent is presented in the appendix). Consequently, lens L_1 focusses this diffracted light to a line

(continued on page 11)

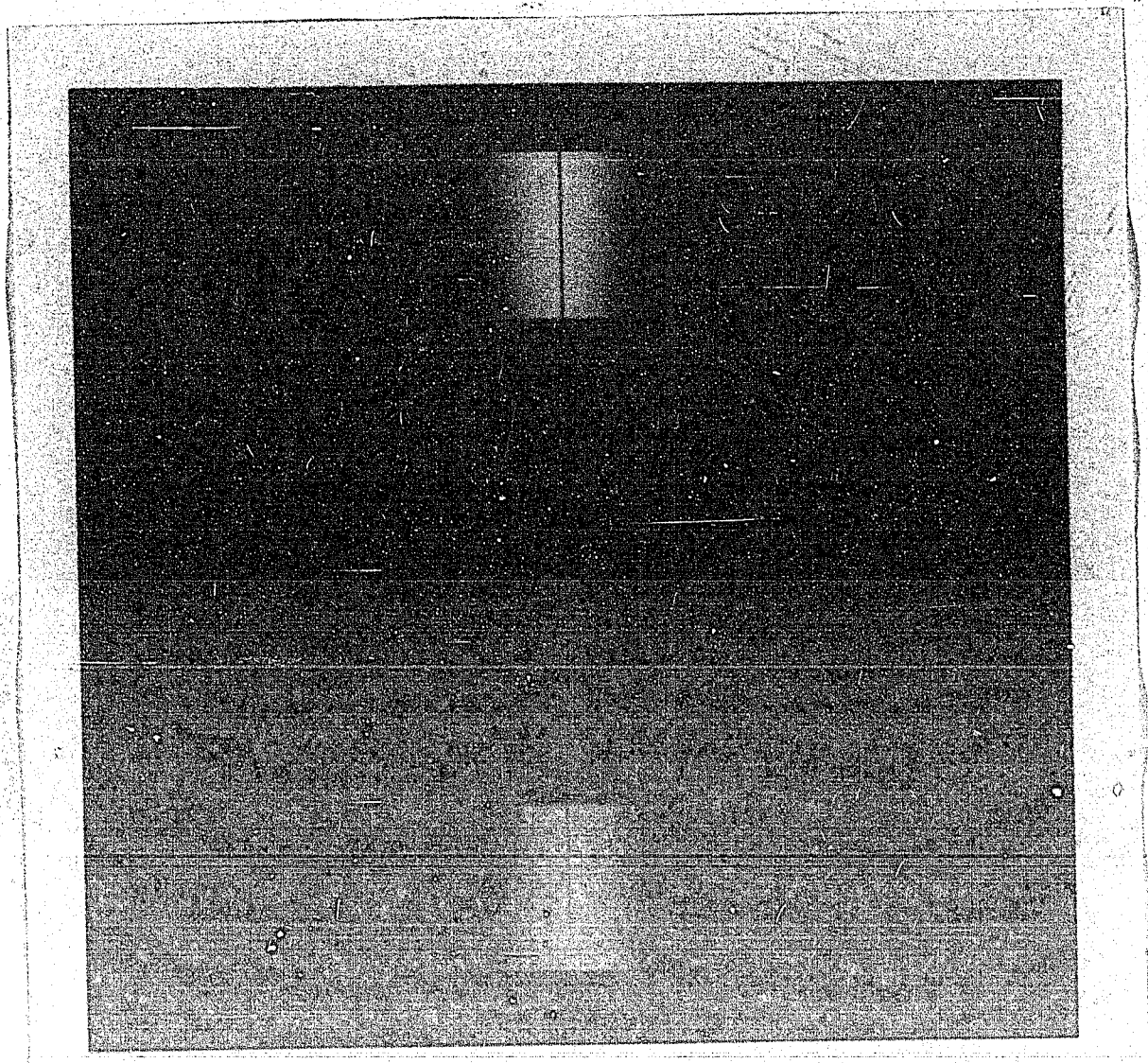

Figure 7: A composite showing the variation of the lateral fringes with wavelength. The top photograph was taken in white light. The next photographs were taken respectively in blue light (wavelength 4352 A), green light (wavelength 5461 A) and yellow light (wavelength 5780 A).

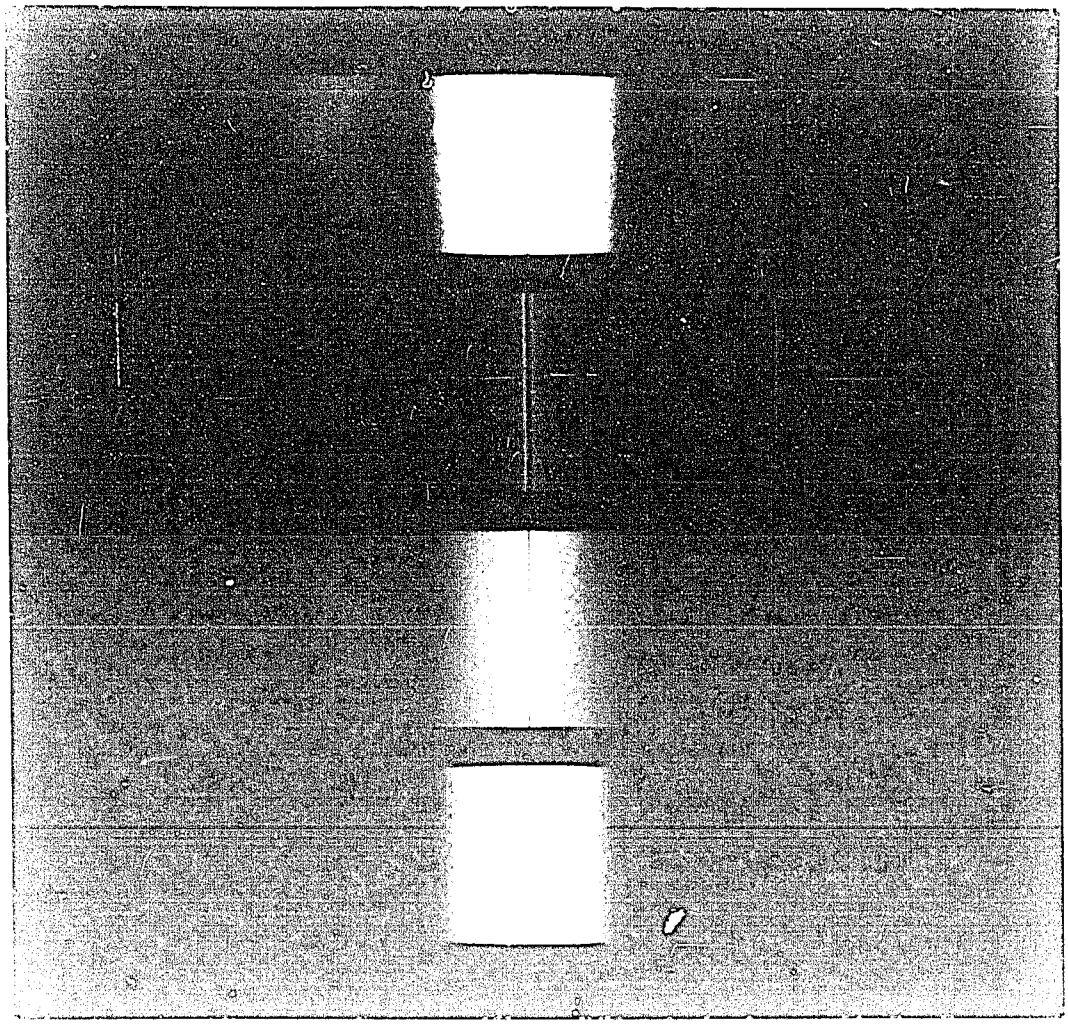

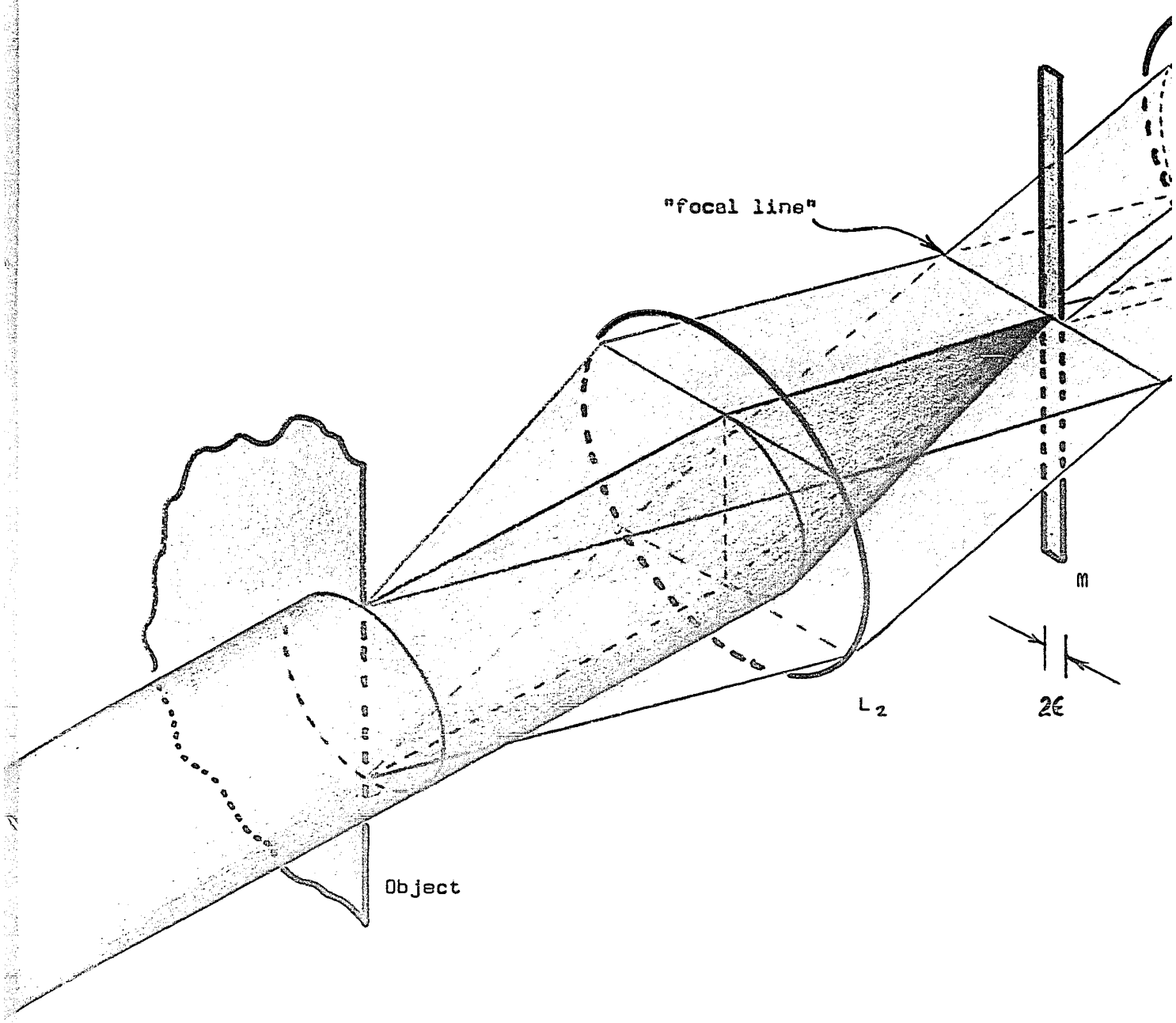
"focal line"
M
L_2
2ϵ
Object

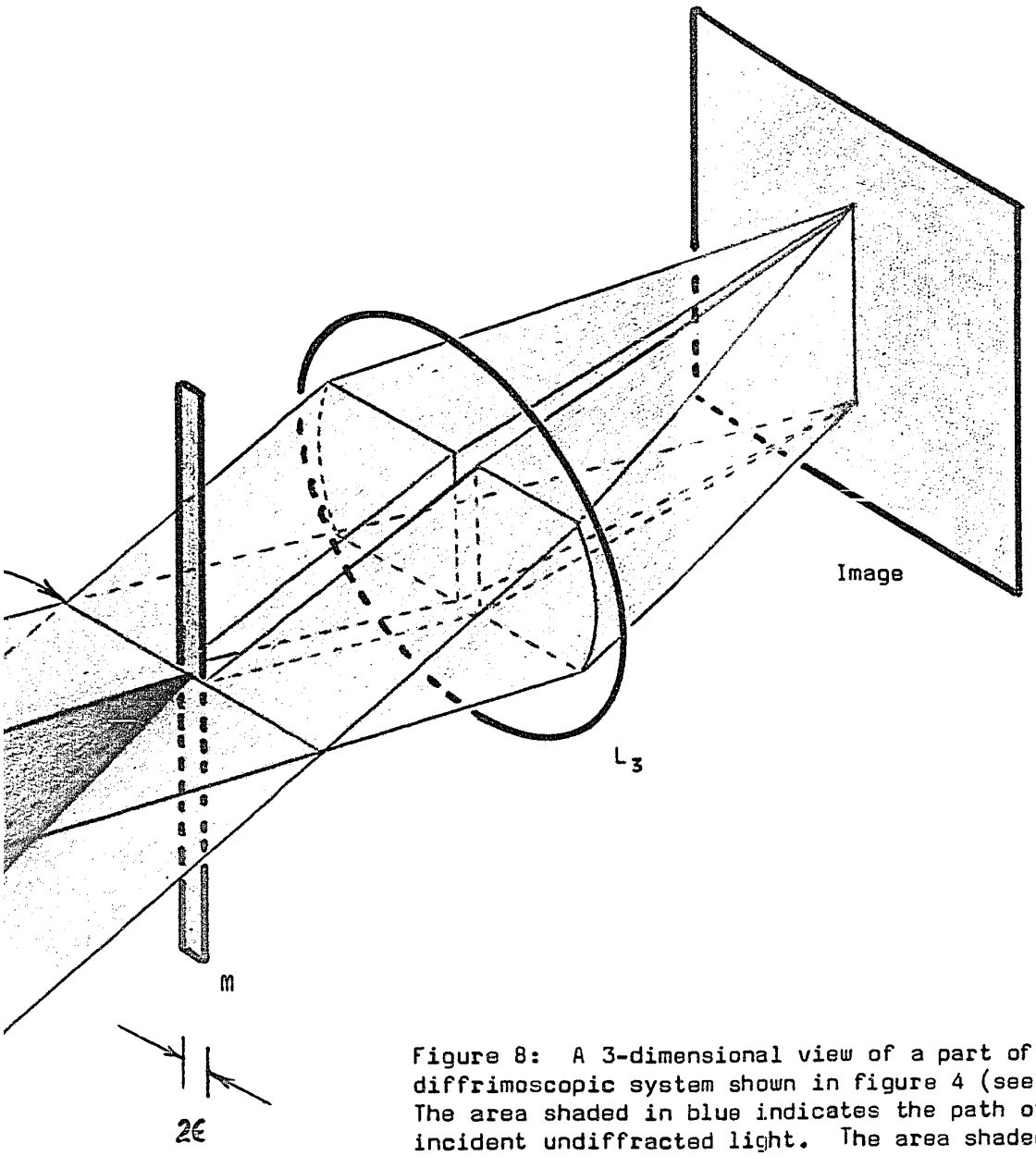

Figure 8: A 3-dimensional view of a part of the diffrimoscopic system shown in figure 4 (see page 4). The area shaded in blue indicates the path of the incident undiffracted light. The area shaded in red indicates the path followed by the diffracted light through the diffrimoscopic system. The so-called "focal line" is here indicated. The mask M is placed one focal length away from lens L_2 which in turn is one focal length away from the diffracting object. The distance from lens L_3 to the image plane is also one focal length.

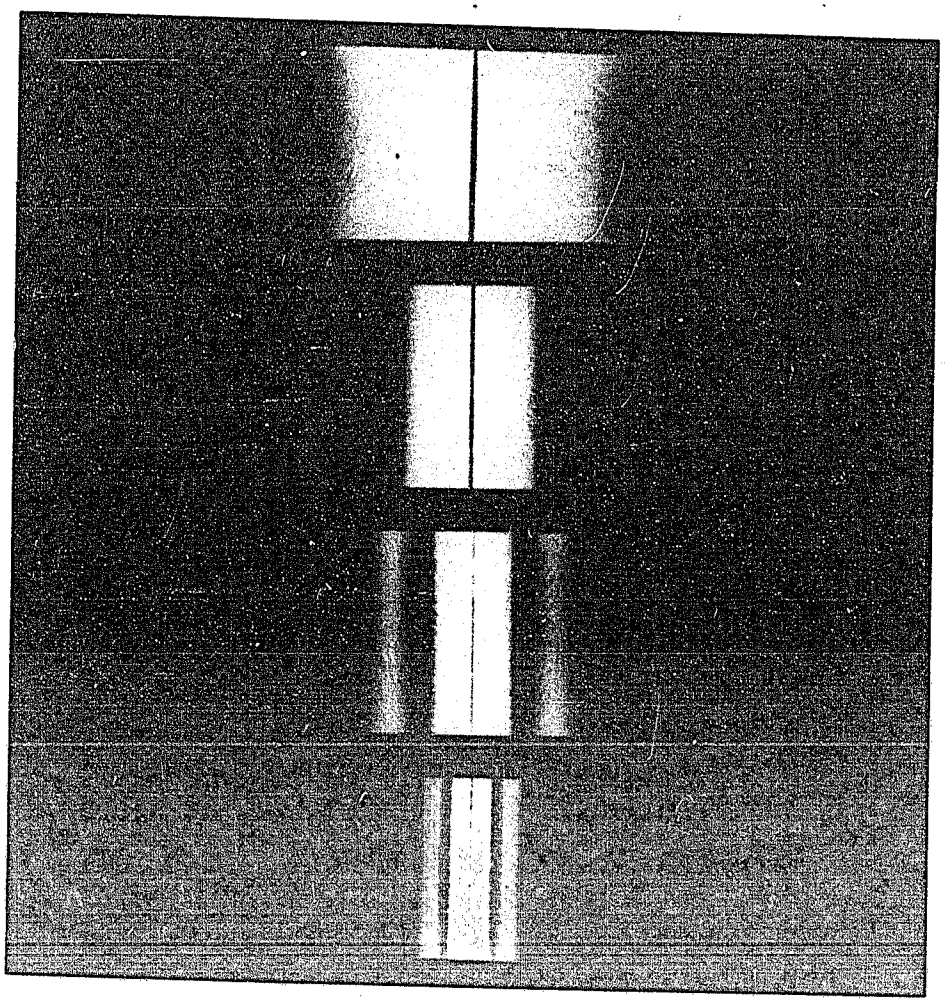

Figure 9 - A composite of photographs showing the variation of the diffrimoscopic image with mask width. From the top, these distributions of light were formed with a .5mm mask, a 1mm mask, and a 2mm mask and 4mm mask respectively.

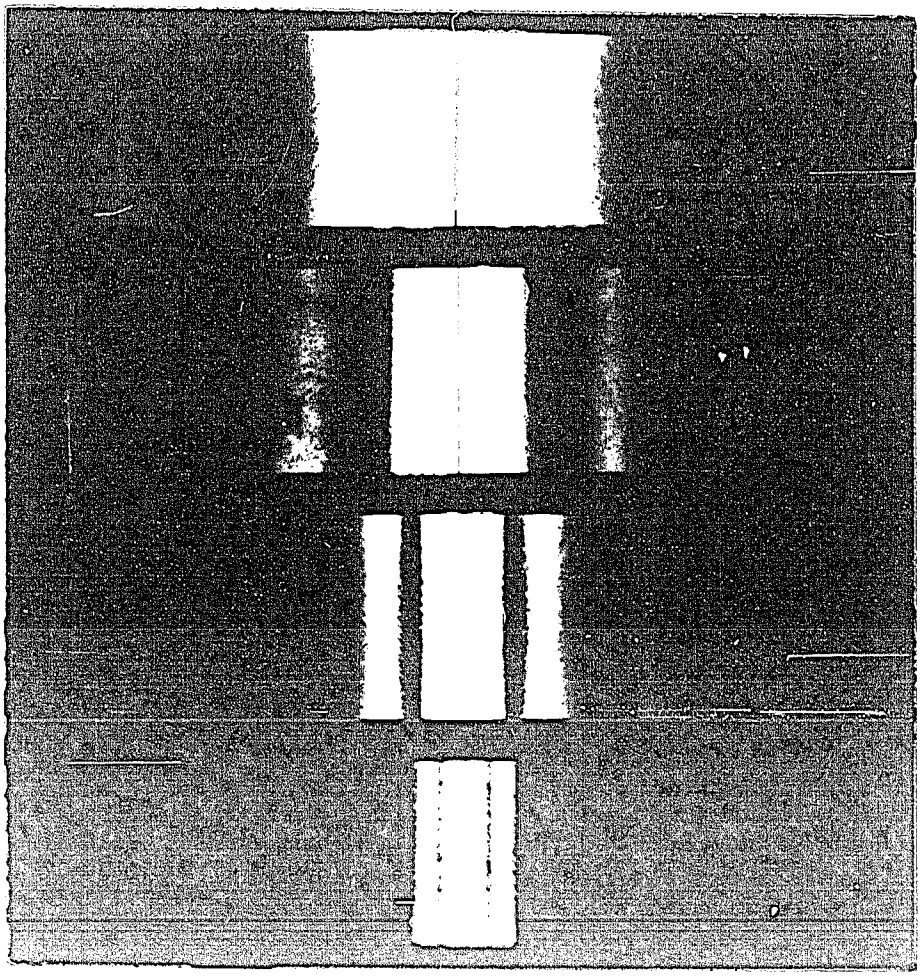

in the plane of the mask. This line is perpendicular to the edge of the object and therefore perpendicular to the strip mask. The diffracted light which is not stopped by the mask is gathered by lens L_3 and focussed to a diffrimoscopic image as shown. This picture treats both the incident beam and the diffracted light as bundles of rays and, consequently, is subject to the limitations of any picture which tries to portray a wave phenomenon through the use of rays.

The effect that the width (2ϵ) of the mask M has on the final image will now be demonstrated. In figure 9 (see page 10) as the width of the mask is varied through the values .5mm, 1mm, 2mm and 4mm, it can be seen that the lateral fringes are brought even closer to the central black fringe. This may be interpreted as a re-diffraction from the edges of the mask of the beam of diffracted light. A more correct theoretical explanation for the variation of fringe position with mask width will be dealt with in a later section.

The lateral fringes have thus been shown to be linked to the mask width and to the wavelength of the light.

Some Remarks on the Formation of the Diffrimoscopic Image.

Figure 10 (see page 12) shows five photographs of a straight edge, all taken with the same diffrimoscopic system. The two photographs to the left show the image inside the focus of lens L_3, the middle photograph shows the correctly focussed image and the two photographs to the right show the image formed outside the focus. In this figure can be seen the evolution of the diffrimoscopic image in space.

These photographs have three important characteristics. First, all the images, whether out of focus or not, present a central minimum. Secondly, the images are all symmetrical with respect to this central black fringe. Thirdly, images which have an equal defect of focus either inside or outside the focal position are identical. These aspects of the diffrimoscopic image play an important role in the preliminary theory which was developed and of which more will be said later.

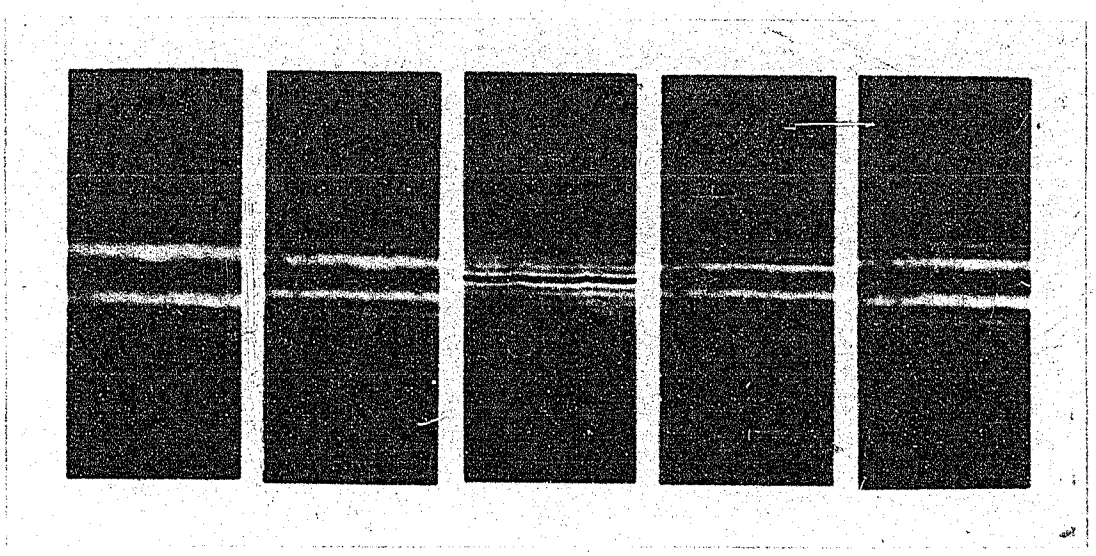

Figure 10 - A composite showing the evolution of the diffrimoscopic image in front of, and behind the focal plane. From the left, the photographs show the distribution of light formed 6mm and 3mm in front of the focal plane respectively. The central photograph shows the image formed at the focus. The next two photographs show the distribution formed 3mm and 6mm behind the focal plane respectively.

Figures 11 and 12 (see pages 13 & 14) indicate the manner in which the next photographs were taken. A stop was introduced in the plane of the mask in such a way as to permit only half of the light diffracted by the edge to continue and form an image. Two of the photographs in figure 13 (see page 15) show the images formed with only half of the diffracted light, the third shows the normal diffrimoscopic image. All the images here are correctly focussed. It is noted that the images formed with either half of the diffracted light are identical. Both images present a central maximum and are symmetrical with respect to this maximum.

(continued on page 16)

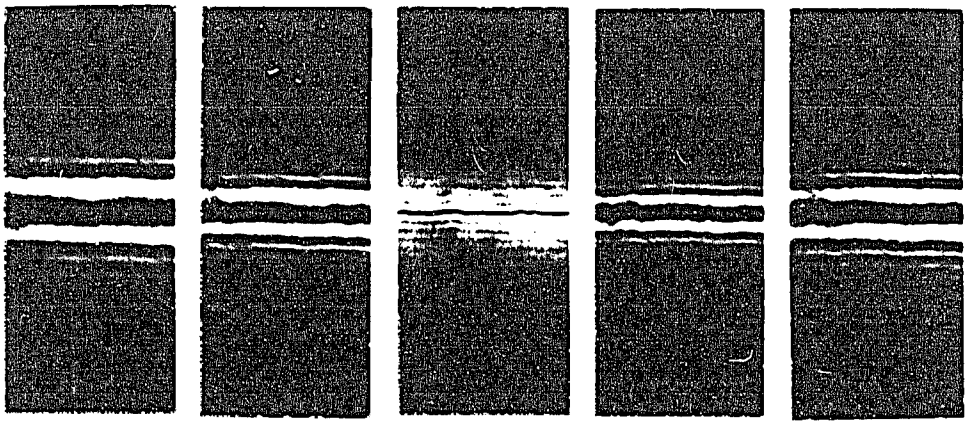

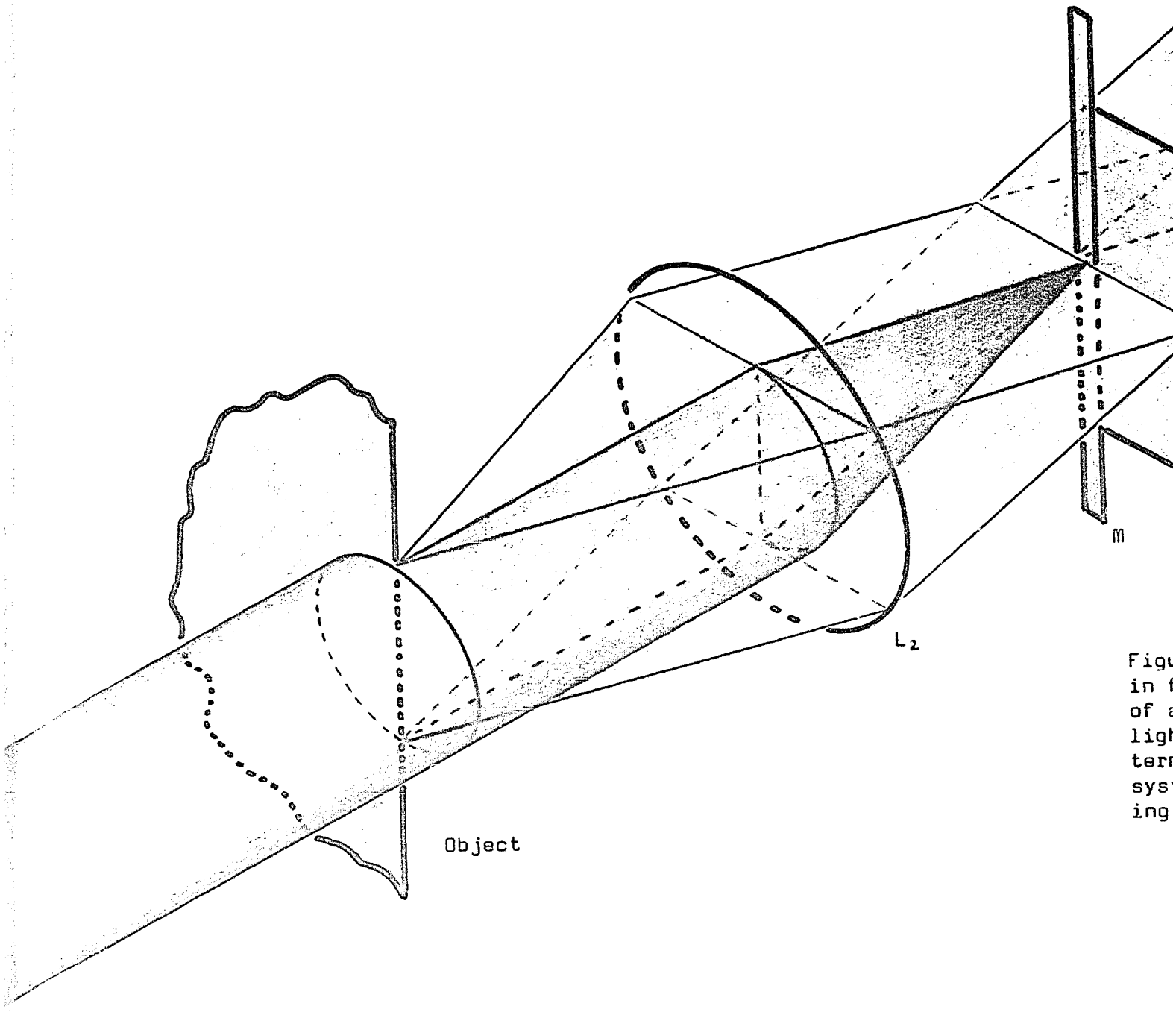

Figu
in t
of a
ligh
terr
sys
ing

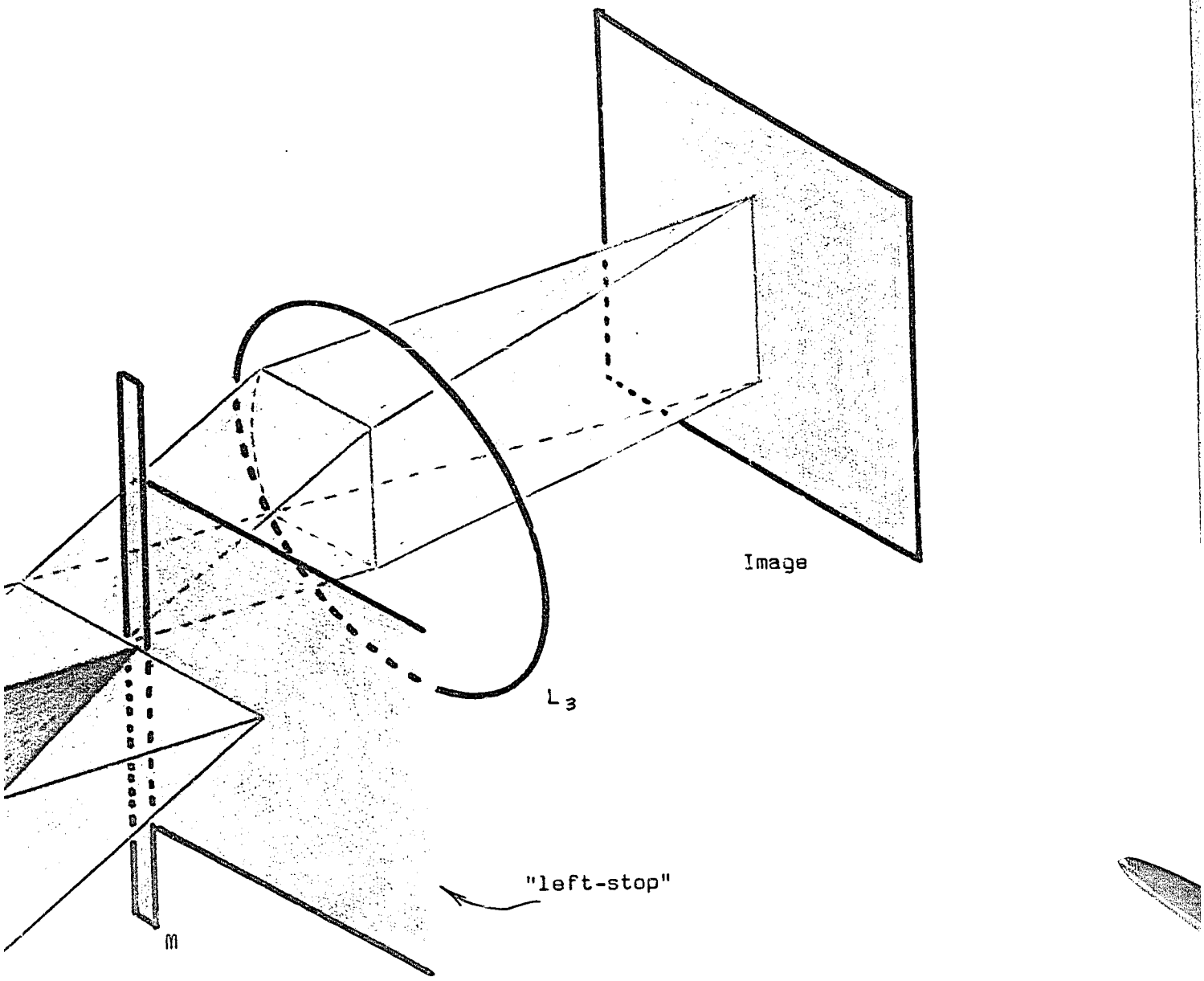

Figure 11 - A 3-dimensional view of the diffrimoscopic system shown in figure 8 (see page 9). In this figure can be seen the presence of a "left-stop" in the mask plane. This stop cuts out all the light diffracted to the left of the optic axis. In this paper the terms "left" and "right" will refer to the two sides of the optical system as seen by an observer standing at the image plane and looking toward the light source.

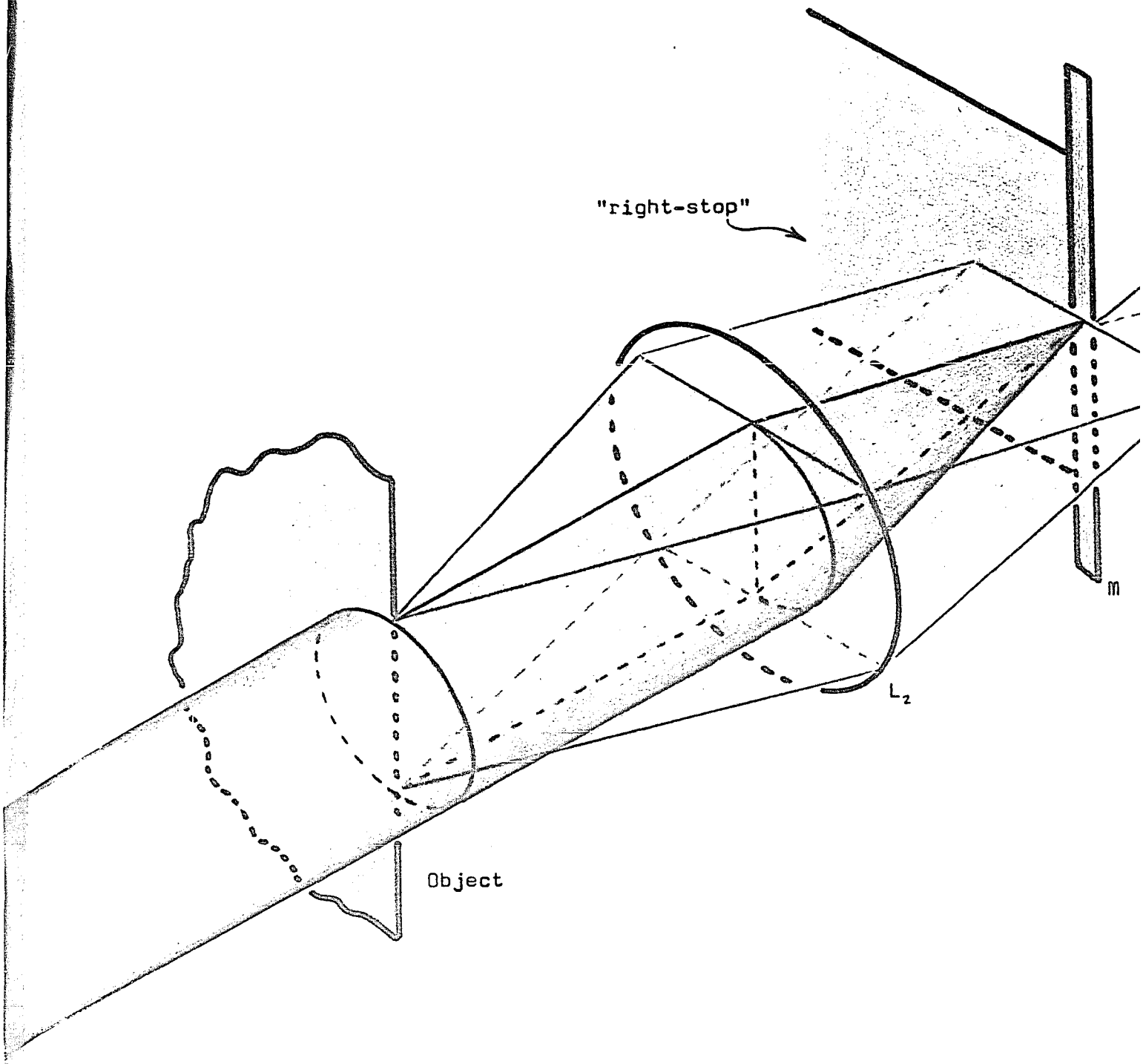
"right-stop"
L_2
m
Object

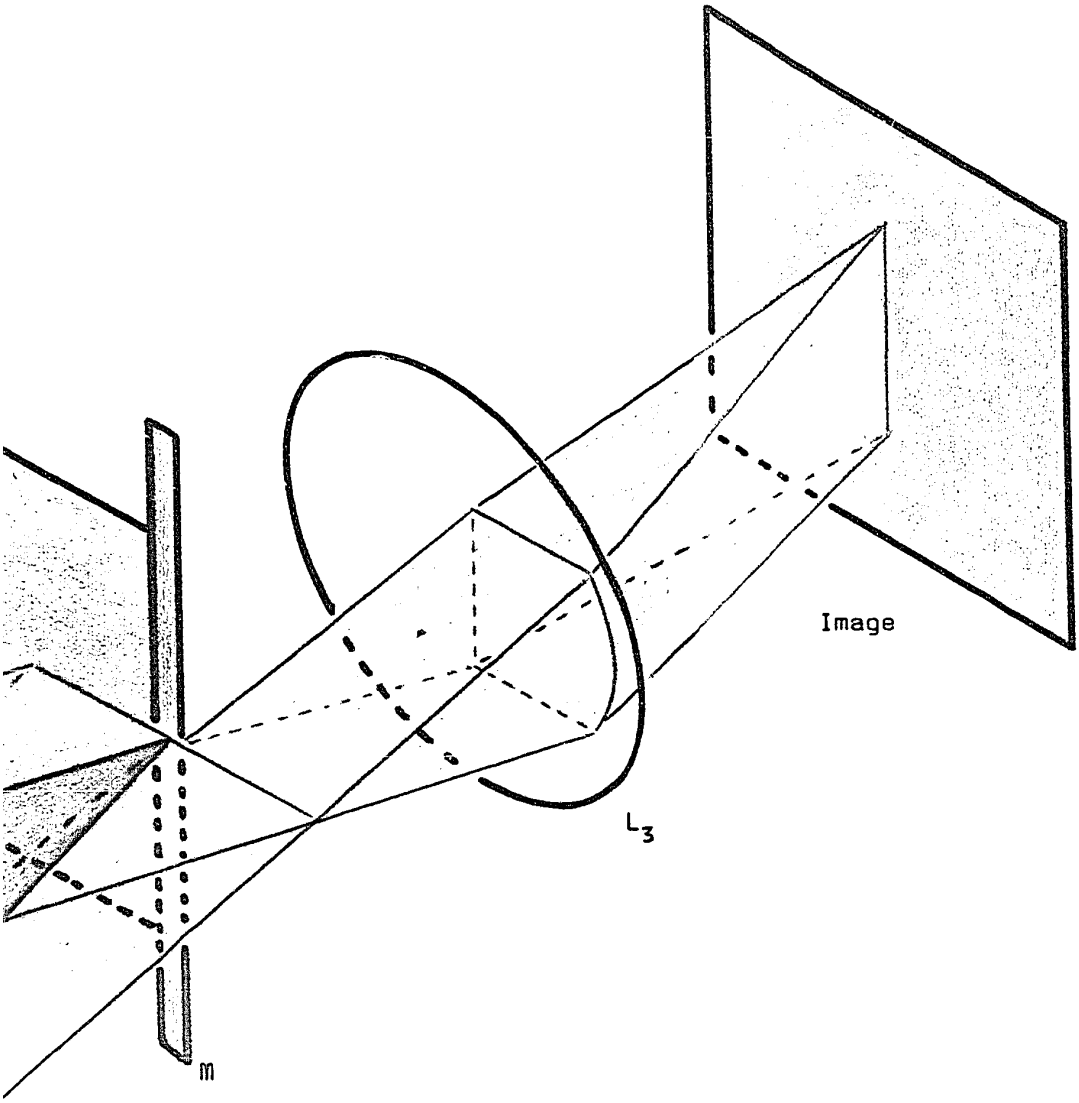

Figure 12 - A 3-dimensional view of the diffrimoscopic system with a "right-stop" in the plane of the mask.

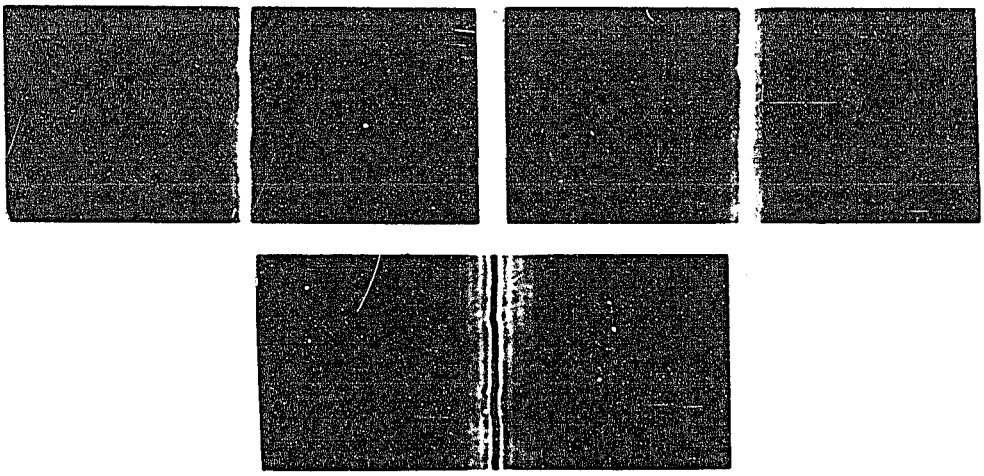

Figure 13 - The two images at the top were formed with half-masks. The image at the left was formed with a left half-mask as shown in figure 11 (see page 13). The image at the right was formed with a right half-mask as shown in figure 12 (see page 14). The lower photograph shows the normal diffrimoscopic image. All images are in focus.

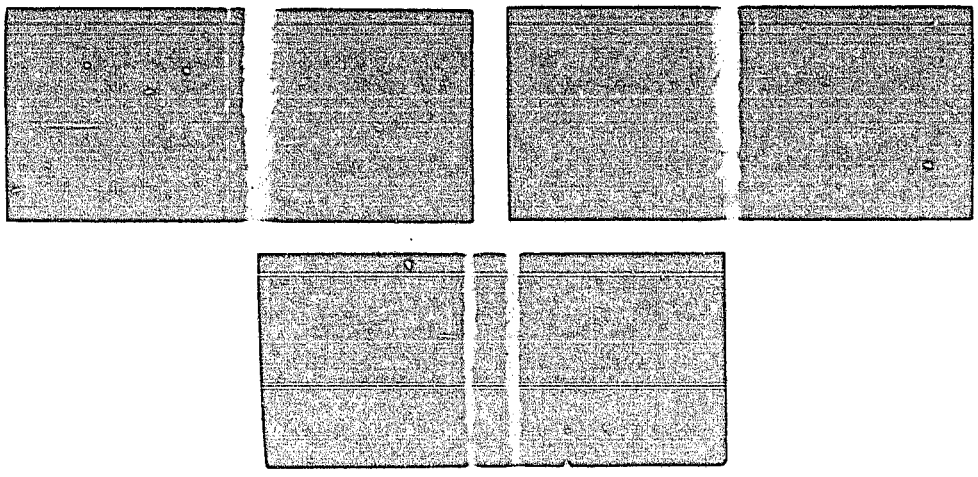

Figure 14 - These images correspond to those of figure 13 but taken 8mm inside the focus of lens L_y.

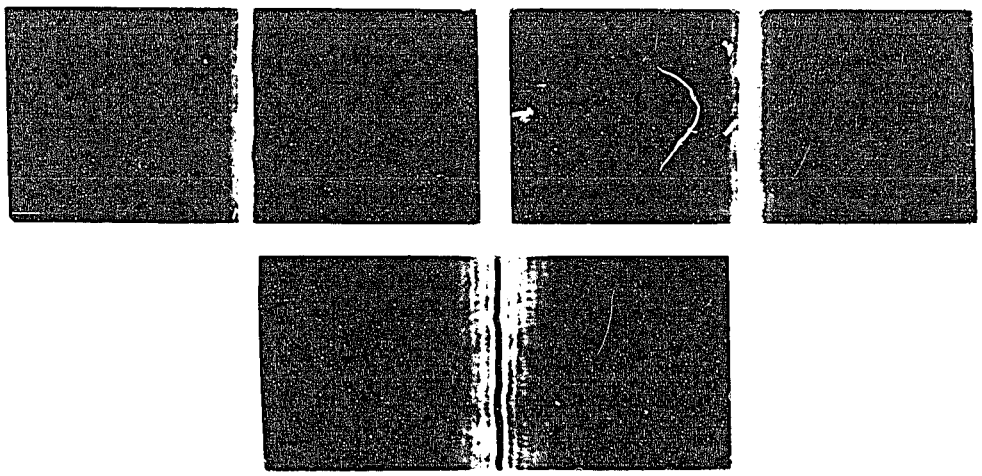

Figure 13 - [illegible] formed with half-masks. The [illegible] with a left half-mask as shown [illegible]. The image at the right was [illegible] as shown in figure 12 (see [illegible] shows the normal diffraction [illegible] in focus.

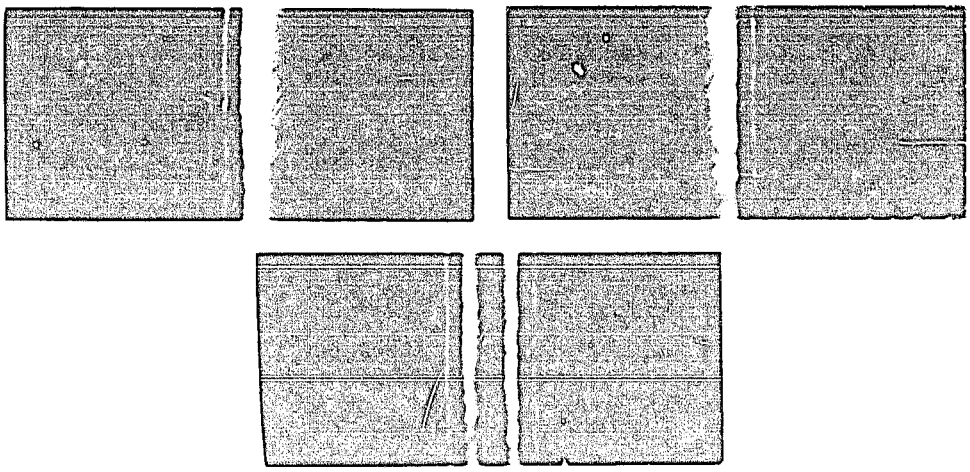

Figure [illegible] - [illegible] taken [illegible]

The photographs in figure 14 (see page 15) correspond exactly to those of figure 13 (see page 15) except now the system is out of focus. In this case the images taken with a right or a left stop are asymmetrical. They can, however, be considered to have a certain mirror symmetry with respect to the optic axis. Moreover, the two images taken with stops indicate how the out-of-focus diffrimoscopic image is formed. If it is imagined that the two distributions of light formed when a stop is present are out of phase by one-half wavelength, and a mental superposition of these two patterns is made, it may be seen that the distribution shown in the third photograph would be the result. This same procedure may now be applied to the photographs shown in figure 13 (see page 15) although there the result is not so easy to visualize.

The supposition that the light which passes on one side of the mask is out of phase with that which passes on the other side is supported by the fact that all diffrimoscopic images (see figure 10 on page 12) present a central minimum. Indeed, by using the simple expedient of introducing a phase reversal plate in the plane of the mask as shown in figure 15, it was possible to change the minimum in the normal diffrimoscopic image to a maximum.

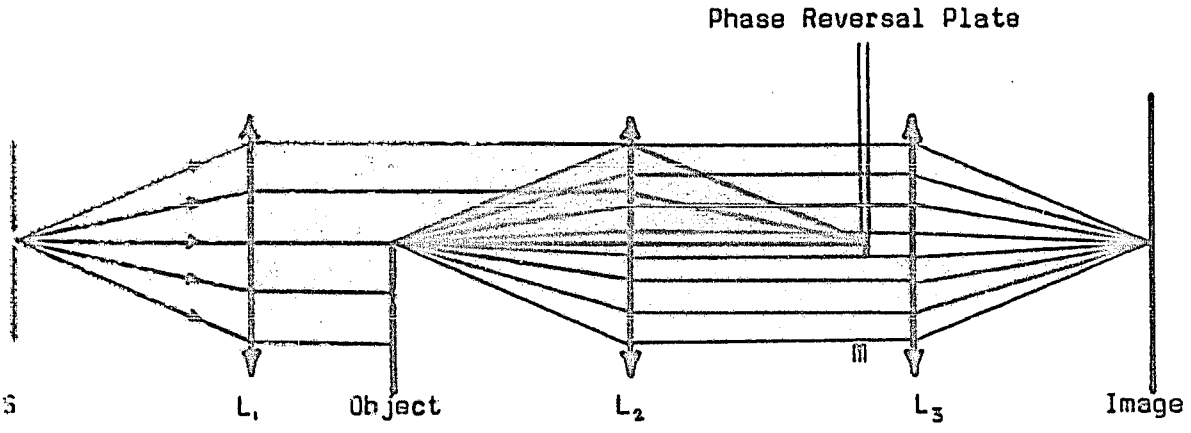

Figure 15 - This diagram of a diffrimoscopic system shows a phase reversal plate inserted half-way into the mask plane. The presence of this plate changes the central minimum of the diffrimoscopic pattern to a maximum.

The following section will serve as an introduction to the formalism used in the derivations as well as an indication of one of the theoretical arguments supporting the assumption that the light on one side of the mask is out of phase with the light on the other side by one-half wavelength.

A Short Theoretical Argument.

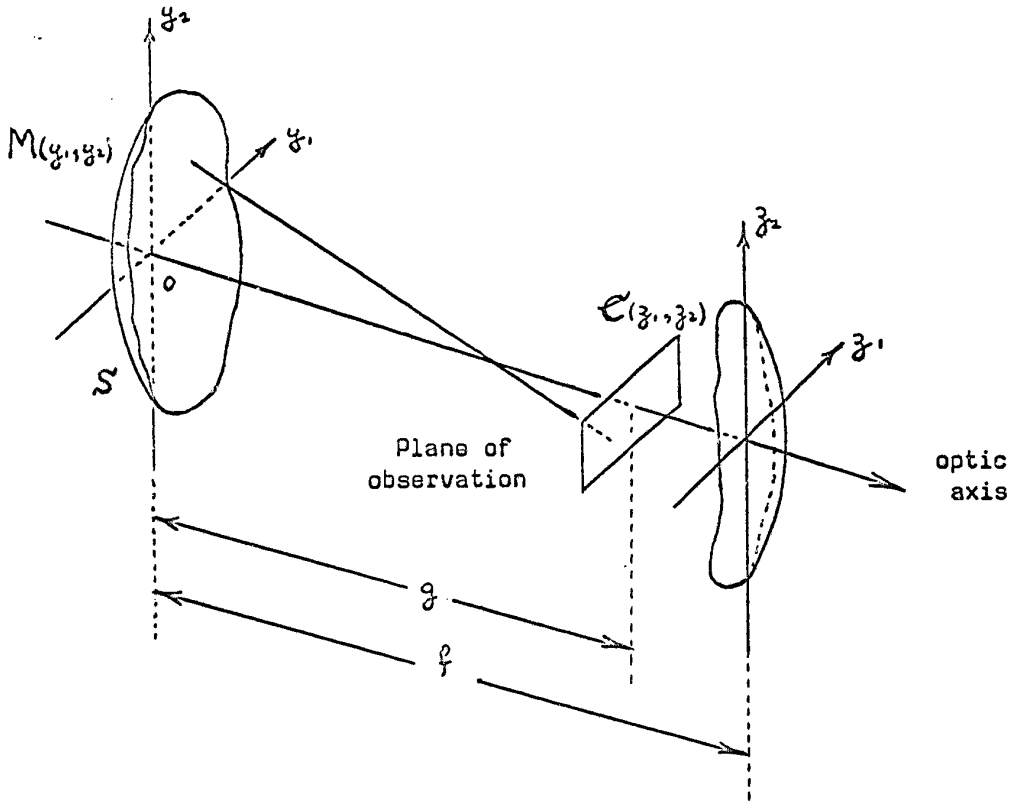

In the Fourier transform theory of diffraction phenomena, the distribution of light in the image plane of an aberration free system is given as:

$$\mathcal{E}(z_1,z_2) = \iint M(y_1,y_2)\cdot e^{i\pi(1-\frac{f}{g})(y_1^2+y_2^2)}\cdot e^{-i2\pi(y_1z_1+y_2z_2)}\, dy_1\, dy_2 \qquad (1)$$

where $\mathcal{E}(z_1,z_2)$ and $M(y_1,y_2)$ are the complex amplitudes in the image and pupil planes respectively.

f - is the focal length of the system

g - is the distance from the pupil at which the image is observed.

---

* Lansraux, G. - Diffraction Instrumentale, Ed. de la Revue d'Optique theorique et instrumentale, 1953.

$$M(y_1, y_2) = m(y_1, y_2) \cdot e^{i\mu(y_1, y_2)} \qquad (2)$$

where $m(y_1, y_2)$ is the amplitude function in the pupil

and $\mu(y_1, y_2)$ is the phase function in the pupil

Let $\alpha = \pi(1 - f/z)$ (3)

The factor α might be called a focussing factor. When the image is observed in the focal plane $z = f$ and $\alpha = 0$.

The origin of the system of co-ordinates is taken as the point "O", where the optic axis meets the pupil.

$$C_{(z_1, z_2)} = \iint_S M_{(y_1, y_2)} \cdot e^{i\alpha(y_1^2 + y_2^2)} \cdot e^{-i2\pi(y_1 z_1 + y_2 z_2)} \, dy_1 \, dy_2 \qquad (4)$$

The complex amplitude function in the plane in which the <u>diffraction</u> occurs will be represented by the symbol "D". In the <u>mask</u> plane it will be represented by the symbol "M" and in the plane which is <u>conjugate</u> to the object plane it will be denoted by the symbol "C".

In this case the pupil plane is the plane of the mask. Choosing the y_1-axis to coincide with the focal line mentioned earlier and using the one-dimensional form of the above equation gives:

$$C_{(z_1)} = \int_L M_{(y_1)} \cdot e^{i\alpha y_1^2} \cdot e^{-i2\pi y_1 z_1} \, dy_1 \qquad (5)$$

where L is the diameter of the pupil.

The integration must actually be carried out over two domains $-L/2 \rightarrow -\epsilon$ and $\epsilon \rightarrow L/2$, because of the presence of the strip mask. The quantity "ϵ" here is one-half the width of the mask.

For simplicity the following notation will be introduced:

$$\int_{-L/2}^{-\epsilon} M_{(y_1)} \cdot e^{i\alpha y_1^2} \cdot e^{-i2\pi y_1 z_1} \, dy_1 + \int_{\epsilon}^{L/2} M_{(y_1)} \cdot e^{i\alpha y_1^2} \cdot e^{-i2\pi y_1 z_1} \, dy_1 = \int_{-L/2}^{L/2} M_{(y_1)} \cdot e^{i\alpha y_1} \cdot e^{-i2\pi y_1 z_1} \, dy_1 \qquad (6)$$

Also, $C_{(z_1)}$ may be said to be a function of "α".

Thus,

$$C_{(z_1,\alpha)} = \int_{-L/2}^{L/2} M_{(y_1)} \cdot e^{i\alpha y_1^2} \cdot e^{-i2\pi y_1 z_1} \, dy_1 \qquad (7)$$

At $z_1 = 0$

$$C_{(0,\alpha)} = \int_{-L/2}^{L/2} M_{(y_1)} \cdot e^{i\alpha y_1^2} \, dy_1 \qquad (8)$$

Letting $M_{(y_1)} = M_e(y_1) + M_o(y_1)$ (9)

where $M_e(y_1)$ is an even function of y_1

and $M_o(y_1)$ is an odd function of y_1

Thus:

$$C_{(0,\alpha)} = \int_{-L/2}^{L/2} M_e(y_1) \cdot e^{i\alpha y_1^2} \, dy_1 + \int_{-L/2}^{L/2} M_o(y_1) \cdot e^{i\alpha y_1^2} \, dy_1 \qquad (10)$$

But

$$\int_{-L/2}^{L/2} M_o(y_1) \cdot e^{i\alpha y_1^2} \, dy_1 = 0 \qquad (11)$$

Thus: $$C_{(0,\alpha)} = \int_{-L/2}^{L/2} M_e(y_1) \cdot e^{i\alpha y_1^2} \, dy_1 \qquad (12)$$

Now $|C_{(0,\alpha)}|^2 = 0$. This states that all diffrimoscopic images whether out of focus or not, have a black central fringe on the optic axis (see figure 10, page 12). From this follows that $C_{(0,\alpha)} = 0$.

$$\therefore \int_{-L/2}^{L/2} M_e(y_1) \cdot e^{i\alpha y_1^2} \, dy_1 \equiv 0 \qquad \text{for all } \alpha. \qquad (13)$$

$$\therefore \quad M_e(y_1) = 0 \qquad (14)$$

The useful part of the complex amplitude $M(y_1)$ in the plane of the mask is thus purely an odd function of y_1. This result supports the assumption which was made on page 16 and will be derived in another fashion later.

Thus,

$$C(z_1,\alpha) = \int_{-L/2}^{L/2} M(y_1)\cdot e^{i\alpha y_1^2}\cdot e^{-i2\pi y_1 z_1}\, dy_1 \qquad (7)$$

At $z_1 = 0$

$$C(0,\alpha) = \int_{-L/2}^{L/2} M(y_1)\cdot e^{i\alpha y_1^2}\, dy_1 \qquad (8)$$

Letting $M(y_1) = M_e(y_1) + M_o(y_1)$ (9)

where $M_e(y_1)$ is an even function of y_1

and $M_o(y_1)$ is an odd function of y_1

Thus:

$$C(0,\alpha) = \int_{-L/2}^{L/2} M_e(y_1)\cdot e^{i\alpha y_1^2}\, dy_1 + \int_{-L/2}^{L/2} M_o(y_1)\cdot e^{i\alpha y_1^2}\, dy_1 \qquad (10)$$

But

$$\int_{-L/2}^{L/2} M_o(y_1)\cdot e^{i\alpha y_1^2}\, dy_1 = 0 \qquad (11)$$

Thus: $$C(0,\alpha) = \int_{-L/2}^{L/2} M_e(y_1)\cdot e^{i\alpha y_1^2}\, dy_1 \qquad (12)$$

Now $|C(0,\alpha)|^2 = 0$. This states that all diffrimoscopic images whether out of focus or not, have a black central fringe on the optic axis (see figure 10, page 12). From this follows that $C(0,\alpha) = 0$.

$$\therefore \int_{-L/2}^{L/2} M_e(y_1)\cdot e^{i\alpha y_1^2}\, dy_1 \equiv 0 \qquad \text{for all } \alpha. \qquad (13)$$

$$\therefore \quad M_e(y_1) = 0 \qquad (14)$$

The useful part of the complex amplitude $M(y_1)$ in the plane of the mask is thus purely an odd function of y_1. This result supports the assumption which was made on page 16 and will be derived in another fashion later.

In the last short section something was learned concerning the complex amplitude distribution in the plane of the mask by making use of experimental evidence provided in the image plane. The result that $M(y_1)$ was found to be an odd function of y_1 will be checked more thoroughly in the next section. The information gained in one plane will give knowledge of the nature of the light distribution in the Fourier transform plane.

The next step in this research project was to make a closer investigation of the complex amplitude distribution in the plane of the mask. The purpose of this was twofold. First, a knowledge of this distribution would give an explanation of the structure of the diffrimoscopic images. Secondly, the mask plane and the object plane being linked by the Fourier transform, it was hoped that information could be gained about the distribution of amplitude and phase in the object plane.

11 - Diffrimoscopy as a Tool in the Study of Diffraction Phenomena.

In the plane of the mask, as was mentioned earlier (see page 7 and figure 8), a luminous line of light is formed. Normal diffrimoscopic images were formed while stopping down the aperture until only a small horizontal slit was left to permit the passage of the diffracted light. In figure 17 (see page 21) the mask holder with and without the baffles used to cut down the aperture is shown. Figure 18 (see page 22) shows two diffrimoscopic images, one of which was formed while the baffles were in position. The two images are identical. No information whatsoever was lost by introducing the baffles in the plane of the mask. The distribution of light in the "focal line" determines the character of the diffrimoscopic image and it is this focal line which will now be studied more closely.

(continued on page 25)

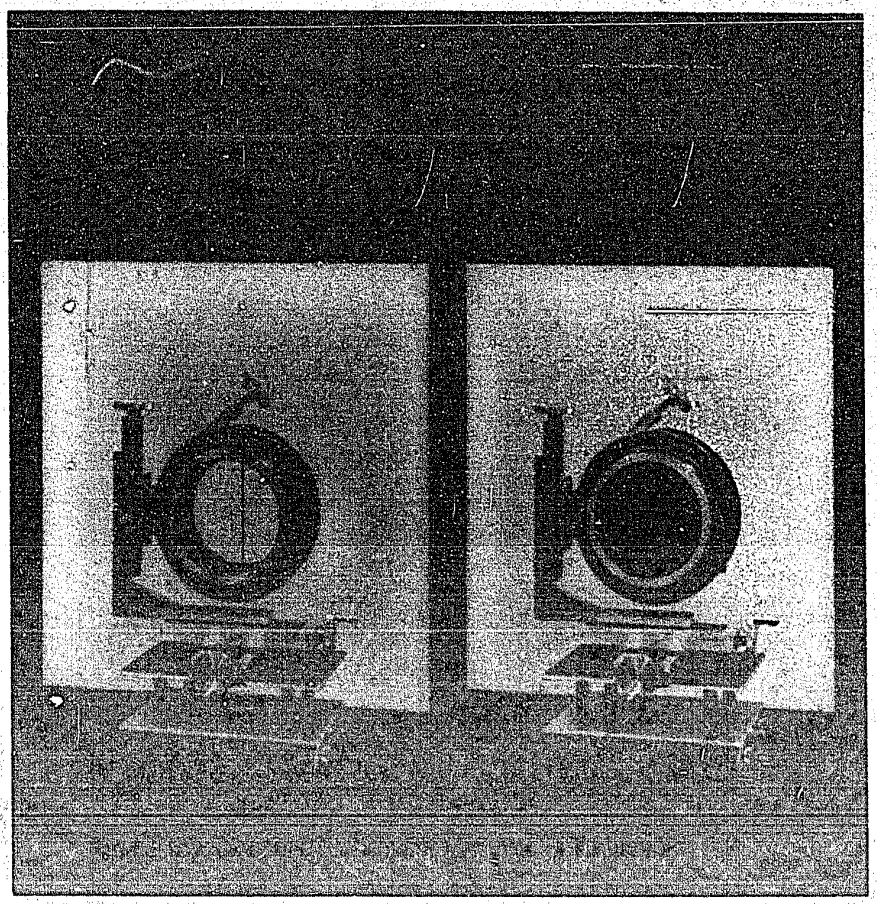

Figure 17 - Two photographs of the mask holder. This support was designed to provide motion along 3 perpendicular axes along with one rotation about the optic axis. The two photographs above show the 1mm strip mask which was used in some of the experiments. One of the photographs shows the baffles which were used to cut down the aperture to a slit 1mm in width.

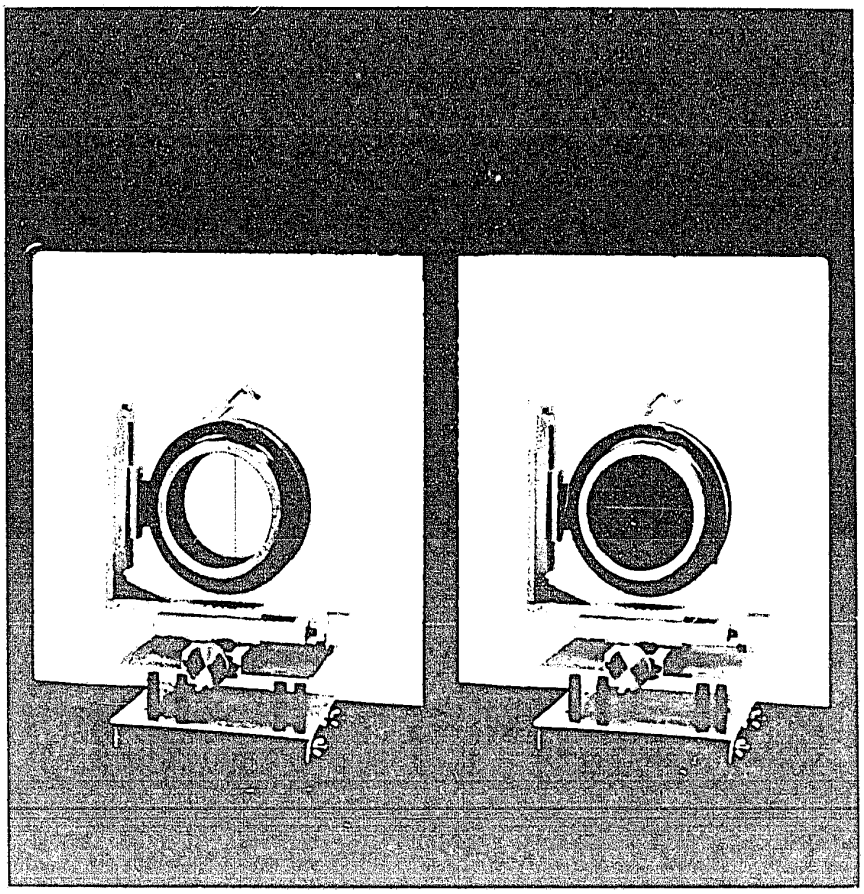

[illegible] photographs of the model rocket. This support was designed [illegible] section shows 3 perpendicular axes along with one [illegible] about the model axis. The two photographs above show [illegible] model which was used in some of the experiments [illegible] photographs show the baffles which were used [illegible]

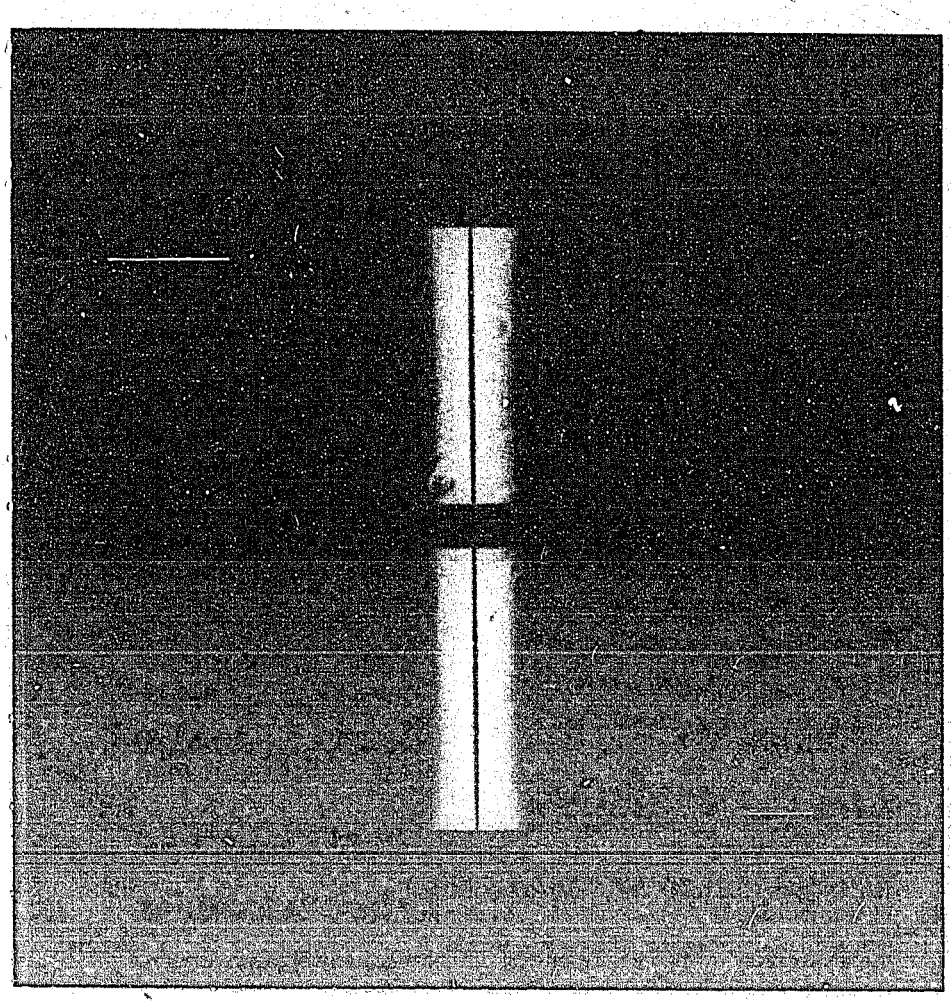

Figure 18 - A composite showing two identical diffrimoscopic images. The image at the top was photographed with the baffles shown in figure 17 (see page 21) whereas the image at the bottom was photographed without baffles.

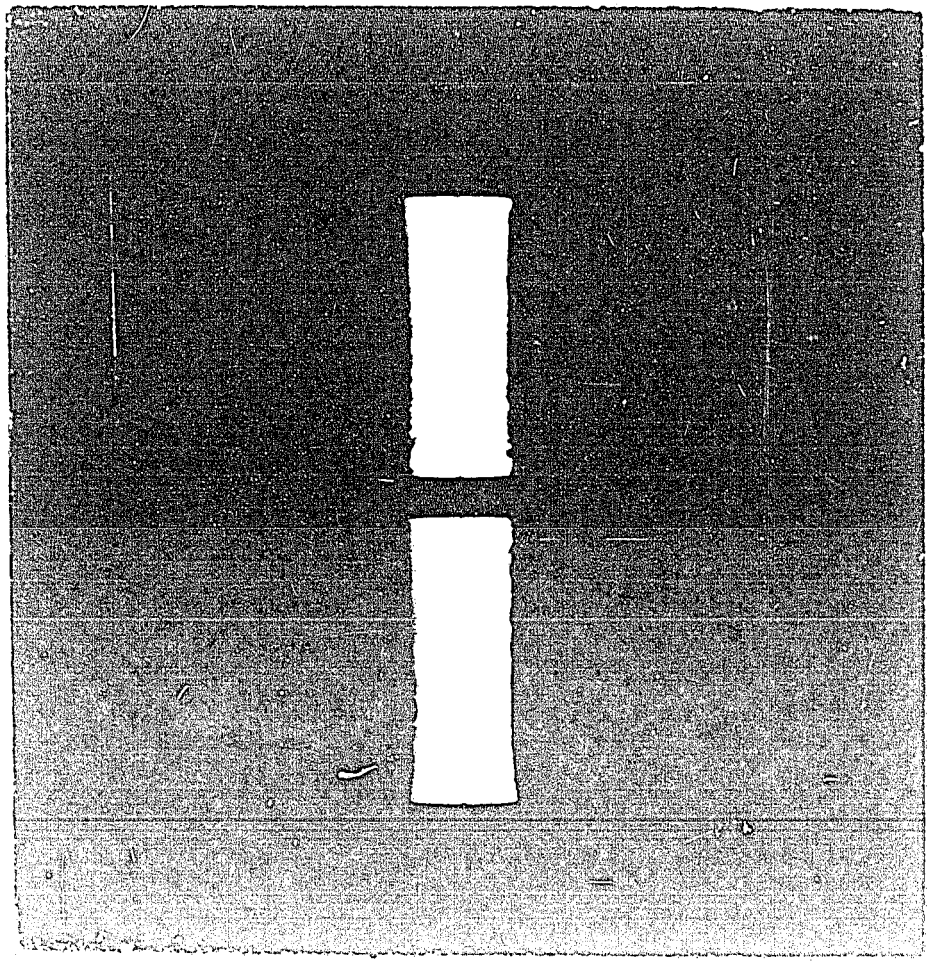

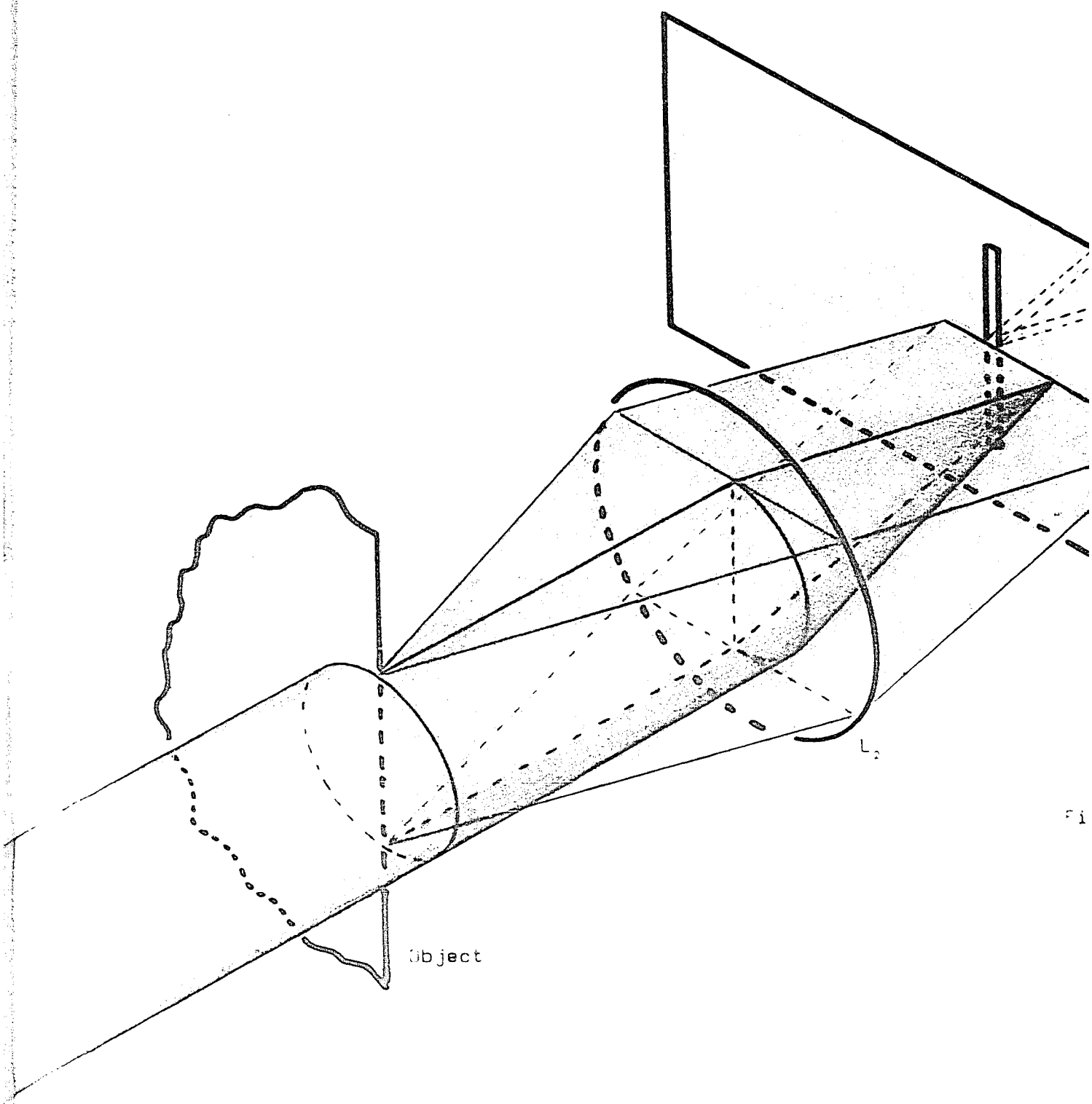

Fi

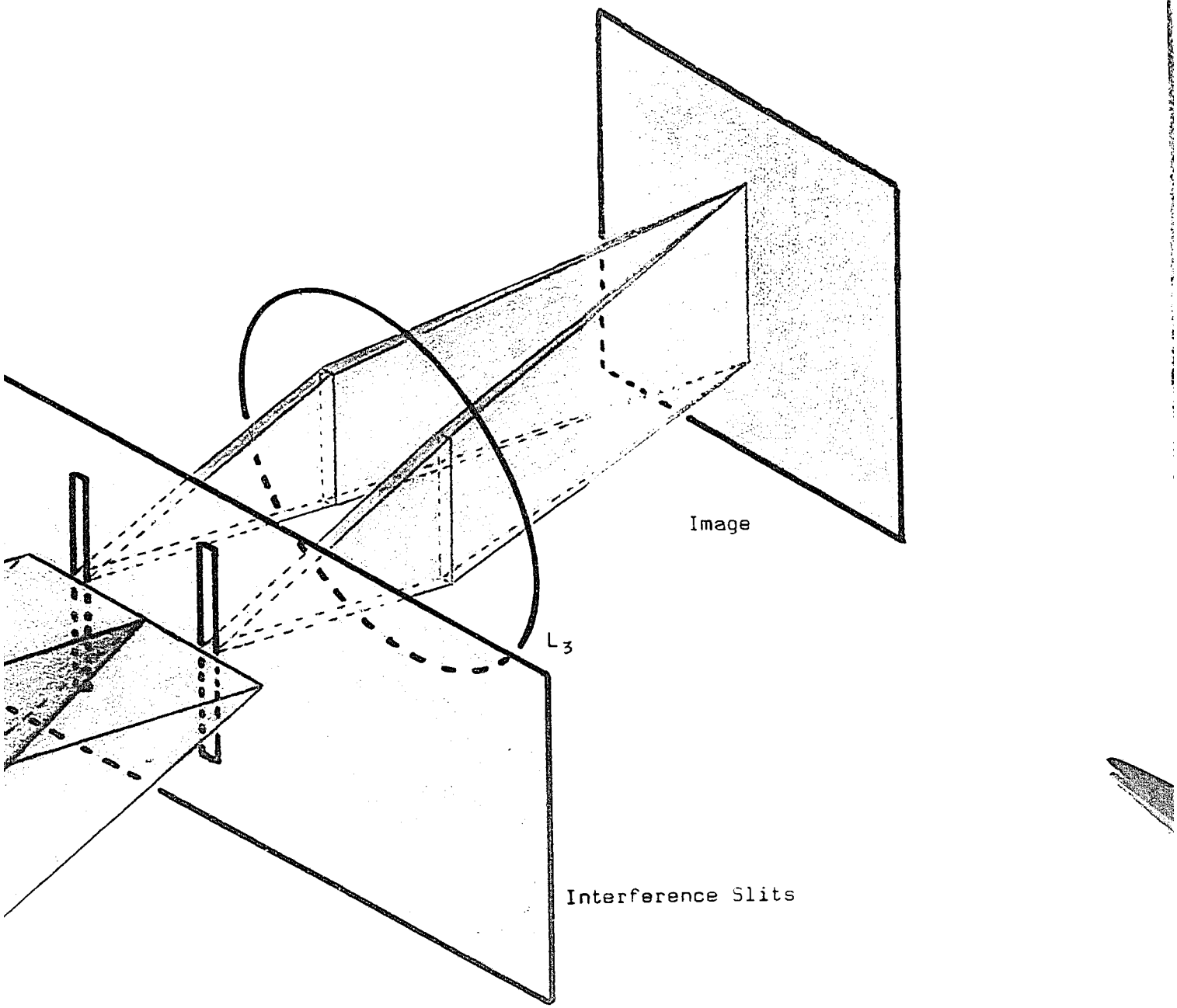

Figure 19 - A 3-dimensional view of the diffrimoscopic system with slits placed in the mask plane and astride the optic axis. A difference of phase between the two branches of the focal line will be detected in the interference pattern formed in the image plane.

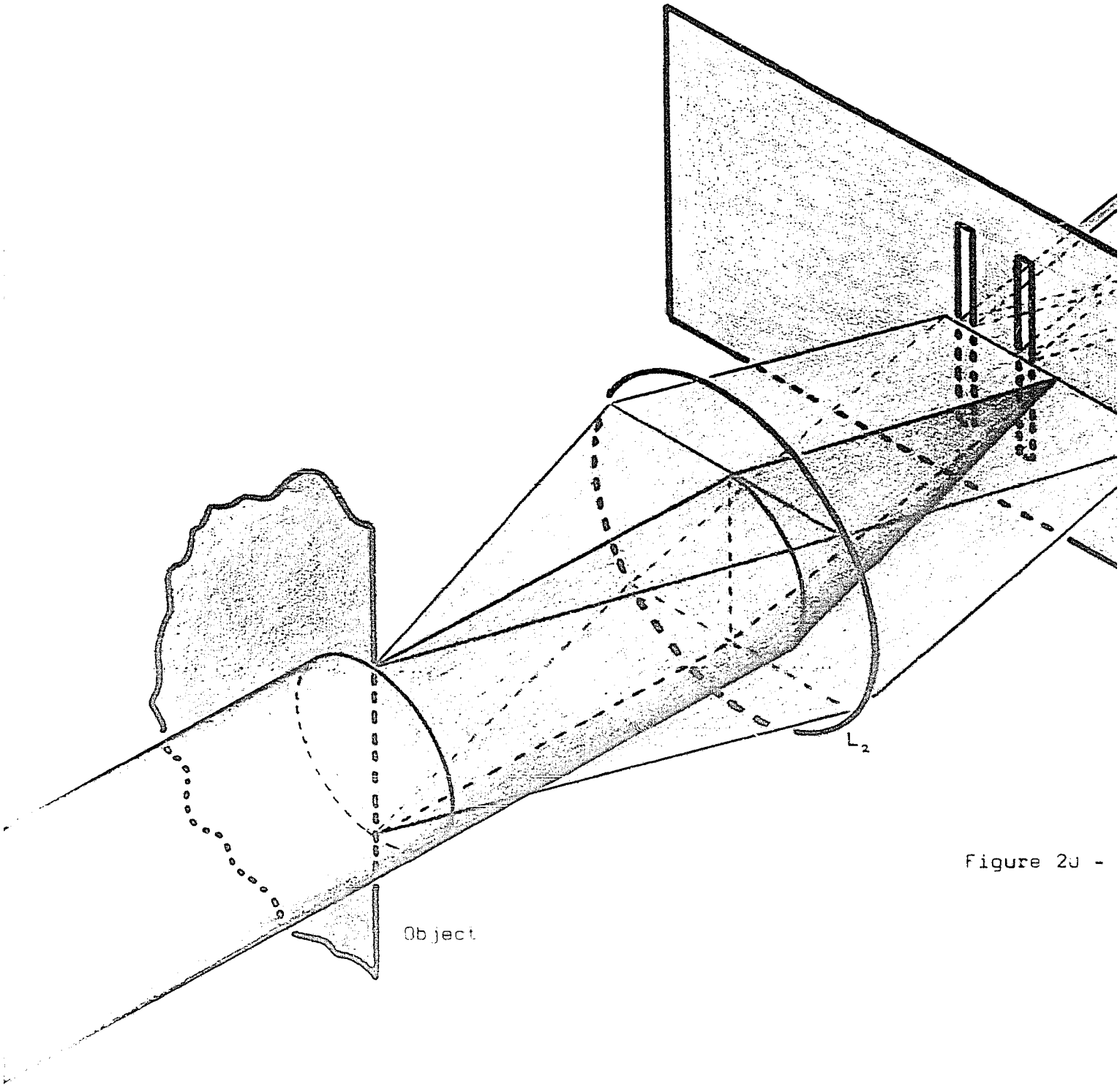

Figure 2J -

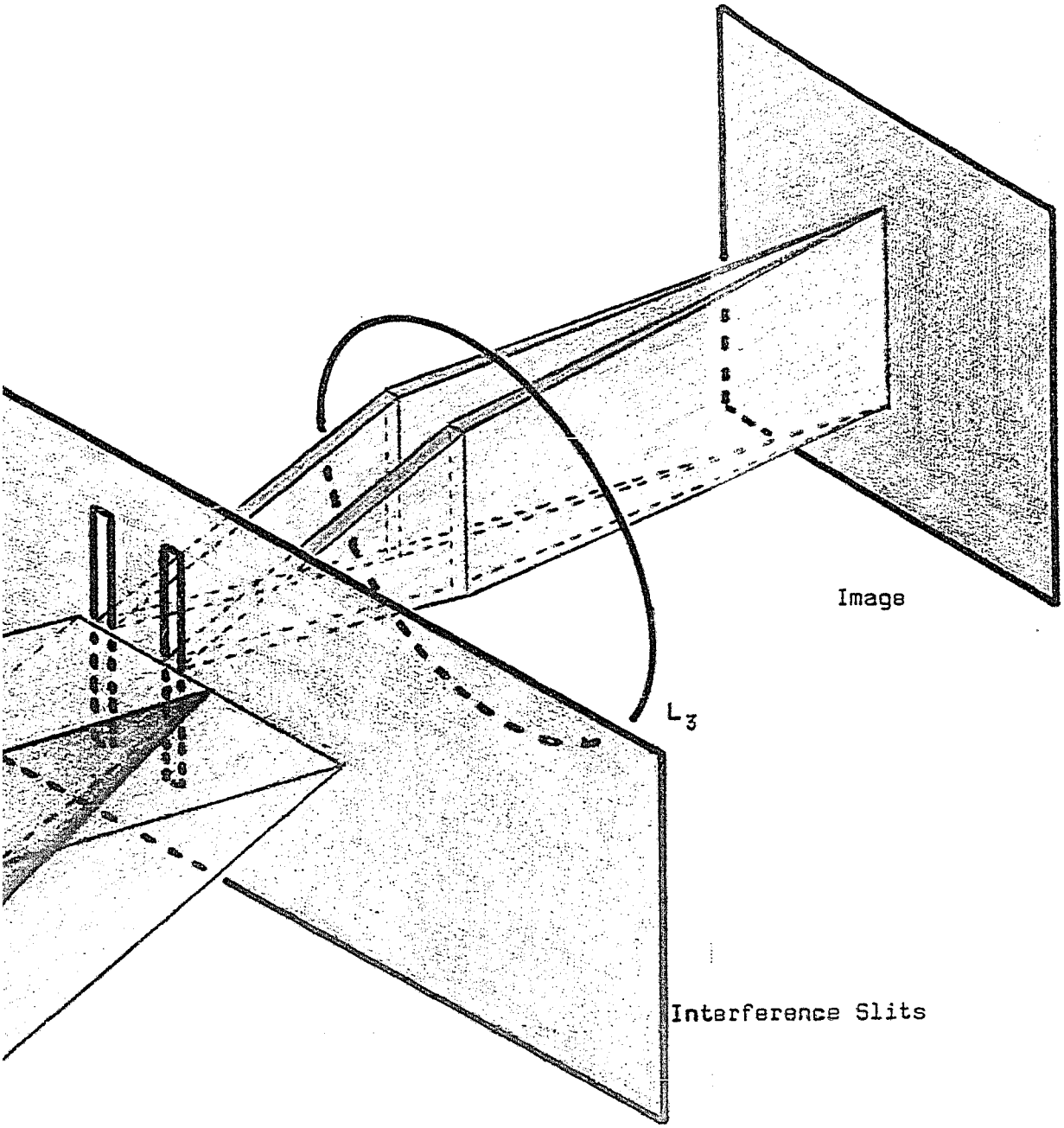

Figure 2J - A 3-dimensional view of the diffrimoscopic system with slits placed in the mask plane of the optic axis. Experiments were also performed with the slits on the left of the optic axis. From these arrangements it was shown that the phase is constant along each of the branches of the focal line.

Experimental Investigation of the Phase Distribution in the Mask Plane.

The phase distribution along the focal line was investigated with the use of slits as indicated in figures 19 and 20 (see pages 23 & 24). The relative phases of the two slits will determine the position of the interference fringes observed in the image plane. In one case the slits were positioned astride the optical axis as shown in figure 19. In another case the slits were both placed to one side of the optical axis as shown in figure 20. This last experiment was, of course, performed on each of the branches of the focal line. The effect of changing the distance between the slits was investigated as was the effect of changing the width of the slits themselves.

The result of performing this type of experiment with slits 200 microns wide and 1000 microns apart is shown in figure 21 (see page 26). The cross-hairs shown in this figure were located in the image plane when the system was operating in the normal diffrimoscopic manner, without the slits. The black central line of the diffrimoscopic image was chosen as the reference point when first positioning the cross-hairs. The top photograph shows the result of placing both slits on the left branch of the focal line. In this paper, right and left will refer to the two sides of the optical system as seen by an observer standing at the image plane and looking toward the light source. The middle photograph shows the result of placing the slits such that one slit was on each side of the optical axis. The bottom photograph shows the result obtained when both slits are on the right hand branch of the focal line. All these photographs show a regular two-slit interference pattern which is modulated by the diffraction pattern from the slits themselves. The top and bottom photographs show a central maximum indicating that the phases at the two slits are the same. The central photograph, however, shows a central minimum indicating that the phases at the two slits were in opposition. The negatives for these photographs were exposed in green monochromatic light (wavelength 5461 A). The same experiment was also performed with white light and it was most striking

(continued on page 29)

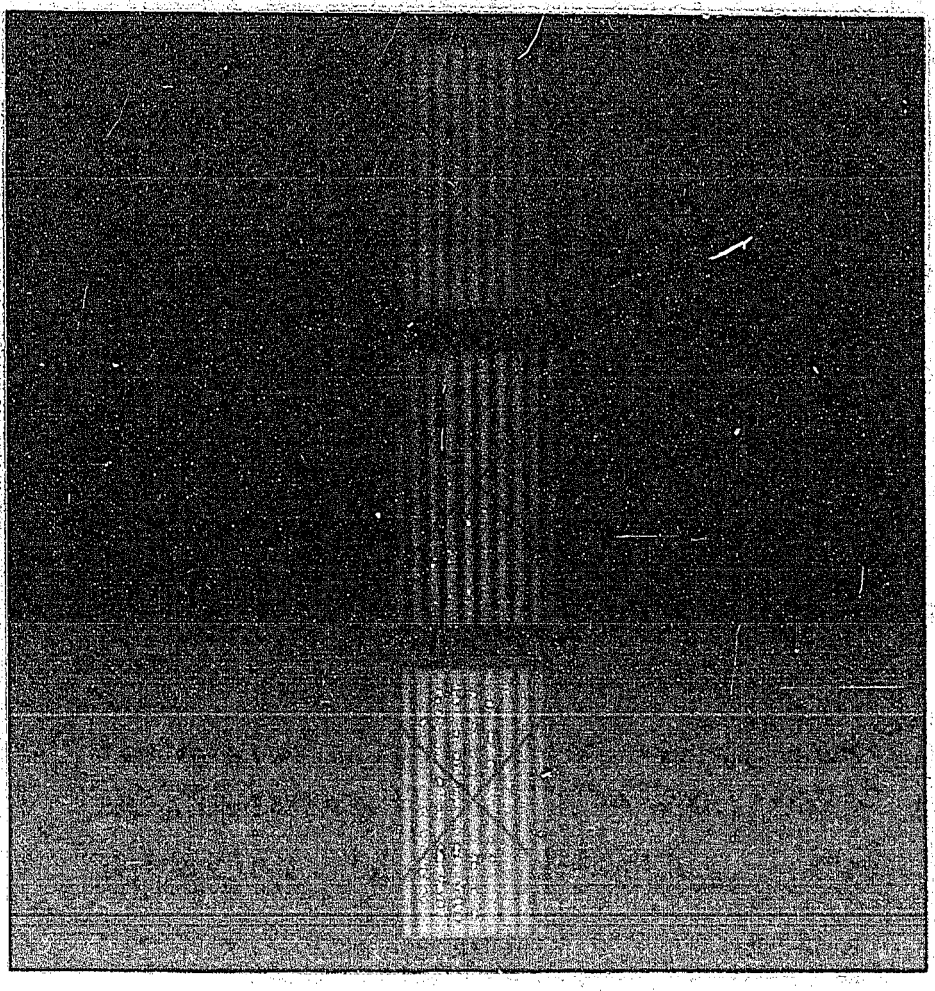

Figure 21 - A composite showing the interference patterns of two slits of width 200 microns separated by a strip 1000 microns wide. The cross-hairs in each photograph indicate the position of the central fringe. The top photograph shows the result of placing the two slits on the left branch of the focal line. The central fringe in this case is a maximum. The result is the same if the slits are placed on the right branch of the focal line as shown in the bottom photograph. The middle photograph, which shows a central dark fringe, is the result of an arrangement such that the slits are astride the optic axis (as shown in figure 19 on page 23).

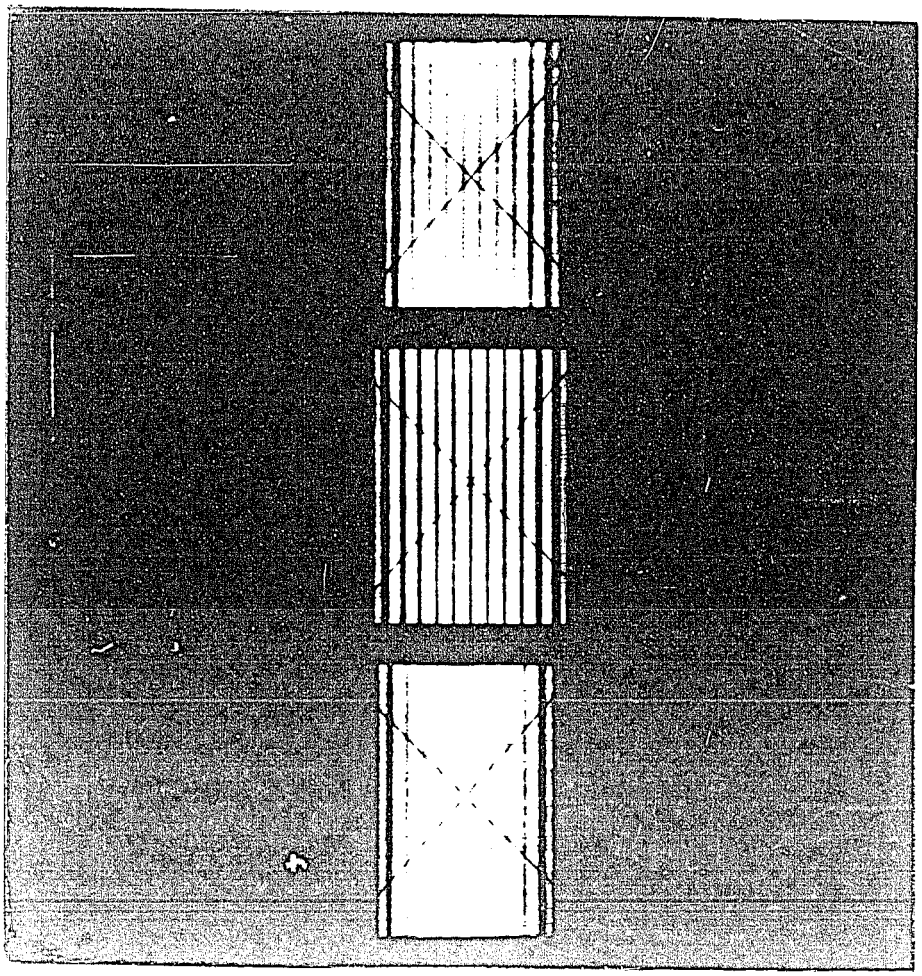

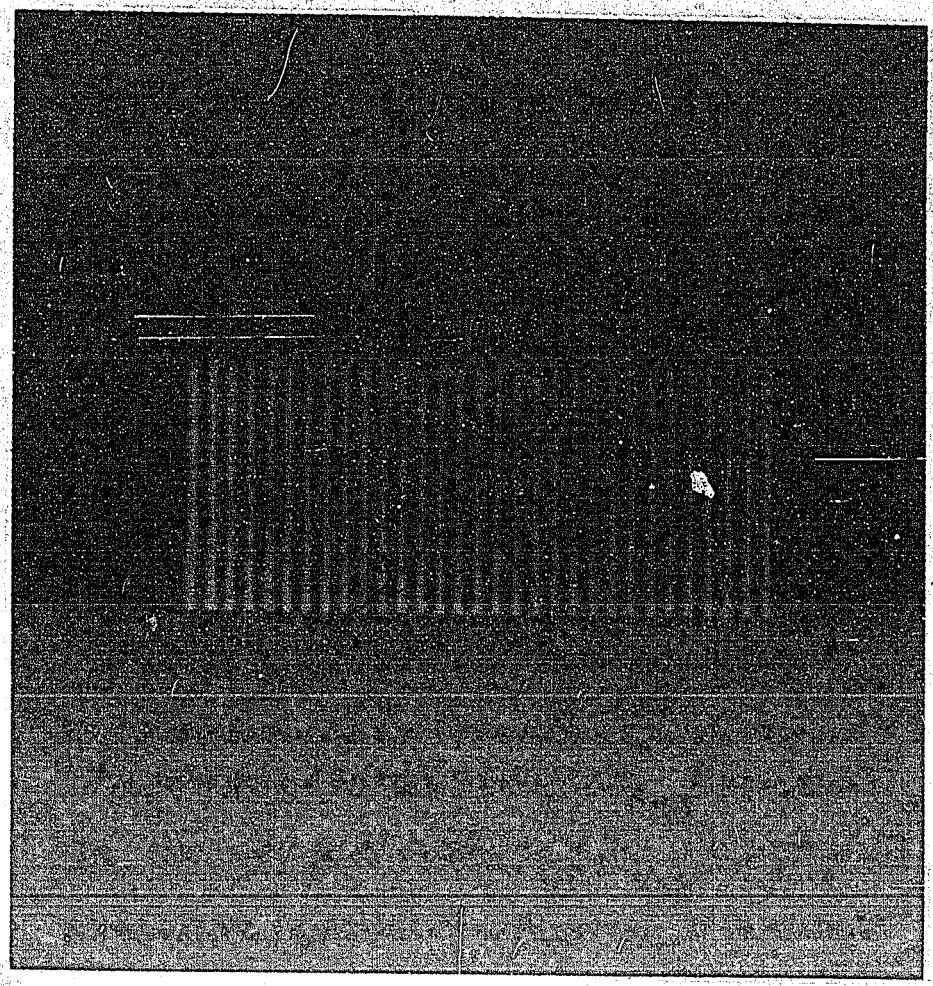

Figure 22 - A composite showing the interference patterns of two slits of width 20 microns separated by a strip 1000 microns wide. The arrangement of the photographs here is the same as in figure 21. The central fringes were aligned to form a vertical straight line. The diffraction fringes which modulated the previous patterns are no longer in the field of view.

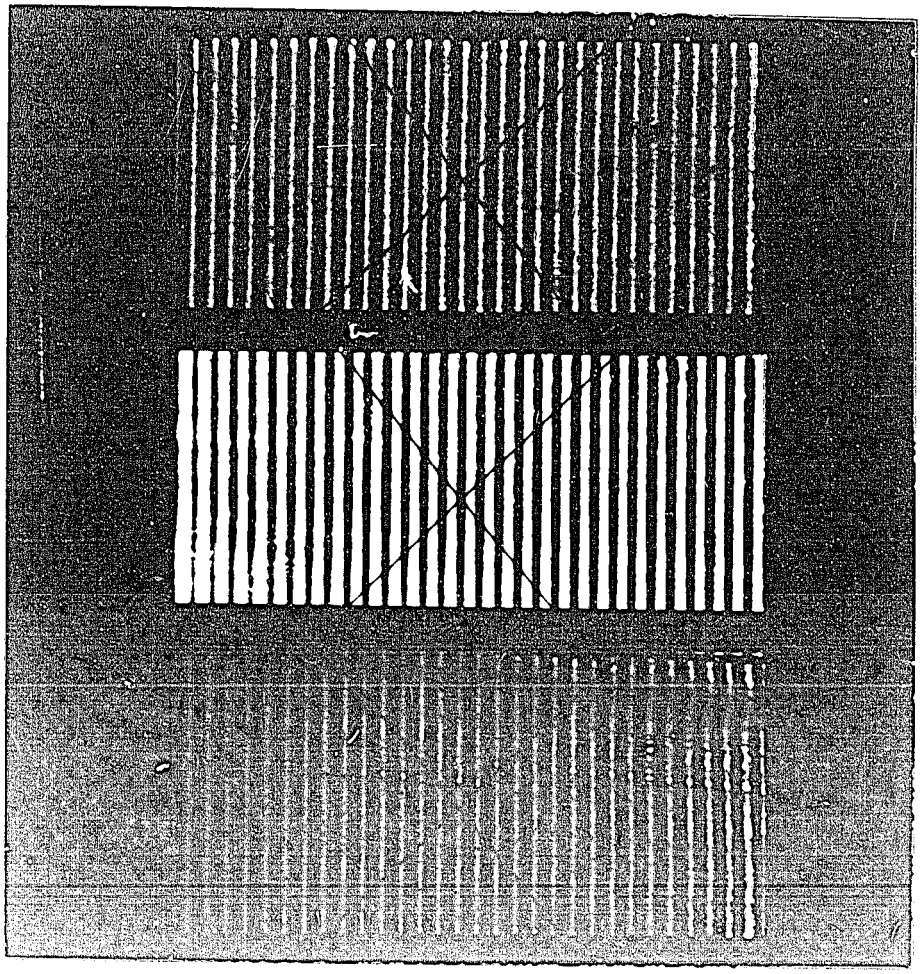

[illegible] photograph here is the same as [illegible]
[illegible] fringes were aligned to form a [illegible]
[illegible] the diffraction fringes which [illegible]
[illegible] ons are no longer in the field [illegible]

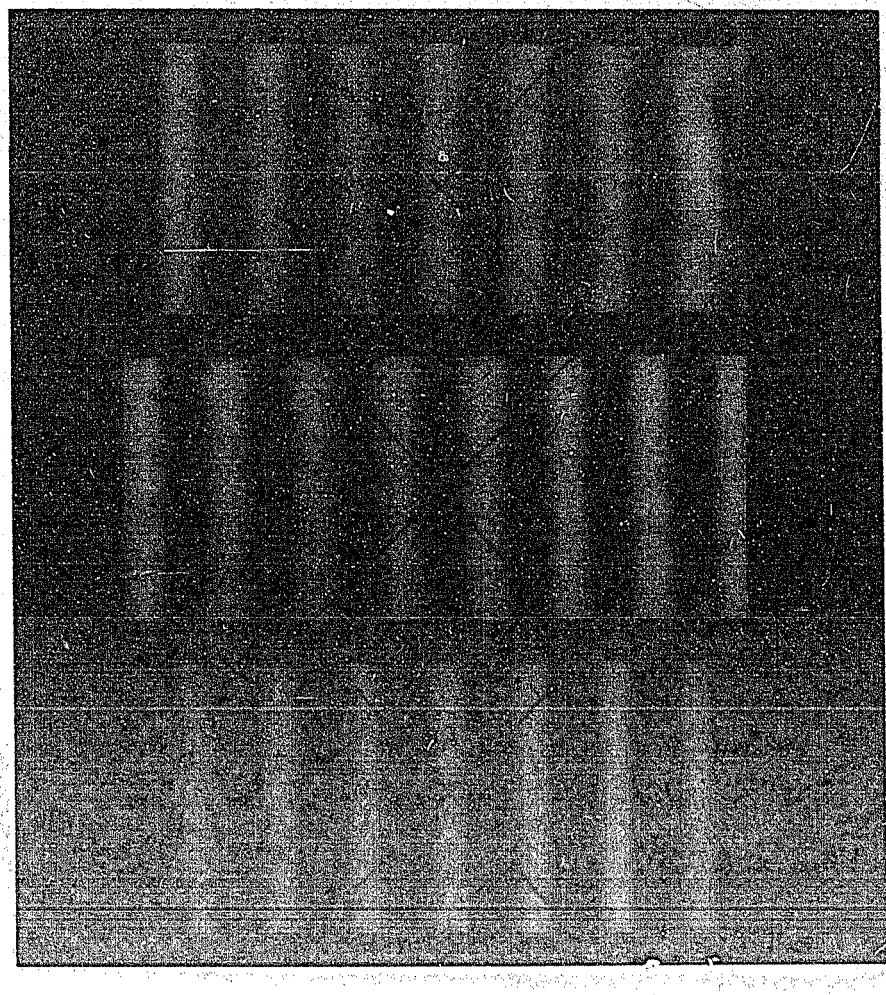

Figure 23 - A composite showing the interference patterns of two slits of width 20 microns separated by a strip 200 microns wide. Again, the arrangements of the photographs is the same as in figure 21.

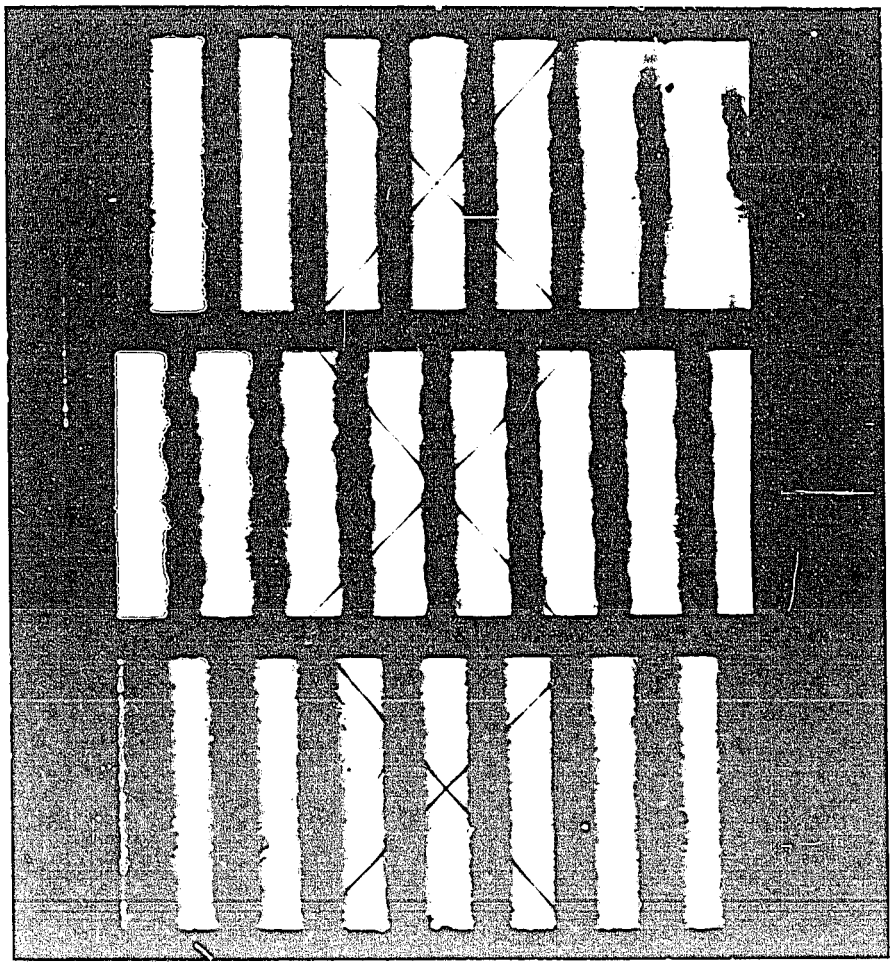

[illegible] interference patterns of two [illegible] separated by a strip 20J [illegible], the arrangements of the photo- [illegible] as in figure 21.

that the central fringe in each case was the only fringe which was achromatic.

Figure 22 (see page 27) shows the results of performing the same type of experiments but with the slits reduced to 20 microns in width while their separation remained at 1000 microns. As was to be expected the diffraction minima which modulated the previous patterns have spread further apart and are no longer in the field of view. The arrangement of the photographs corresponds exactly to the arrangement described for figure 21. The results here are the same as those in figure 21, that is, a bright central fringe being observed in the top and bottom photographs while a dark fringe is present at the center of the middle photograph.

In figure 23 (see page 28) the result of reducing the slits separation to 200 microns while keeping the slit widths at 20 microns is shown. Again the arrangement of the photographs is the same as that in figure 21. In this case the interference fringes themselves have broadened but the result of the experiment has remained unchanged.

Another experiment was performed with slits 200 microns wide and 1000 microns apart. In this case the slits were slowly moved from the left to the right side while an observer looked at the phenomenon through an ocular. While the slits were being moved along the left-hand branch of the focal line no change was noticed in the positions of the interference fringes. The luminosity of the fringes did change and the reason for this will become apparent in the next section. An abrupt change occured when the slits were moved far enough to the right that one slit was on each branch of the focal line. When the slits themselves cross the optic axis, it must be remembered that nothing is left to obstruct the direct incident light and the field of view for the observer is momentarily flooded with too much light. This however, is not the abrupt change which is mentioned above. The change which was observed is the same change recorded in the top and middle photographs in figure 21. As the

slits continued to move to the right no further change occured until the left-hand slit crossed the optic axis. With both slits moving along the right-hand branch of the focal line no further change in the positions of the fringes was observed.

The results of these experiments suggest that the phases in the two branches of the focal line are in opposition and that the phase along any one branch of the focal line is constant. These results will be used in the theory which will be developed later.

Experimental Investigation of the Intensity Distribution in the Mask Plane.

A photomultiplier tube was attached to a moving carriage in the mask plane. Its axis of motion was set perpendicular to both the optic axis and to the object edge. The light entered the photomultiplier tube through a slit mounted parallel to the object edge. The width of the slit was 10 microns. The carriage was adjusted so that the focal line was sharply focussed in the plane of the slit.

A second photomultiplier probe was arranged so that it measured the luminosity of the incident undiffracted beam. The output of these two probes was then fed into an electronic circuit which produced a value for the ratio of these two outputs. This arrangement was used in order that any fluctuations of the light source would not affect the readings.

The luminosity (more correctly a relative luminosity) along the focal line was recorded in 100 micron steps for a total distance of 15 millimeters.

Figure 24 (see page 32) shows the curve obtained when making such a scanning of the focal line. The numerical data is listed on the following page.

The two graphs on pages 34 and 35 show the plots which were made of log $|M(y_i)|^2$ versus the logarithm of the distance from the center of distribution along each of the two branches of the focal line. The slopes of these two lines indicate that $|M(y_i)|^2$ is proportional to y_i^{-2} along each branch.

In the case when no object is present in the object plane the complex amplitude in the mask plane is represented by:

$$M_{(y_1,y_2)} = \int_{-1}^{+1} \int_{-\sqrt{1-x_1^2}}^{\sqrt{1-x_1^2}} D(x_1,x_2) \cdot e^{-i2\pi(x_1y_1 + x_2y_2)}\, dx_1\, dx_2 \qquad (15)$$

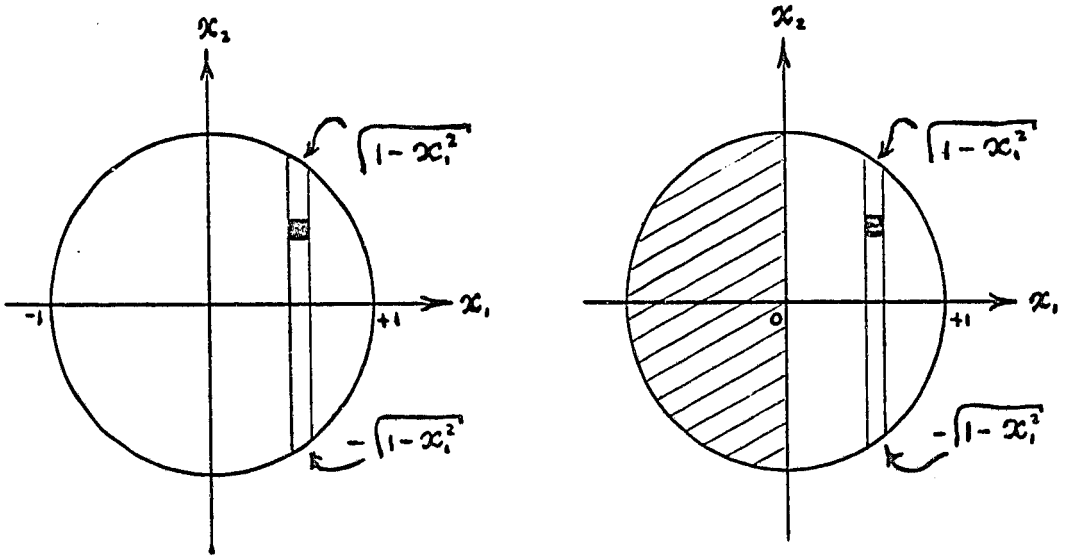

object absent object present

In the case of a uniformly transparent and uniformly illuminated pupil $D(x_1,x_2) = 1$.

$$\therefore\ M_{(y_1,0)} = \int_{-1}^{+1} e^{-i2\pi x_1 y_1}\, dx_1 \int_{-\sqrt{1-x_1^2}}^{\sqrt{1-x_1^2}} dx_2$$

$$= 2\int_{-1}^{+1} \sqrt{1-x_1^2} \cdot e^{-i2\pi x_1 y_1}\, dx_1 \qquad (16)$$

(continued on page 36)

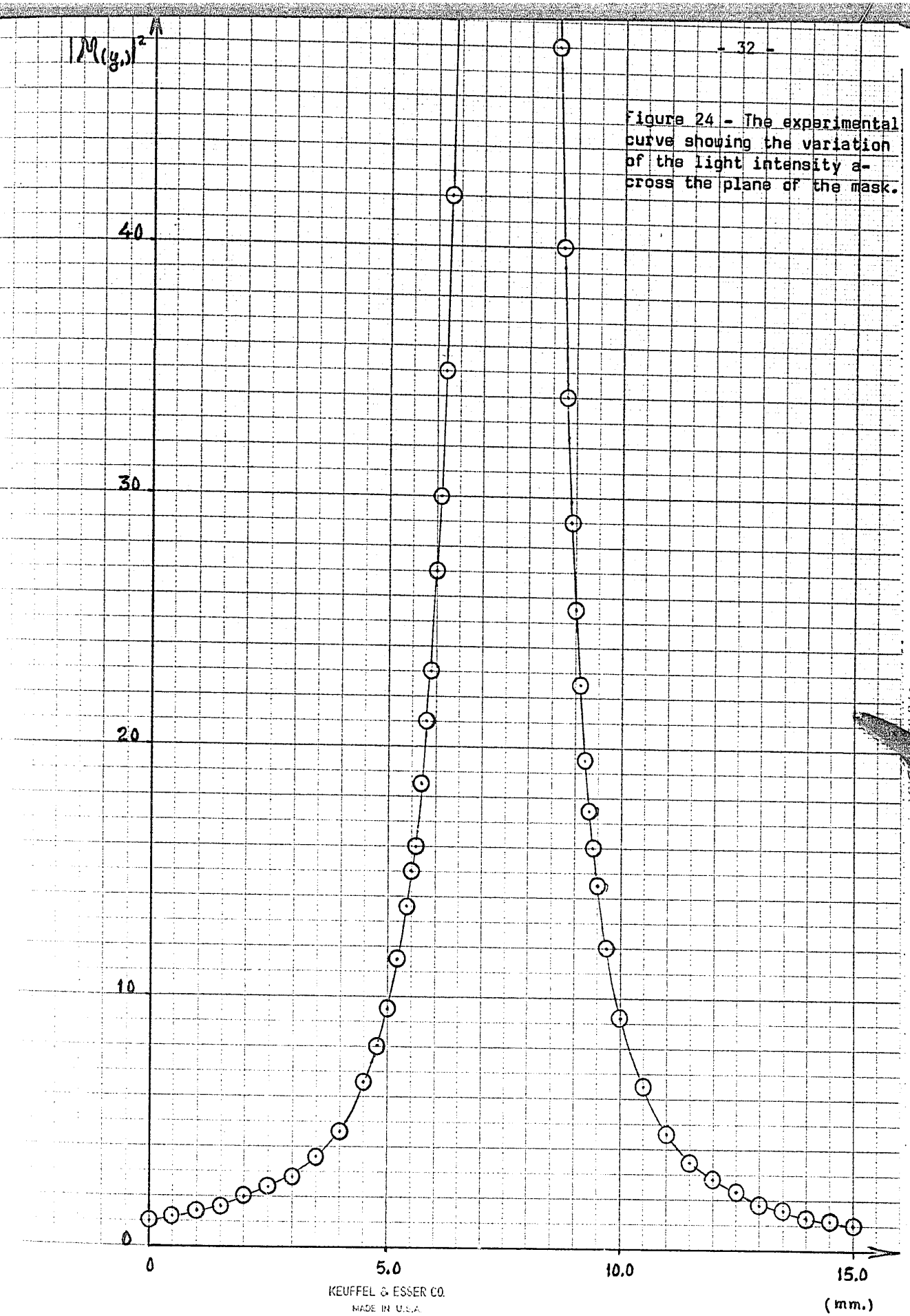

Figure 24 - The experimental curve showing the variation of the light intensity across the plane of the mask.

Scanning of the Focal Line

Distance (mm)	Ratio A/B	Distance (mm)	Ratio A/B	Distance (mm)	Ratio A/B
0	1.05	5.0	.95 x10	10.0	.92 x10
.1	1.07	5.1	1.05 x10	10.1	.85 x10
.2	1.10	5.2	1.15 x10	10.2	.81 x10
.3	1.15	5.3	1.25 x10	10.3	.74 x10
.4	1.17	5.4	1.37 x10	10.4	.69 x10
.5	1.23	5.5	1.50 x10	10.5	.65 x10
.6	1.27	5.6	1.60 x10	10.6	.61 x10
.7	1.30	5.7	1.85 x10	10.7	.57 x10
.8	1.35	5.8	2.1 x10	10.8	.53 x10
.9	1.38	5.9	2.3 x10	10.9	.50 x10
1.0	1.42	6.0	2.7 x10	11.0	.46 x10
1.1	1.47	6.1	3.0 x10	11.1	.44 x10
1.2	1.53	6.2	.35 $x10^2$	11.2	.415 x10
1.3	1.58	6.3	.42 $x10^2$	11.3	.39 x10
1.4	.16 x10	6.4	.51 $x10^2$	11.4	.37 x10
1.5	.16 x10	6.5	.63 $x10^2$	11.5	.35 x10
1.6	.165 x10	6.6	.76 $x10^2$	11.6	.33 x10
1.7	.175 x10	6.7	.96 $x10^2$	11.7	.31 x10
1.8	.180 x10	6.8	1.40 $x10^2$	11.8	.31 x10
1.9	.190 x10	6.9	2.00 $x10^2$	11.9	.295 x10
2.0	.20 x10	7.0	3.8 $x10^2$	12.0	.28 x10
2.1	.21 x10	7.1	.44 $x10^5$	12.1	.27 x10
2.2	.22 x10	7.2		12.2	.26 x10
2.3	.225 x10	7.3	.80 $x10^5$	12.3	.245 x10
2.4	.23 x10	7.4	.60 $x10^4$	12.4	.235 x10
2.5	.24 x10	7.5	.60 $x10^4$	12.5	.23 x10
2.6	.25 x10	7.6	4.0 $x10^4$	12.6	.22 x10
2.7	.25 x10	7.7	2.5 $x10^3$	12.7	.21 x10
2.8	.26 x10	7.8	.79 $x10^3$	12.8	.20 x10
2.9	.275 x10	7.9	.375 $x10^3$	12.9	1.95 $x10^0$
3.0	.28 x10	8.0	2.3 $x10^2$	13.0	1.85 $x10^0$
3.1	.30 x10	8.1	1.75 $x10^2$	13.1	1.80 $x10^0$
3.2	.31 x10	8.2	1.26 $x10^2$	13.2	1.75 $x10^0$
3.3	.325 x10	8.3	.91 $x10^2$	13.3	1.70 $x10^0$
3.4		8.4	.72 $x10^2$	13.4	1.65 $x10^0$
3.5	.36 x10	8.5	.58 $x10^2$	13.5	1.60 $x10^0$
3.6	.38 x10	8.6	.48 $x10^2$	13.6	1.55 $x10^0$
3.7	.39 x10	8.7	.40 $x10^2$	13.7	1.50 $x10^0$
3.8	.42 x10	8.8	.34 $x10^2$	13.8	1.425 $x10^0$
3.9	.44 x10	8.9	.29 $x10^2$	13.9	1.375 $x10^0$
4.0	.46 x10	9.0	.255 $x10^2$	14.0	1.35 $x10^0$
4.1	.48 x10	9.1	.225 $x10^2$	14.1	1.30 $x10^0$
4.2	.51 x10	9.2	1.95 x10	14.2	1.25 $x10^0$
4.3	.56 x10	9.3	1.75 x10	14.3	1.25 $x10^0$
4.4	.60 x10	9.4	1.60 x10	14.4	1.20 $x10^0$
4.5	.66 x10	9.5	1.45 x10	14.5	1.17 $x10^0$
4.6	.70 x10	9.6	1.35 x10	14.6	1.13 $x10^0$
4.7	.75 x10	9.7	1.20 x10	14.7	1.10 $x10^0$
4.8	.81 x10	9.8	1.10 x10	14.8	1.06 $x10^0$
4.9	.88 x10	9.9	1.00 x10	14.9	1.03 $x10^0$

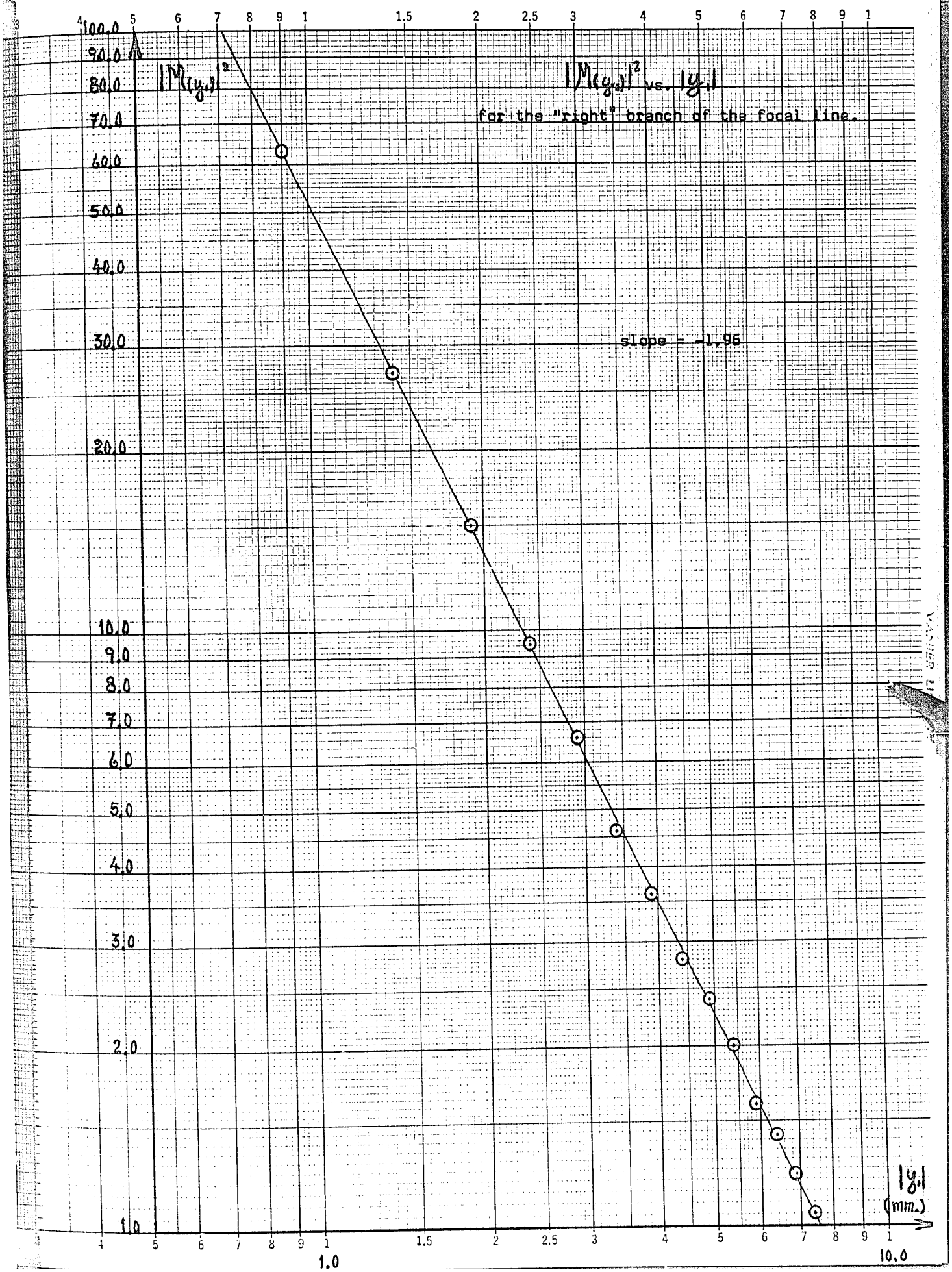
$|M(y_i)|^2$ vs. $|y_i|$
for the "right" branch of the focal line.
slope = -1.96
$|M(y_i)|^2$
$|y_i|$ (mm.)
100.0
90.0
80.0
70.0
60.0
50.0
40.0
30.0
20.0
10.0
9.0
8.0
7.0
6.0
5.0
4.0
3.0
2.0
1.0
1.0
10.0

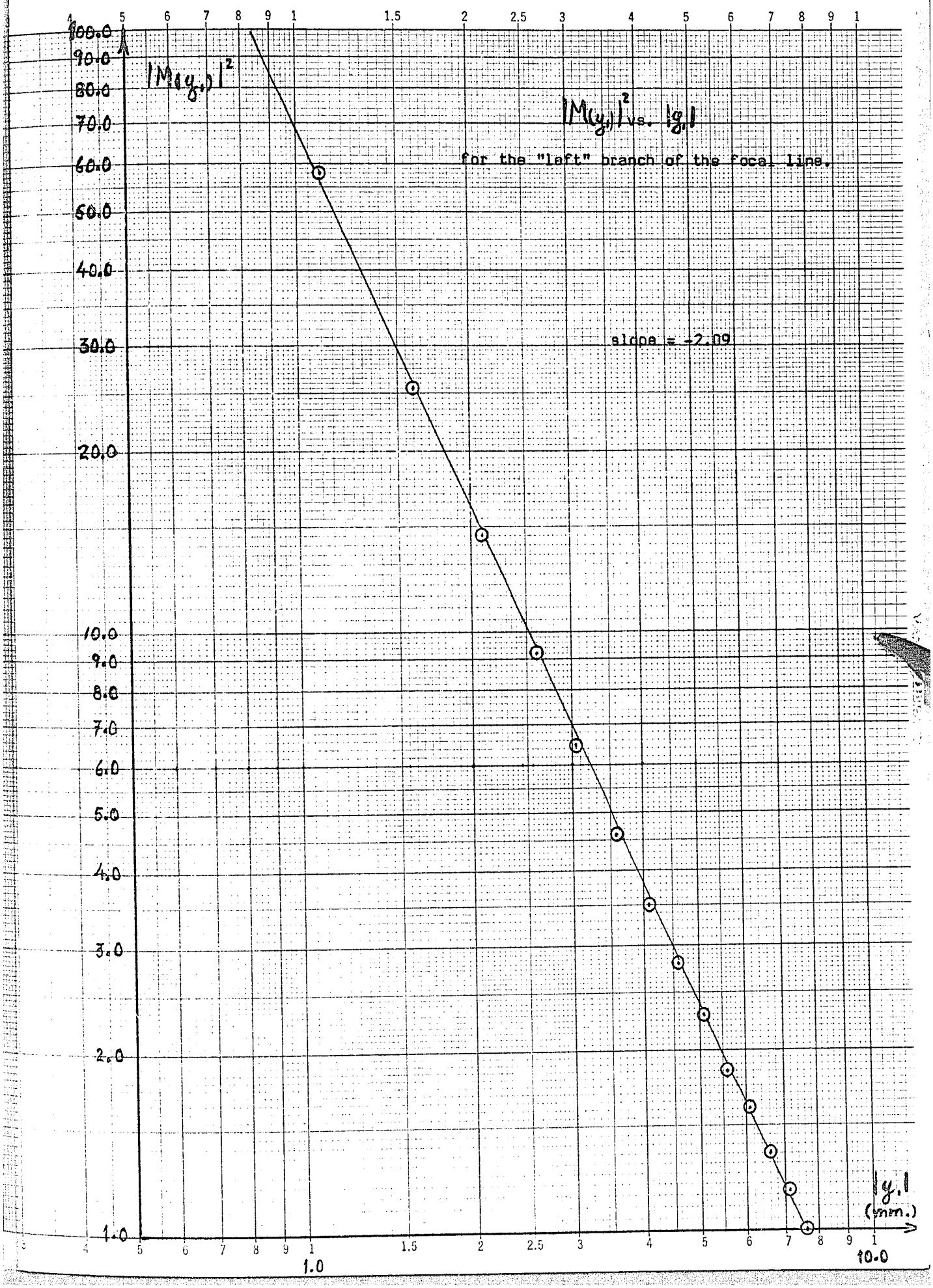
$|M(y_1)|^2$
$|M(y_1)|^2$ vs. $|y_1|$
for the "left" branch of the focal line.
slope = -2.09
100.0
90.0
80.0
70.0
60.0
50.0
40.0
30.0
20.0
10.0
9.0
8.0
7.0
6.0
5.0
4.0
3.0
2.0
1.0
1.0
10.0
$|y_1|$ (mm.)

$$\therefore M(y_1,0) = 2\int_{-1}^{+1} \sqrt{1-x_1^2}\,\cos(2\pi x_1 y_1)\,dx_1 \qquad (17)$$

$$\text{or } M(y_1,0) = 4\int_{0}^{1} \sqrt{1-x_1^2}\,\cos(2\pi x_1 y_1)\,dx_1 \qquad (18)$$

$$\therefore M(y_1,0) = \frac{J_1(2\pi y_1)}{y_1} \qquad (19)$$

where $J_1(2\pi y_1)$ is the first order Bessel function.

For large values of y_1 it is known * that $J_1(2\pi y_1)$ varies as $1/y_1^{1/2}$. Thus it is seen $M(y_1,0)$ is proportional to $y^{-3/2}$ in this region.

The presence of the object edge in the pupil changes the expression for $M(y_1,0)$ as follows:

$$M(y_1,0) = \int_0^1 e^{-i2\pi x_1 y_1}\,dx_1 \int_{-\sqrt{1-x_1^2}}^{\sqrt{1-x_1^2}} dx_2$$

$$= 2\int_0^1 \sqrt{1-x_1^2}\; e^{-i2\pi x_1 y_1}\,dx_1$$

$$= 2\int_0^1 \sqrt{1-x_1^2}\,\cos(2\pi x_1 y_1)\,dx_1 - 2i\int_0^1 \sqrt{1-x_1^2}\,\sin(2\pi x_1 y_1)\,dx_1 \qquad (20)$$

* See page 132 of "La Theorie des Fonctions de Bessel" (Centre National de Recherche Scientifique). 1955

It has already been shown that the first integral is proportional to $y_1^{-3/2}$.

The second integral in equation 20 may be found in Watson* as:

$$H_1(2\pi y_1) = \frac{2(\frac{1}{2}2\pi y_1)}{\Gamma(3/2)\,\Gamma(1/2)} \cdot \int_0^1 (1-x_1^2)^{1/2} \cdot \sin(2\pi y_1 x_1)\, dx_1 \qquad (21)$$

where $H_1(2\pi y_1)$ is Struve's function of order 1,

and $\Gamma(1+a) = a!$ is known as the "factorial function".

Jahnke-Emde** give the values of $\Gamma(3/2)$ and $\Gamma(1/2)$ as $\sqrt{\pi}/2$ and $\sqrt{\pi}$ respectively. Thus it is seen that

$$\int_0^1 (1-x_1^2)^{1/2} \cdot \sin(2\pi x_1 y_1)\, dx_1 = \frac{H_1(2\pi y_1)}{4y_1} \qquad (22)$$

Watson*** quotes an asymptotic expansion for $H_1(2\pi y_1)$ when $2\pi y_1$ is large.

$$H_1(2\pi y_1) \simeq Y_1(2\pi y_1) + \frac{1}{\pi}\frac{\Gamma(1/2)}{\Gamma(3/2)} + \cdots$$

$$\simeq Y_1(2\pi y_1) + \frac{2}{\pi} + \cdots \qquad (23)$$

In the same volume, on page 199, may be found an asymptotic expansion for $Y_1(2\pi y_1)$. Consequently, for large values of $2\pi y_1$, it is seen that $H_1(2\pi y_1) \simeq 2/\pi$.

Thus

$$\int_0^1 (1-x_1^2)^{1/2} \cdot \sin(2\pi y_1 x_1)\, dx_1 \simeq 1/2\pi y_1 \qquad (24)$$

The second integral in equation 20 thus varies as $(2\pi y_1)^{-1}$.

---

* Watson, G.N., A treatise on the Theory of Bessel Functions, Camb. Univ. Press (1962) p. 328, equation 1.

** Jahnke E., Emde, F., Tables of Functions - Dover (1945) p.11.

*** Watson, G.N., p. 333, equation 2.

The expression for the intensity in the plane of the mask is

$$|M(y_1,0)|^2 = 4\left[\int_0^1 (1-x_1^2)^{1/2}\cdot\cos(2\pi x_1 y_1)\,dx_1\right]^2 + 4\left[\int_0^1 (1-x_1^2)^{1/2}\cdot\sin(2\pi x_1 y_1)\,dx_1\right]^2 \quad (25)$$

But

$$\left[\int_0^1 (1-x_1^2)^{1/2}\cdot\cos(2\pi x_1 y_1)\,dx_1\right]^2 \propto 1/y_1^3$$

And

$$\left[\int_0^1 (1-x_1^2)^{1/2}\cdot\sin(2\pi x_1 y_1)\,dx_1\right]^2 \propto 1/y_1^2$$

It is seen that the first term in equation 25 varies much more rapidly with y_1 than does the second term. Consequently, in the regions of large $|y_1|$, the intensity in the plane of the mask will be adequately represented by the second term of the equation.

The first term of equation 25 is the representation of that part of the intensity which is blocked by the mask.

It is seen that the $1/y^2$ variation of the second term confirms the power law found in the scanning performed with the probes. This term is the square of the integral of an odd function. This prediction that the branches of the focal line are represented by an odd function of y_1 is also in agreement with the results of the phase scanning mentioned earlier.

The theoretical calculations indicated above are well known and were presented here with the object of providing a convenient basis for the discussion of the experimental data.

The following treatment is due to Prof. Lansraux. It provides an expression for $C(z_1)$, the complex amplitude in the image plane. A system of infinite aperture (integration carried over the domain $-\infty \to +\infty$) will be dealt with first, and then the case of the finite aperture will be discussed.

a) Infinite Aperture.

The complex amplitude in the image plane is given by:

$$C(z_1) = \int_{-\infty}^{\infty} M(y_1)\, e^{-i\,2\pi y_1 z_1}\, dy_1$$

$$C(z_1) = \int_{-\infty}^{\infty} \left[-2i \int_0^1 (1-x_1^2)^{1/2} \cdot \sin(2\pi x_1 y_1)\, dy_1 \right] e^{-i 2\pi y_1 z_1}\, dy_1$$

$$= \int_{-\infty}^{\infty} \left[-2i \cdot \frac{1}{2\pi y_1} \right] e^{-i 2\pi y_1 z_1}\, dy_1$$

$$= \int_{-\infty}^{\infty} \left[-2i \cdot \frac{1}{2\pi y_1} \right] \cdot \left[-i \sin(2\pi y_1 z_1) \right] dy_1$$

$$= Cst. \int_{-\infty}^{\infty} \frac{\sin(2\pi y_1 z_1)}{2\pi y_1}\, dy_1 \qquad (26)$$

Let $2\pi y_1 z_1 = t \qquad y_1 = \frac{t}{2\pi z_1} \qquad dy_1 = \frac{dt}{2\pi z_1}$ (27)

$$C(z_1) = 2\, Cst. \int_{+\epsilon}^{\infty} \frac{\sin(2\pi y_1 z_1)}{2\pi y_1}\, dy_1$$

$$= \pm 2\, Cst. \int_{2\pi|z_1|\epsilon}^{\infty} |z_1| \cdot \frac{\sin t}{t} \cdot \frac{dt}{2\pi|z_1|} \qquad \text{for } z_1 \gtrless 0$$

$$= \pm \frac{Cst.}{\pi} \int_{2\pi|z_1|\epsilon}^{\infty} \frac{\sin t}{t} \cdot dt$$

$$= \pm \frac{Cst.}{\pi} \left[\int_0^{\infty} \frac{\sin t}{t} \cdot dt - \int_0^{2\pi|z_1|\epsilon} \frac{\sin t}{t} \cdot dt \right]$$

$$= \pm \frac{Cst.}{\pi} \left[\frac{\pi}{2} - Si(2\pi|z_1|\epsilon) \right] \qquad (28)$$

The function $C(z_1)$ for both positive and negative values of z_1 is shown in figures 27 and 28 on pages 41 and 42 respectively. The curve of $Si(2\pi\epsilon z_1)$ was found in Jahnke-Emde*.

Figure 28 is a composite of the curve $C(z_1)$ and a diffrimoscopic image. It is seen that the theoretical curve represents reasonably well the distribution of light formed in the image plane. This figure also shows that $C(z_1)$ is an odd function of z_1, that is, that the two branches of the complex amplitude curve are out of phase. There is a particularly good agreement between the predicted broad minima and those found in practice. Furthermore, it is seen that the curve $C(z_1)$ represented in figure 27 crosses the $2\pi\epsilon z_1$ axis at some value of the argument, say, $2\pi\epsilon z_1 = p$. It is seen immediately that the position z_1 of the lateral fringes is linked directly to the width 2ϵ of the mask.

This leads immediately to an explanation of the phenomenon known as "ultramicroscopy". Ultramicroscopic images of a pin are shown in figure 29 (see page 43) which shows the transition between diffrimoscopy and ultramicroscopy. As the diameter of the masks is reduced the interior of the pin becomes the luminous area whereas a classical system would present the interior of the pin as a dark zone surrounded by a bright background.

The next figure shows a schematic figure of the curve presented on page 41. The shaded areas have been marked with plus and minus signs according to whether the amplitude of the $C(z_1)$ curve is positive or negative in this region. It shall be assumed at present that the amplitude is positive on the shadow side of the object edge.

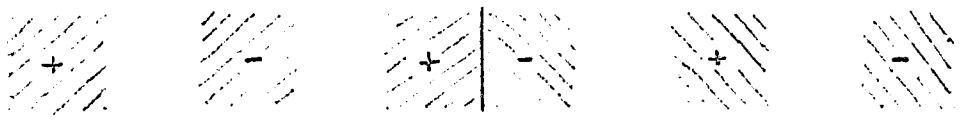

* Jahnke-Emde - "Tables of Functions" (Dover) - 1954 - p.1.

(continued on page 44)

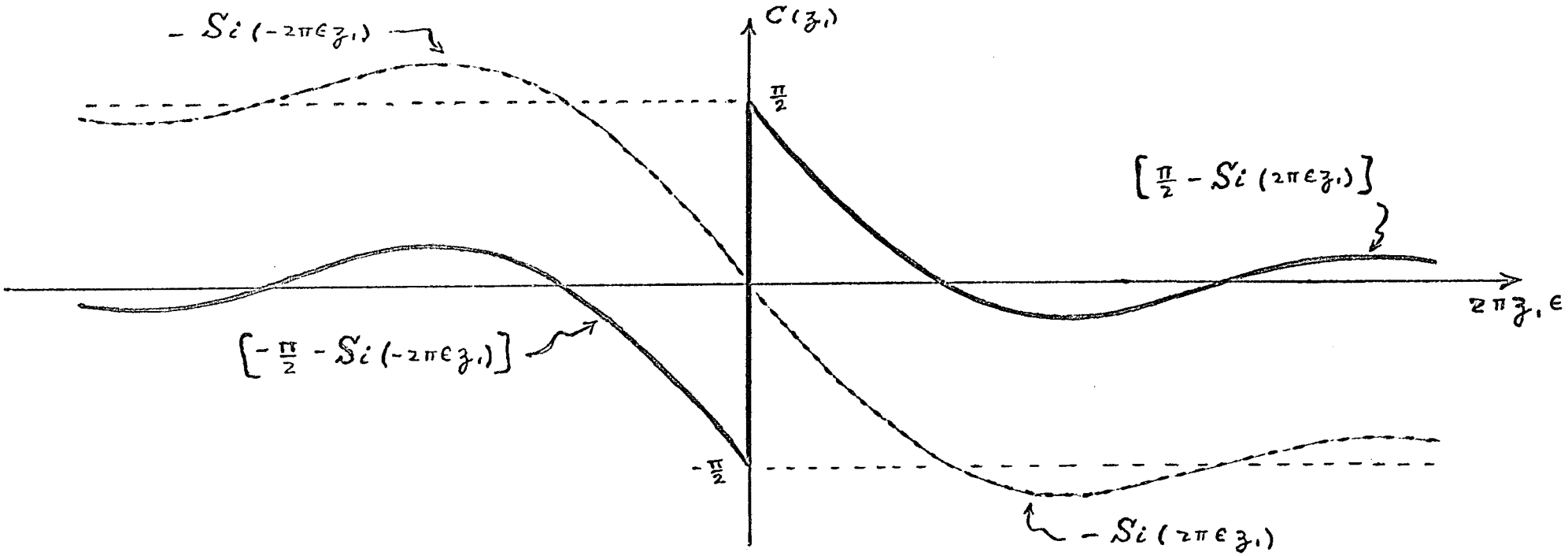

Figure 27 - A graph (heavy line) showing the complex amplitude distribution $C(z_1)$ in the image plane. This represents approximately the theoretically predicted distribution when a half-plane bounded by a straight edge is used as object. The two other curves (dotted lines) show the functional variation of $-Si(2\pi\epsilon z_1)$ and $-Si(-2\pi\epsilon z_1)$. These curves oscillate about $-\pi/2$ and $\pi/2$ respectively.

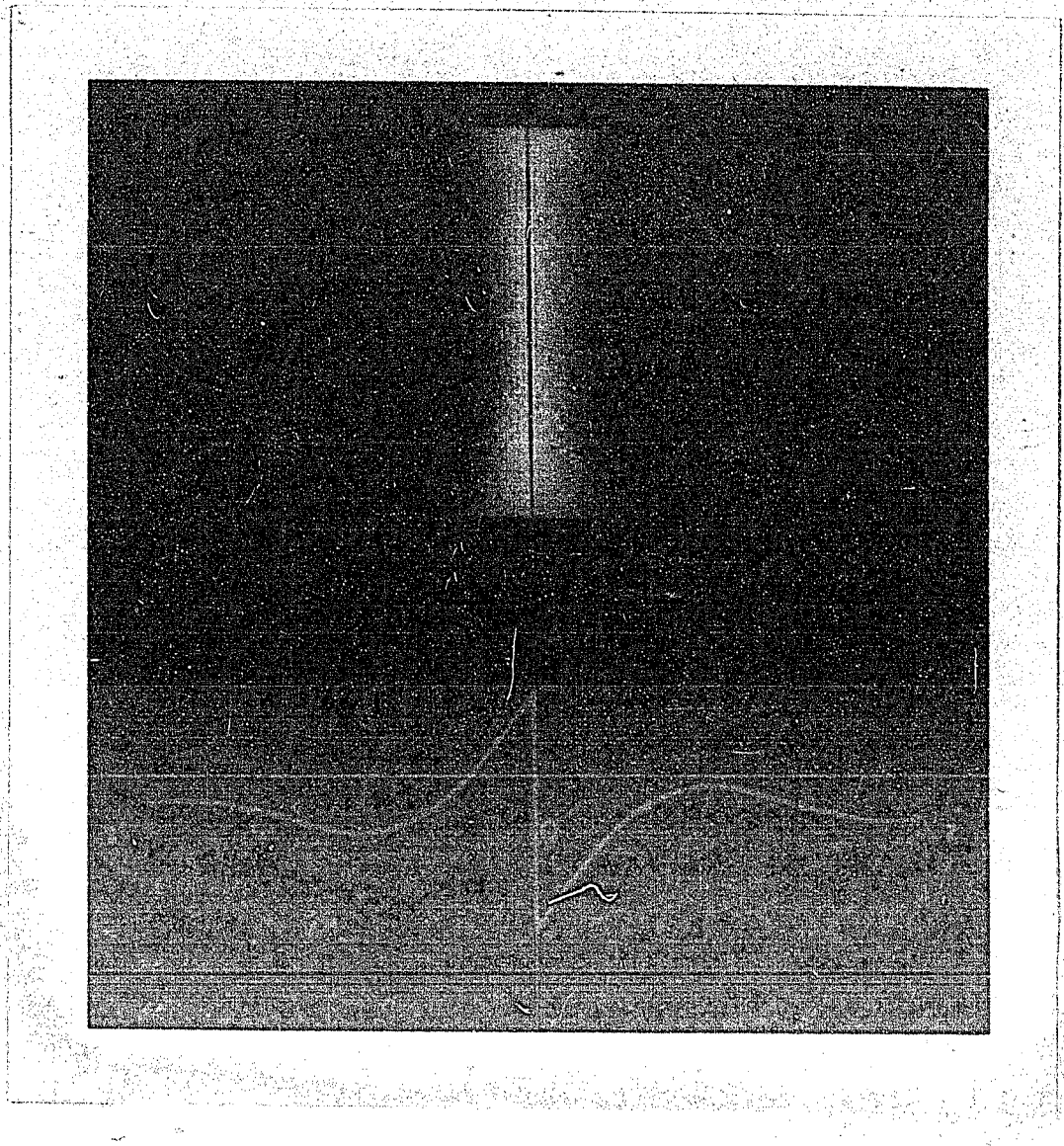

Figure 28 - A composite of the complex amplitude and the diffrimoscopic image. The positions of the minima in the two figures were made to correspond to each other.

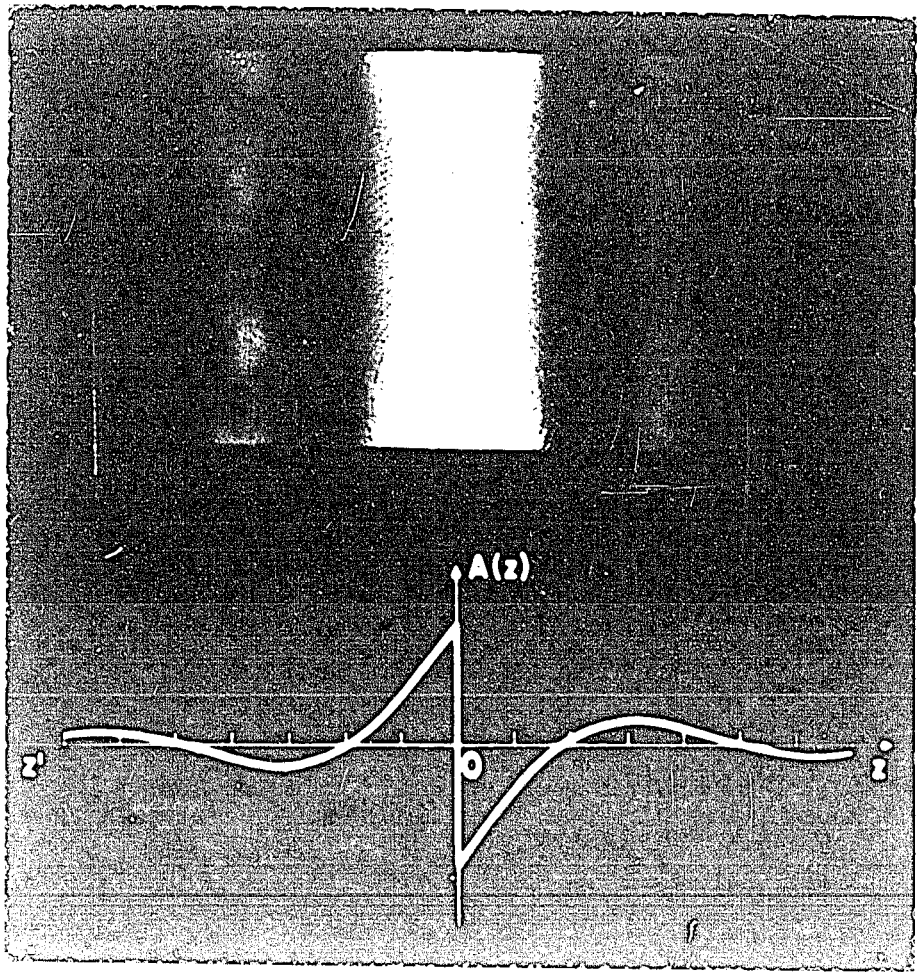
A(z)
z'
0
z

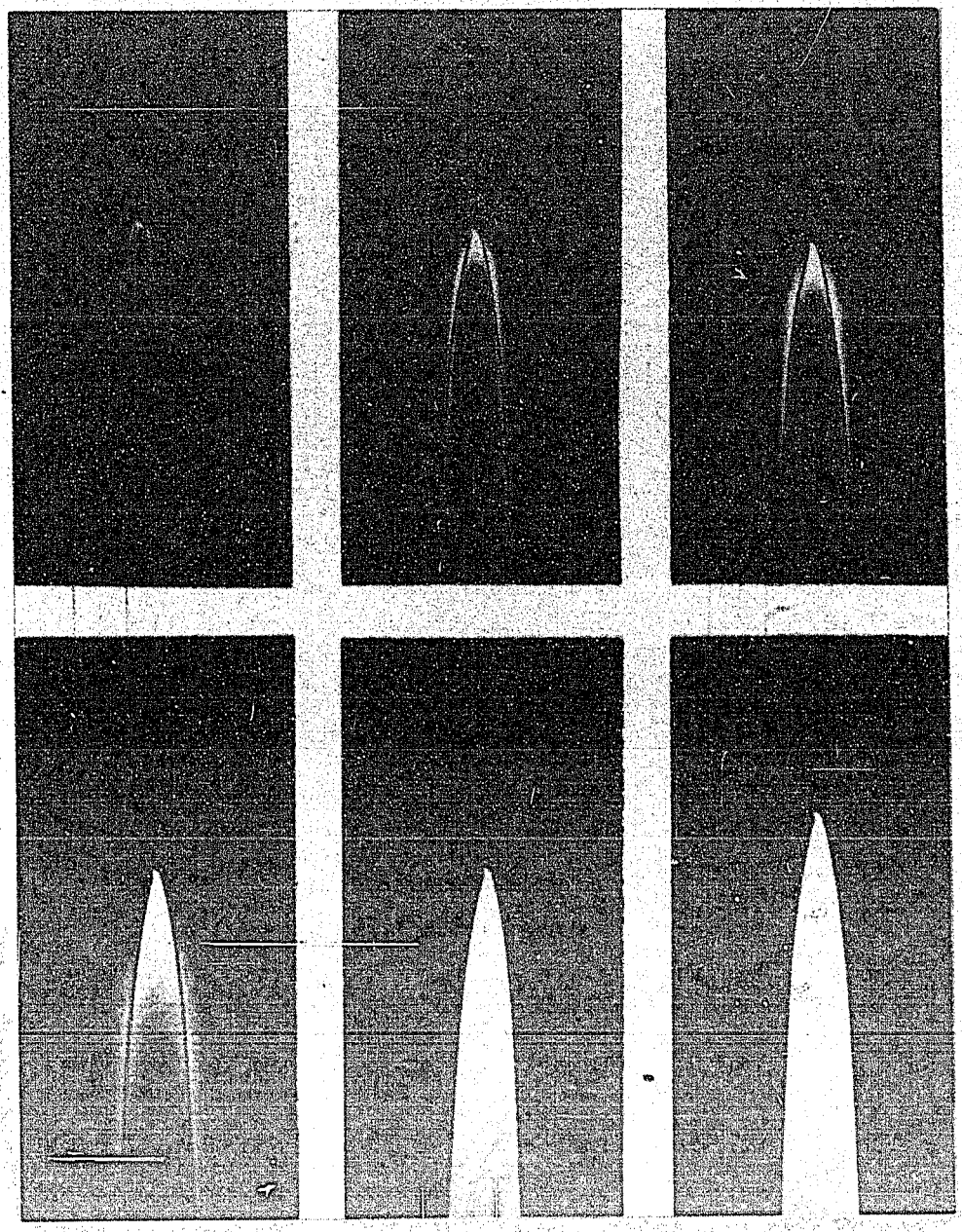

Figure 29 - A composite of images of a needle point showing the transition from diffrimoscopy to ultramicroscopy. Starting at the top left the mask diameters are 8mm, 4mm, 2mm, 1mm, 0.6mm and 0.3mm respectively. Since the object in this case does not present a straight edge, a circular mask mounted on the surface of a lens had to be used.

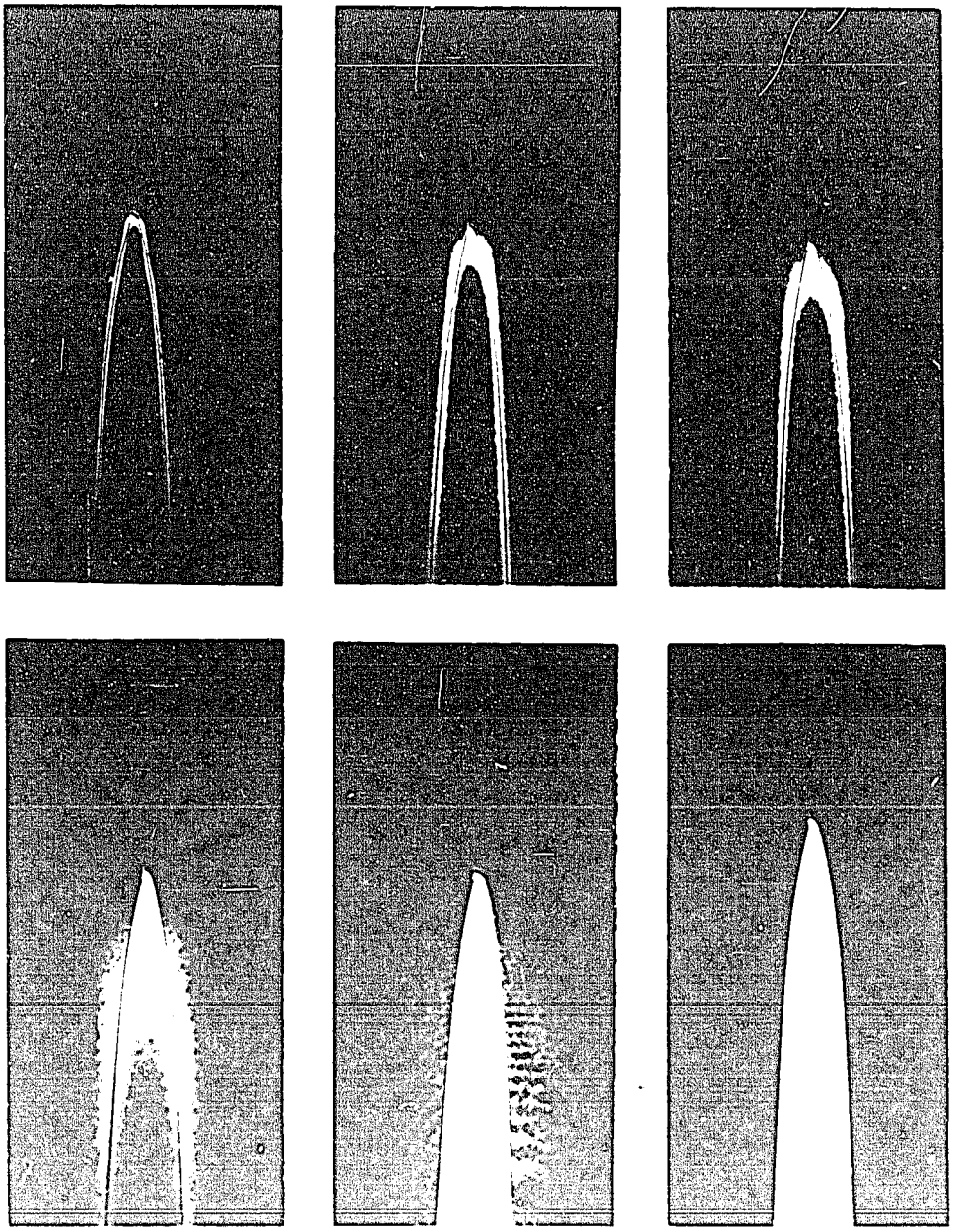

The next figure shows the effect (see figure 9 on page 10) that a narrowing of the mask has on the amplitude distribution in the image plane. The luminous areas immediately adjacent to the central minimum are broadened, in this case, to fill the entire field of view.

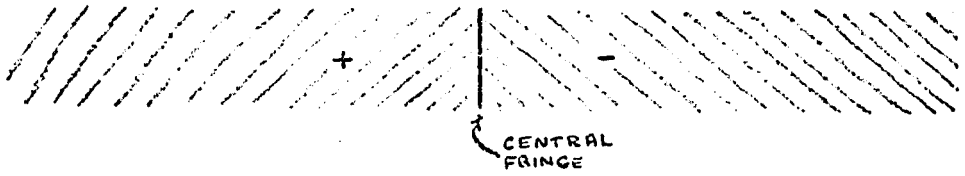

The effect of adding another diffracting edge in the object plane is to create a zone of destructive interference outside the region bounded by the two edges while the region within the edges is luminous as shown in this next figure.

If the shape of a needle were cut out of a piece of sheet-metal and introduced into the object plane the images would have the same aspect as the real needle in figure 29. Ultramicroscopy can be explained as a special case of diffrimoscopy.

b) Finite Aperture.

The complex amplitude in the image plane in the case of an aperture of diameter L is given by:

$$C_{(z_1)} = 2\,Cst \int_{\epsilon}^{L/2} \frac{\sin(2\pi y_1 z_1)}{2\pi y_1}\, dy_1 \qquad (29)$$

Let

$$2\pi y_1 z_1 = t \qquad y_1 = \frac{t}{2\pi z_1} \qquad dy_1 = \frac{dt}{2\pi z_1} \qquad (30)$$

$$\therefore C_{(z_1)} = \frac{C_{st.}}{\pi} \int_{2\pi\epsilon z_1}^{2\pi\frac{L}{2}z_1} \frac{\sin t}{t} \cdot dt$$

$$= \frac{C_{st.}}{\pi} \left[\int_0^{2\pi\frac{L}{2}z_1} \frac{\sin t}{t} \cdot dt - \int_0^{2\pi\epsilon z_1} \frac{\sin t}{t} \cdot dt \right]$$

$$= \frac{C_{st.}}{\pi} \left[Si\,(2\pi\tfrac{L}{2}z_1) - Si\,(2\pi\epsilon z_1) \right] \qquad (31)$$

Equation 31 is a more correct expression for the complex amplitude $C_{(z_1)}$ in the image plane. A comparison with equation 28 on page 39 will show that the only difference between the result of the two treatments is that $\frac{\pi}{2}$ is replaced by $Si(2\pi\frac{L}{2}z_1)$ within the square brackets. This seems to provide an explanation for the small fringes which are close to the black central fringe of the diffrimoscopic phenomenon. For small values of $2\pi\epsilon z_1$, the argument $2\pi\frac{L}{2}z_1$ will be in the region of the Sine-integral function which oscillates slightly about $Si(2\pi\frac{L}{2}z_1) = \frac{\pi}{2}$. At large values of $2\pi\epsilon z_1$ the Sine-integral function will have reached the value $\frac{\pi}{2}$ and no more small fringes would be observed.

Some preliminary experiments have been made which indicate that the small fringes are indeed linked to the width of the aperture. These experiments, however, seemed to indicate that these small fringes were insensitive to small changes in the aperture. This may or may not be explained adequately by the present theory.

It was noticed, also, that a reduction of the aperture did not affect the width of the central fringe. As this central fringe is linked to the resolution of our system it seems paradoxical that the resolution of our system does not strongly depend on the aperture. It is also noted that this central black fringe has not yet been fully

explained. On the basis of the preliminary result contained in equation 28, it would seem that the central black fringe should be infinitely thin. A graphical representation of equation 31 has not yet been made. This curve might have yielded some explanation for the width of the central fringe. From equation 31 it is expected that this possible explanation could only be linked to the aperture of the system, but as has been mentioned earlier, the preliminary experiments do not bear this out. It was possible to reduce the aperture of the system without changing the width of the central fringe. This then remains one of the problems which must be solved with this project. It may be that the central black fringe is insensitive to changes in the aperture when the aperture is large or it may be that this fringe cannot be explained on the basis of a classical theory.

According to Young*, a diffraction pattern is the resultant of the unperturbed incident beam and reradiated Huygen's wavelets from points on the edge of the aperture. Later, other authors (e.g. Bouasse) proposed that the light reradiated into the shadow of the object was out of phase with that reradiated into the illuminated region in order to explain just the type of phenomenon now under study.

A notion which is closely related to those mentioned above has been investigated. It is assumed that the object in some way perturbs the "light field". Estimations of the nature of this perturbation may be calculated by starting from the characteristics observed in the image plane and working back, through the use of Fourier transform theory, to the object plane. The calculations are illustrated in the appendix and the results are summarized below.

The average value of the perturbed amplitude in the object plane was found to be zero. The perturbed wave was calculated to be 90° out of phase with the incident wave and Bouasse's supposition was

---

* See Andrew, C.L. - "Optics of the Electromagnetic Spectrum" - Prentice-Hall (1960) page 300.

verified. The perturbation at the edge itself was found to be zero. This last result does not seem to be in agreement with the results of other workers. These calculations will have to be re-examined but the principle of the investigation of the object plane has been illustrated. It is hoped that with this technique the mechanism of diffraction may be more fully understood. This technique has an advantage over the technique used at microwave frequencies where a probe is used to investigate the electromagnetic field in the vicinity of the object. At microwave frequencies it seems impossible to chart the field in the very close vicinity of the edge because of edge-probe interactions. In diffrimoscopy probes are not necessary and consequently this limitation does not exist.

III. Further Studies in Diffrimoscopy.

a) Direct Experimental Evidence Showing that the Black Fringe is not shifted from the edge.

It may be that the black central fringe is slightly displaced within (or without) the geometrical shadow of the edge.

An experiment should be performed which would prove that the central black fringe lies exactly on the border of the geometrical shadow of the edge. It has been assumed up to now that this is the case. Such an experiment could make use of complementary objects, such as a strip and a slit of identical width. The widths of these objects could then be found by measuring the distance between the two central black fringes in their diffrimoscopic patterns. A shift of the central fringe by an amount σ within (or without) the border of the geometrical shadow would mean that the two widths mentioned above would differ by an amount 4σ. The use of complementary objects thus would provide sufficient sensitivity to detect all but the most minute of shifts.

b) Intensity Scannings.

The intensity scanning of the focal line was performed with the use of a spherical mirror in the off-axis configuration. It is hoped that in the future a better arrangement will be possible with the use of off-axis paraboloids or with the use of beam splitters so that the spherical mirrors could be used in the on-axis configuration. This latter arrangement, it must be remembered, has the disadvantage that the intensity in the focal line under the best conditions would be reduced to ¼ of the original intensity. The use of more sensitive probes together with a better optical system would provide a more rigorously correct scanning.

A scanning of the final diffrimoscopic pattern is also planned in order to provide a more complete verification of the theory. In this case, however, it is felt that probes of increased sensitivity are essential as the luminosity of the diffrimoscopic pattern away from the central area is too low to be measured with the probes presently at hand. A scanning of the diffrimoscopic pattern formed when a phase reversal plate is present (as shown in figure 15 on page 16) would provide a check on the scanning mentioned above and may yield a better explanation of the normal diffrimoscopic pattern.

A complete analysis of this data together with the theory is needed to ensure that the small fringes and the broad fringes of the diffrimoscopic image are indeed correctly and exactly explained.

c) Central black fringe.

Moreover, there remains the problem of the central black fringe which is seemingly not explained on the basis of the theory presented. As was mentioned earlier, this theory predicts that the central fringe should be infinitely thin. This fact may be an expression of the approximate nature of the Fourier transform theory or it may be an expression of a perturbation in the vicinity of the diffracting edge which was not taken into account when formulating the equations.

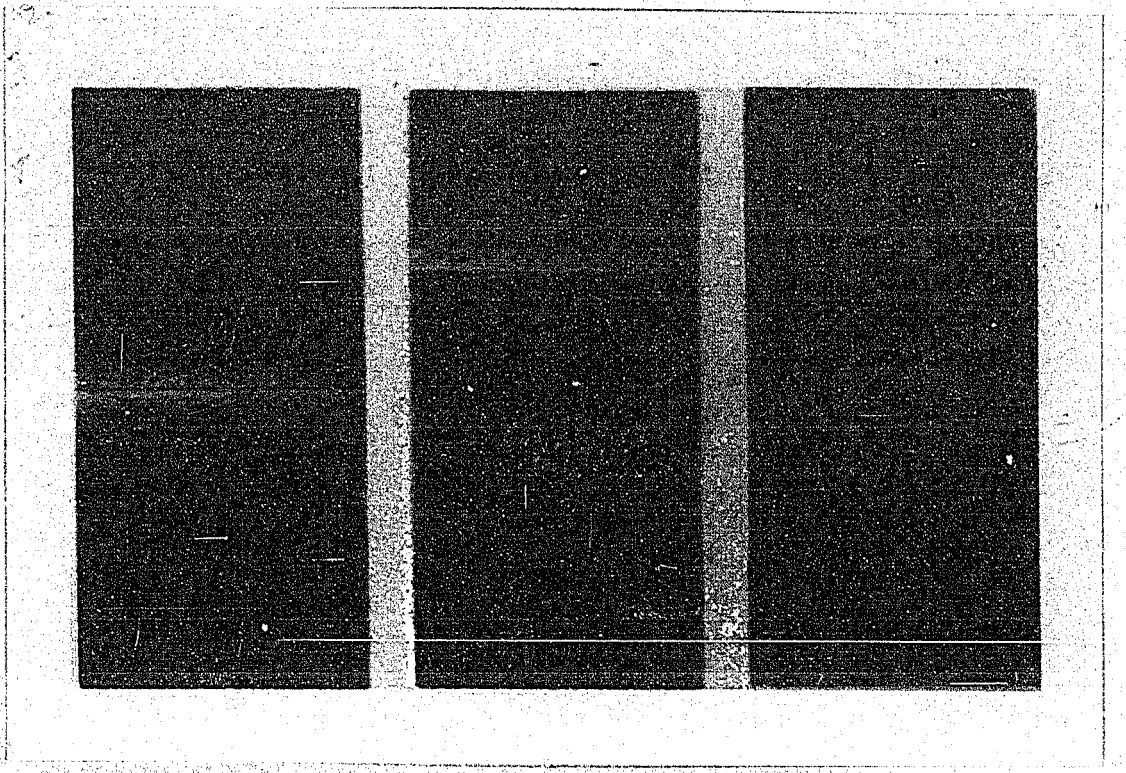

Figure 30 - The diffrimoscopic images of a straight edge, a rod and a ball. The overall magnification here is 19x.

d) Asymmetry for objects whose edge has a large radius of curvature (see figure 30).

The asymmetry present in the case of the rod and ball mentioned on page 5 does not seem to be linked to an interaction of the light diffracted from the various edges. A black fringe is still present but additional work is needed to prove that this fringe is not shifted. It is necessary to know more about the diffraction pattern in the case of a large radius of curvature if the diffrimoscopic technique of measurement is to be applicable to all manner of objects.

IV. Practical Uses of the Diffrimoscopic Technique.

The improvement in the resolution of optical systems which the diffrimoscopic technique permits certainly must be regarded as one

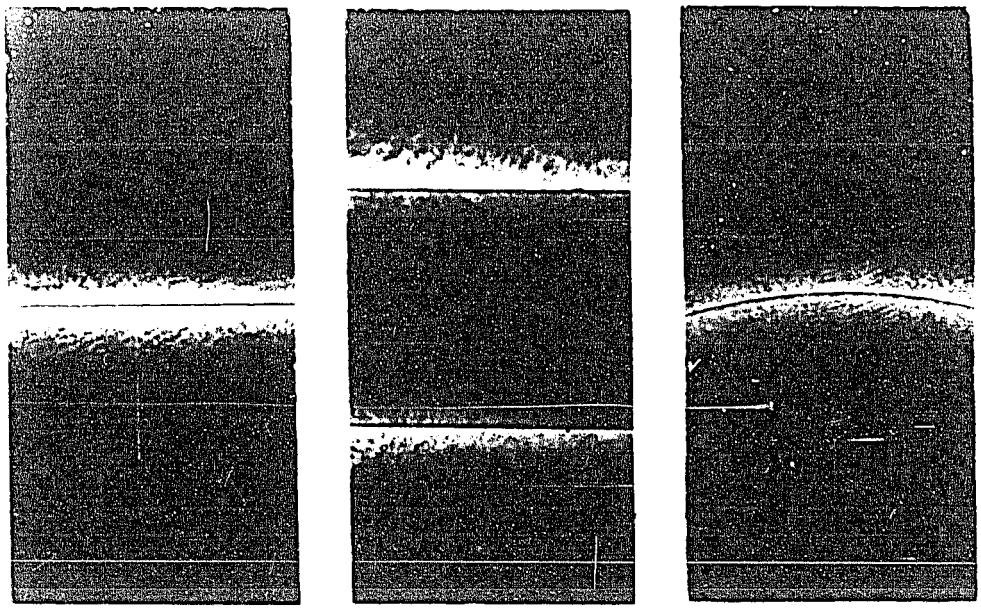

of the more significant practical aspects. From this is derived the principle of the "profiloscope" which was announced by Prof. Lansraux* in a publication in which this author participated. The "profiloscope" would permit metrological pointings of object contours with a much better precision than obtainable in a profile projector.

From the academic point of view, however, the most important aspect of the diffrimoscopic technique is its usefulness, which has already manifested itself, in the fundamental study of diffraction phenomena. It has yielded an explanation of ultramicroscopy**, for example. Moreover, since the phase in the mask plane has been found to be constant it is possible from a scanning of intensity to arrive at the amplitude distribution in this plane. It is then possible to calculate the amplitude distribution both in the image plane and in the object plane.

---

* Lansraux G., "Diffrimoscopy" - Metroligia (April 1965, vol. 1, pp. 31 - 36).

** Professor Lansraux suggested this link between ultramicroscopy and diffrimoscopy after seeing the photographs on page 42. It seems, however, that there are certain ultramicroscopic arrangements which remain best explained on the basis of the Tyndall effect. An example of this would be the ultramicroscopic arrangement used by Siedentopf.

Description of Apparatus.

1. Light Source -

This piece of equipment is shown in the two photographs on page 52. It provides a light - tight housing for an Osram, mercury-filled, super-pressure lamp. The lamp bulb (see figure 31, page 52) is cooled by convection currents rising through the housing. It carries a current of 5 amperes at 100 volts through a small ($\approx$1/16")arc. This ensures a high luminance which is important for experiments in diffraction. The arc is then focussed on to a removable pin-hole which becomes the effective source for the optical system. Pin-holes of 200 microns and 30 microns were used. Provision is made in the design of the housing for adjustment (see figure 32) of the lamp bulb along 3 perpendicular axes so that the arc can always be focussed on to the pin-hole which remains fixed. This facillitates the changing of bulbs without the need for any adjustments to the optical system.

A variable filter housing was designed by the author to fit the light source. Changes in wavelength could then be realized, again, without the need of readjusting the optical system. This housing may hold 4 filters or 3 filters and one "hole" for observations made in polychromatic light.

2. Mask Holder -

The mask holder (shown on page 21) was designed to provide motion along 3 perpendicular directions and a rotation about the optic axis. The linear motion was realized with the use of UniSlide dovetails. The moving surfaces of these slides are coated with nylon to provide smooth movement. The rotation about the optic axis was realized with the use of a 5" diameter Torrington needle bearing. This allowed the strip mask to be adjusted until it was parallel to the diffracting edge and thus perpendicular to the focal line.

Figure 31: The lamp bulb and housing.

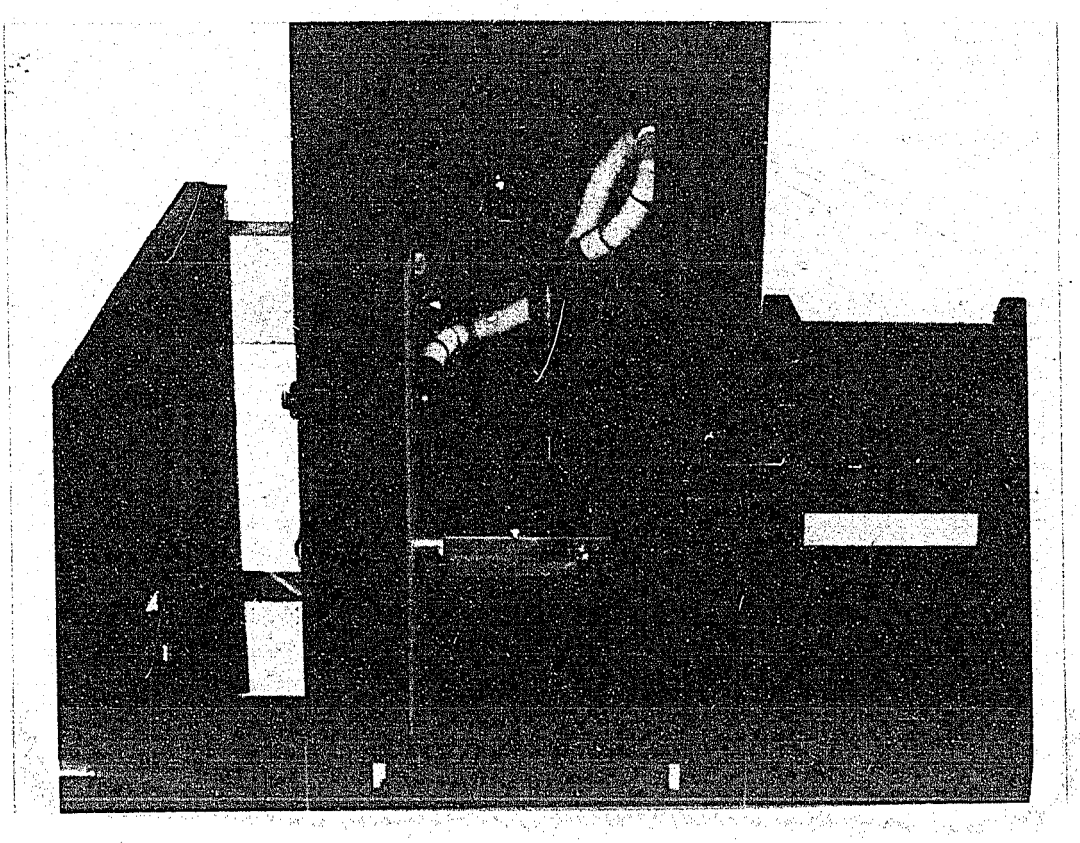

Figure 32: The light source.

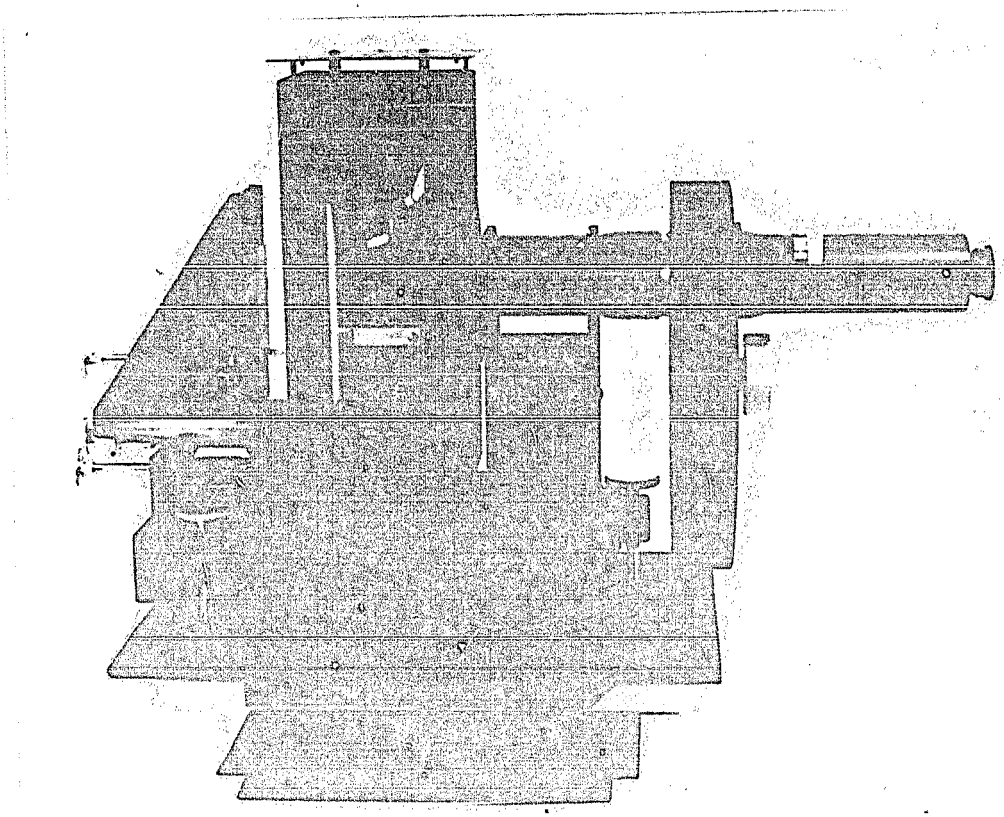

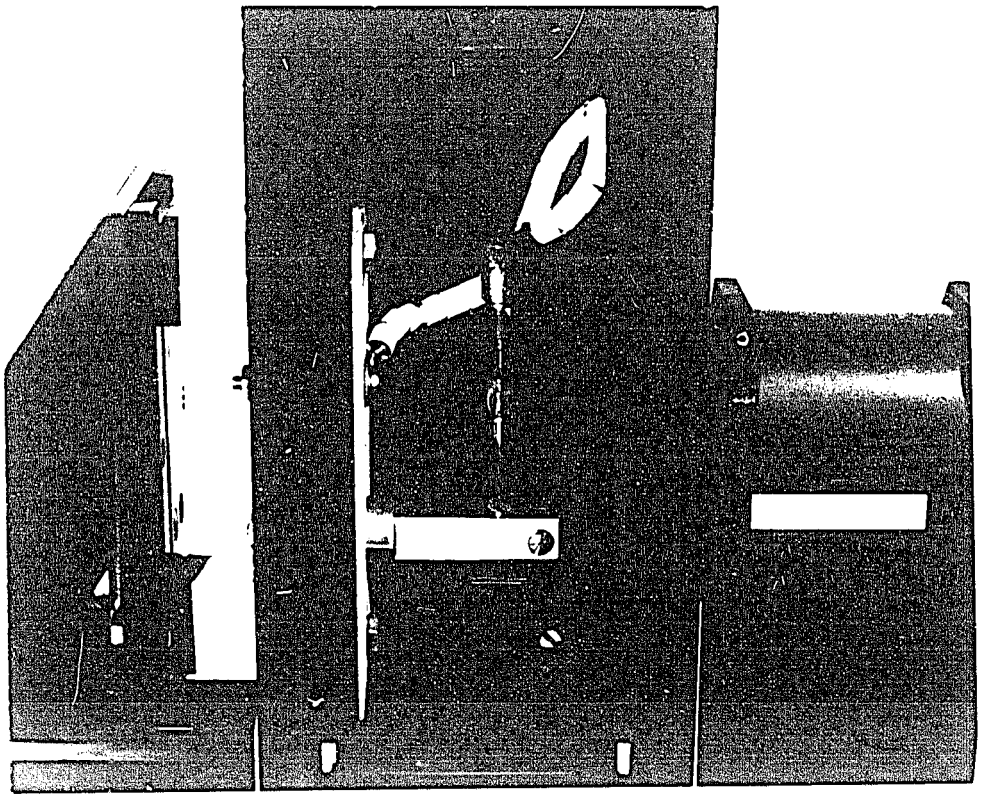

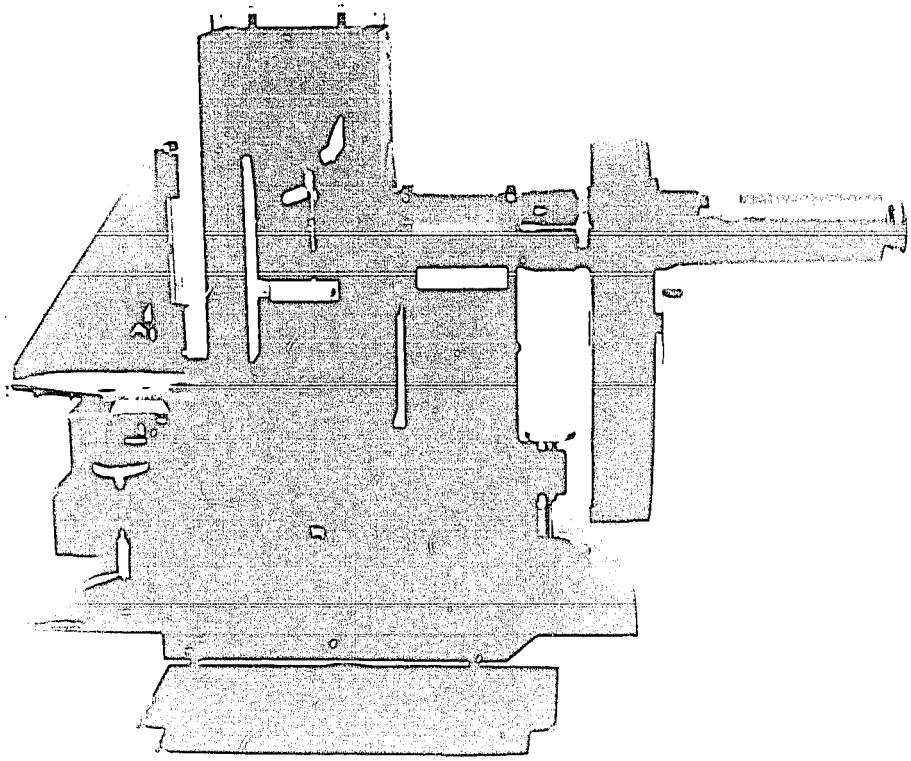

3. Lens Holder -

The holder shown in figure 33 was designed to provide motion along 3 perpendicular directions and rotations about 2 axes perpendicular to the optic axis. The lenses could be correctly positioned and oriented by making use of the reflected light. The lenses themselves are 4" diameter, air-spaced, telescope objectives obtained through the Edmund company.

figure 33:

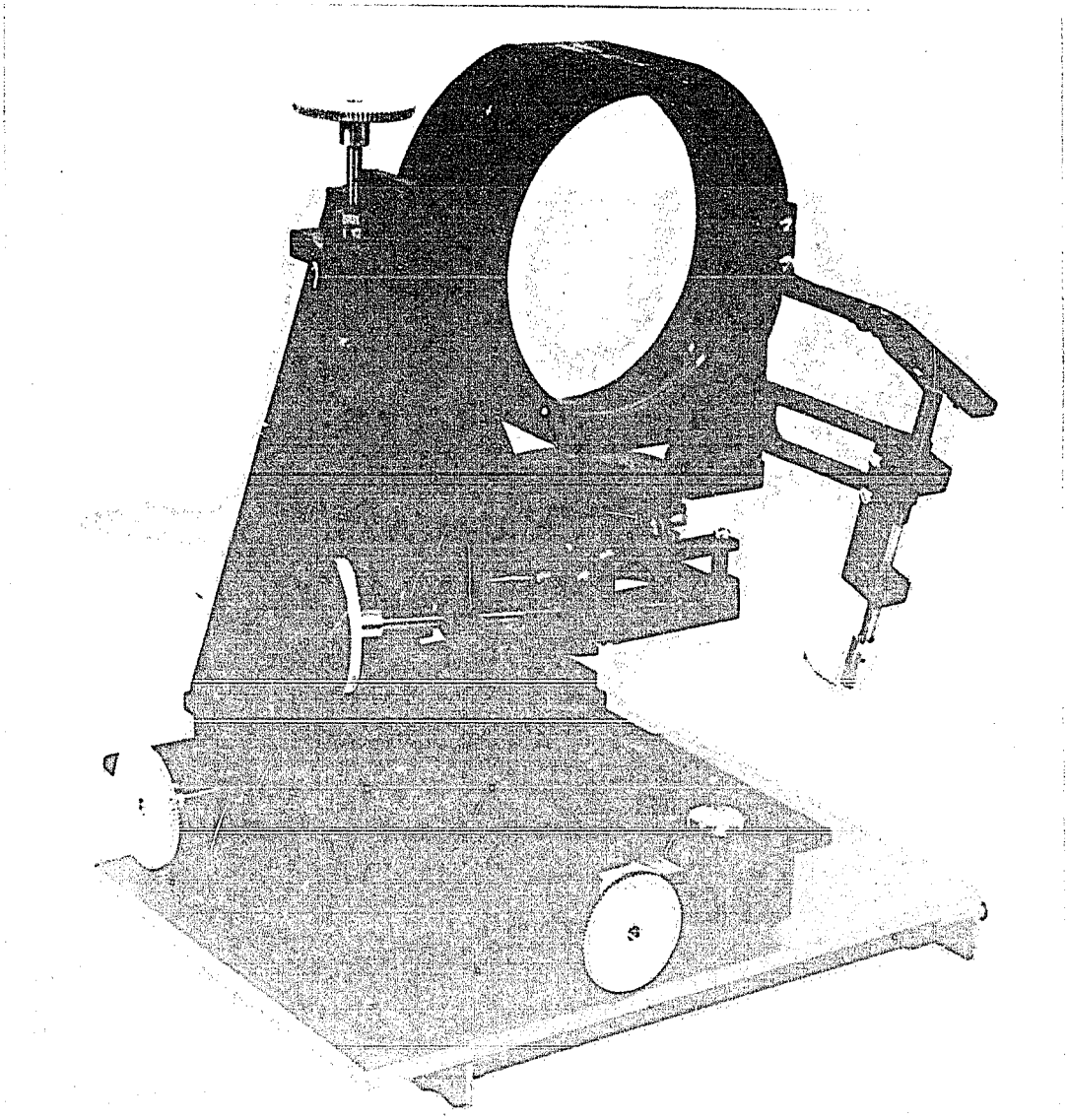

3. Lens Holder -

[illegible] designed to provide motion along 2 perpendicular directions and rotations about 2 axes perpendicular to the optic axis. [illegible] correctly positioned [illegible]

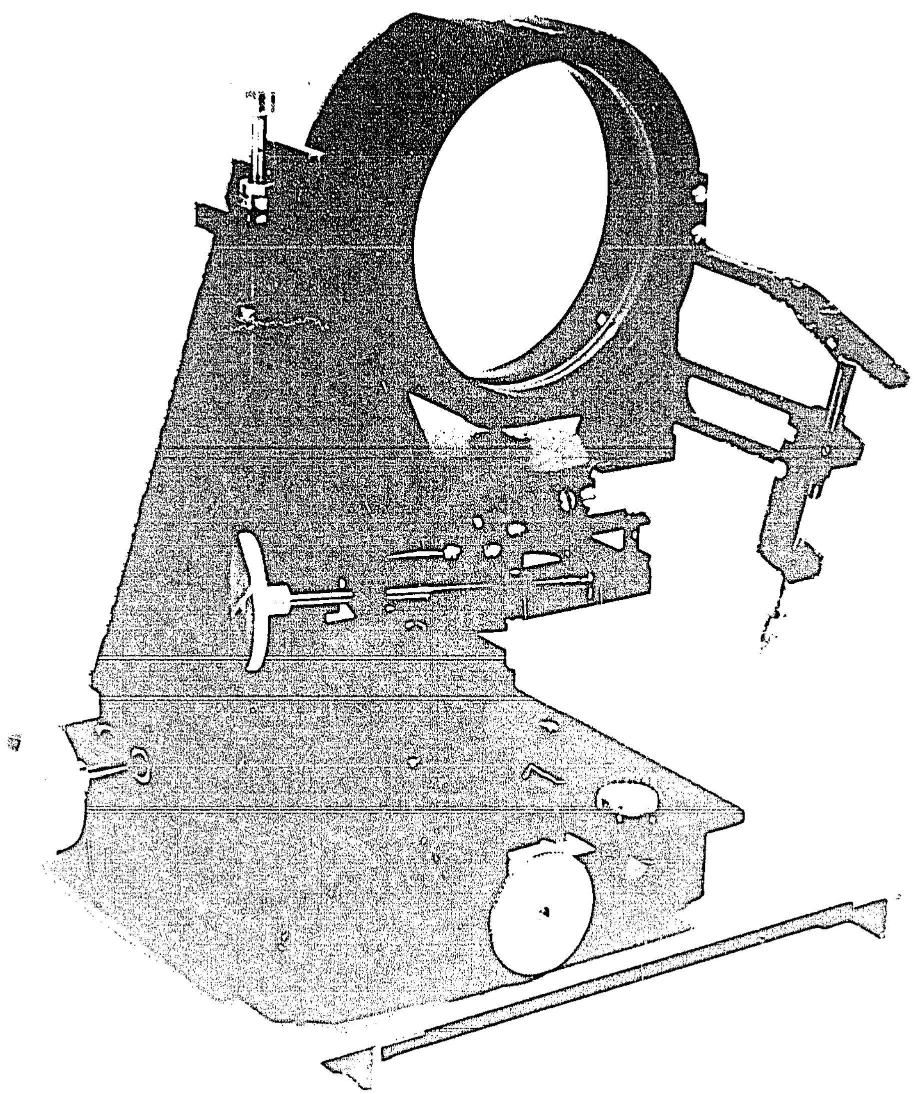

4. Microscope -

This microscope was designed so that it would move along two perpendicular axes in the horizontal plane. The motion of this large end heavy piece of equipment along these directions was made possible with the use of hardened stainless steel rods and adjustable Thompson ball bushings. The pushing force was provided by a special Roton planetary screw. This screw also gives a free-wheeling action when the end of the travel has been reached. A small vertical adjustment was also provided in the design. The microscope was built with a special objective carrier by which one could choose either of two magnifications without the need of refocussing. A removable 90° mirror was built into this system. Visual observations were made with the mirror in place at 90° to the optic axis (figure 34) while photographs could be taken with the removal of the mirror (figure 35). It was necessary to insure that the mirror would return exactly to the same position each time it was moved. Care was also taken to insure that a correctly focussed image observed visually, corresponded to a correctly focussed image in the film plane of the camera. The microscope objectives used were obtained through the Wild Company of Canada.

The construction and a large part of the design of this piece of equipment is due to Mr. M. Ranger.

Figure 34

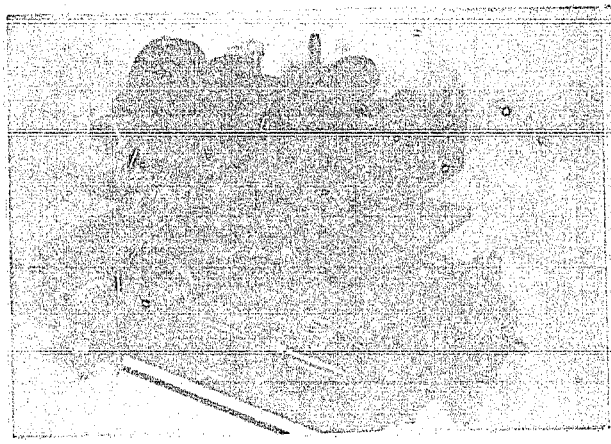

Figure 35

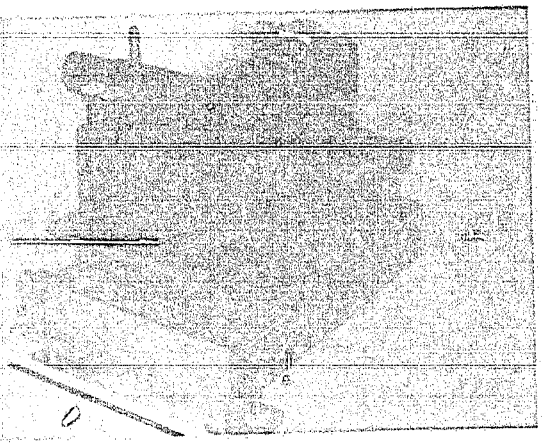

4. Microscope -

This microscope was designed so that it would move along two perpendicular axes in the horizontal plane. The motion of this large and heavy piece of equipment along these directions was made possible with the use of hardened stainless steel rods and adjustable Thompson ball bushings. The pushing force was provided by a special Roton planetary screw. This screw also gives a free-wheeling action when the end of the travel has been reached. A small vertical adjustment was also provided in the design. The microscope was built with a special objective carrier by which one could choose either of two magnifications without the need of refocussing. A removable 90° mirror was built into this system. Visual observations were made with the mirror in place at 90° to the optic axis (figure 34) while photographs could be taken with the removal of the mirror (figure 35). It was necessary to insure that the mirror would return exactly to the same position each time it was moved. Care was also taken to insure that a correctly focussed image observed visually, corresponded to a correctly focussed image in the film plane of the camera. The microscope objectives used were obtained through the Wild Company of Canada.

The construction and a large part of the design of this piece of equipment is due to Mr. M. Dauger.

Figure 34

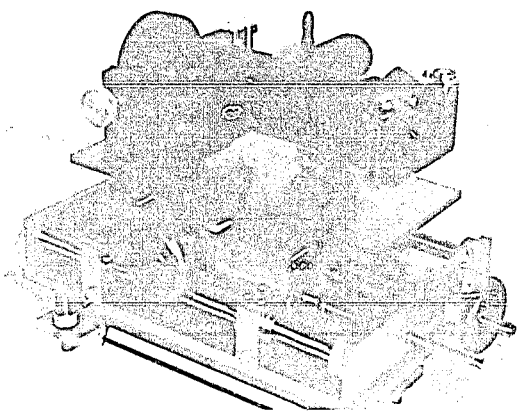

Figure 35

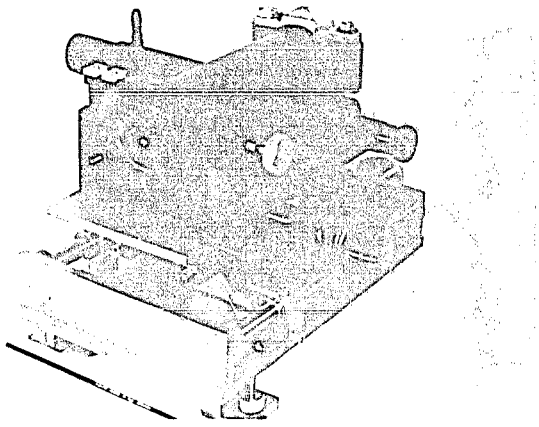

5. Mirror -

A system of spherical mirrors was used for part of the research for this project. The mirror shown below has a radius of curvature of 9' 7" and a 12½" diameter. The particular mirror shown here was used to focus the diffrated light. One of the spot masks which were used to stop the incident light is shown stuck to the center of the mirror. These mirrors were fabricated in the optical shops at the National Research Council.

figure 36:

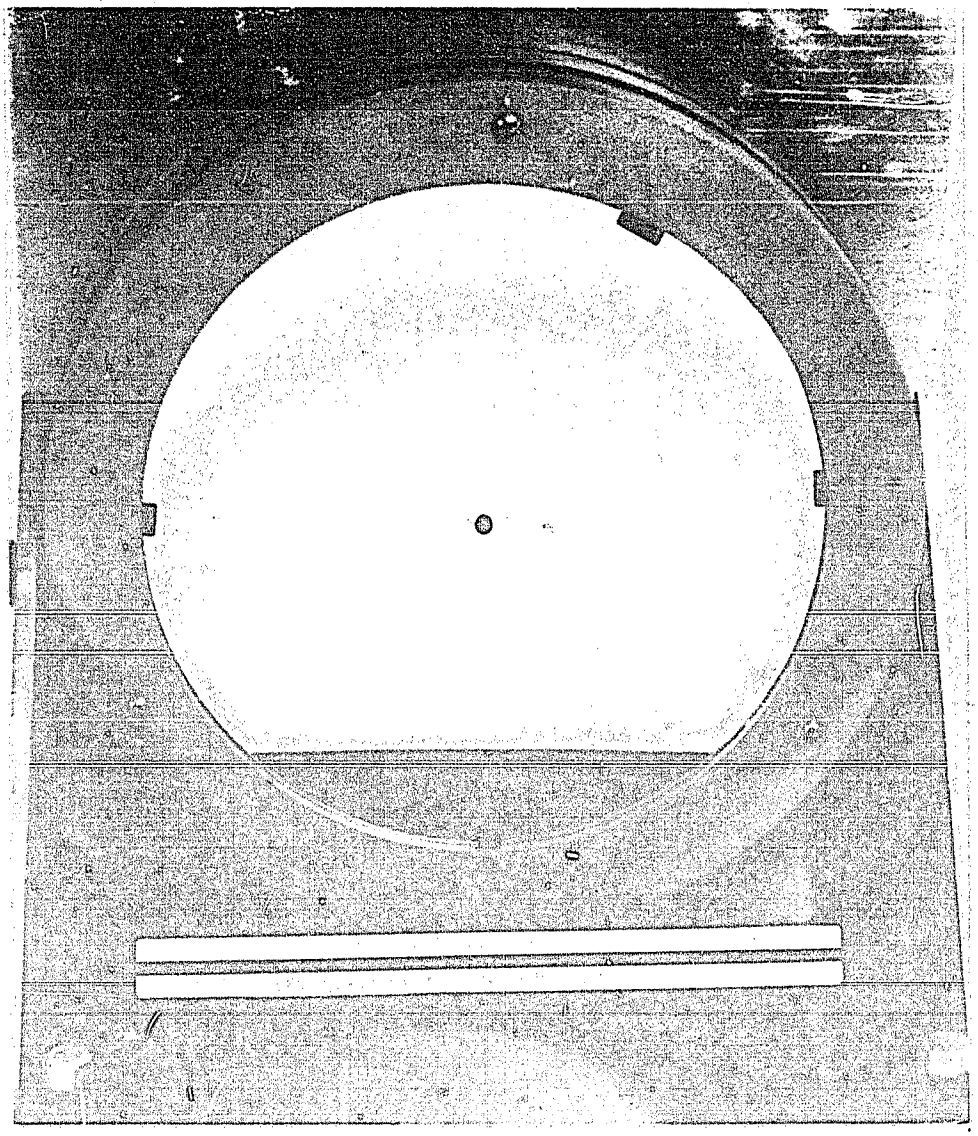

5. Mirror -

A system of spherical mirrors was used for part of the research for this project. The mirror shown below has a radius of curvature of 9' 7" and a 12½" diameter. The particular mirror shown here was used to focus the diffrated light. One of the spot masks which were used to stop the incident light is shown stuck to the center of the mirror. These mirrors were fabricated in the optical shops at the National Research Council.

figure 36:

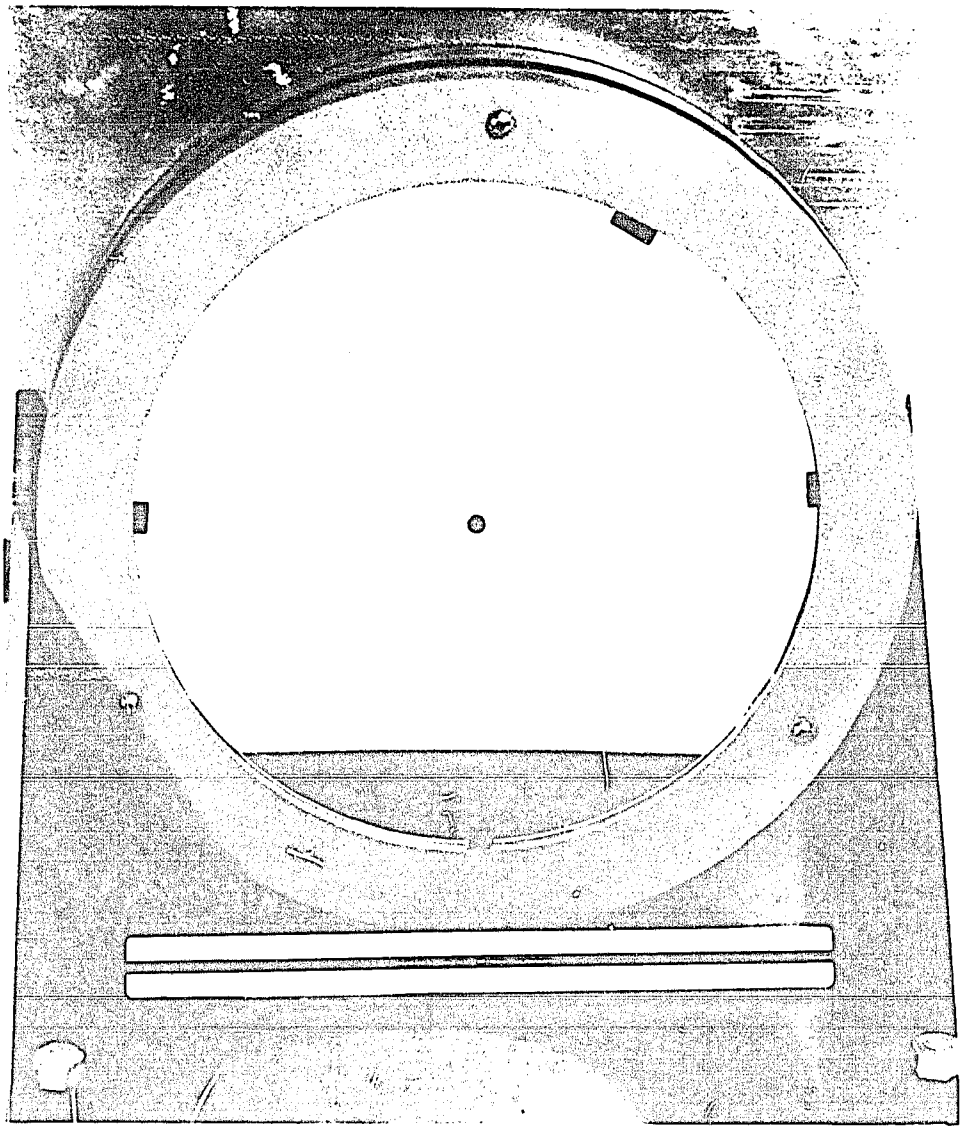

APPENDICES

Appendix A

On page 7 the resolution of the diffrimoscopic system is compared to the same system operating in a conventional manner. This discussion was based essentially on the predicted resolution according to the Rayleigh criterion.

The Rayleigh criterion, however, sets the theoretical limit of resolution under the best conditions. The system used for this research project had a point source which was in fact not a point but a hole 200 microns in diameter. This would thus raise the predicted limit of resolution. In fact it is difficult to predict what resolution might be expected when an object such as a straight edge is used. It seems safe to say, however, that the net classical limit of resolution of the system was in excess of the 25 microns quoted in the text.

An attempt was made to increase the diffrimoscopic resolution of the system by replacing the 200 micron pin-hole with a pin-hole 30 microns in diameter. The width of the central black fringe did not change noticeably. The resolution of the system operating in the diffrimoscopic manner does not seem to be greatly affected by the change in the degree of collimation of the light.

The lenses used in this system were not achromats. This, however, did not affect the resolution of the diffrimoscopic system and the reason for this will be understood from looking at figure 10 on page 12. New achromatic lenses have been received which will improve the overall character of the images but which are not expected to appreciably improve the gain in resolution.

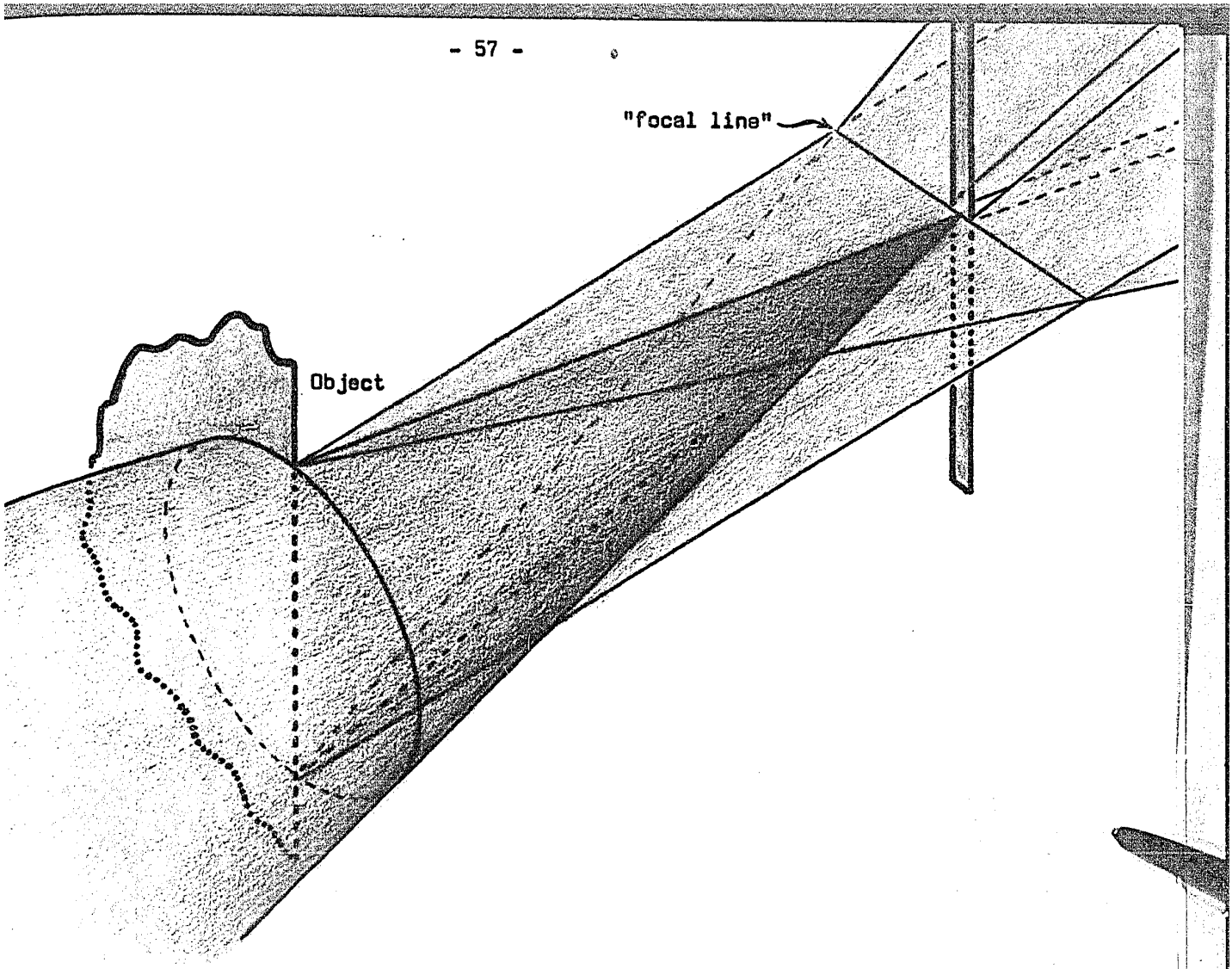

Appendix B

The case in which the object is placed in a beam of convergent light is depicted above. This is a 3-dimensional representation of a part of the system shown in figure 3 on page 3. The incident light (coloured blue) is focussed on to the mask M by the lens L_1 which is not shown in this figure. A strip mask may still be used because the light diffracted by the edge still forms a "focal line" in this case.

A similar argument would show that such a focal line would be formed even in the case where the object is placed in a beam of diverging light.

Appendix C

The complex amplitude distribution in the object plane is $\mathbb{D}(x_1, x_2)$. This may be written as:

$$\mathbb{D}(x_1, x_2) = \mathbb{D}(x_1, x_2) + \mathbb{ID}(x_1, x_2) \qquad (32)$$

where $\mathbb{D}(x_1, x_2)$ is the perturbed complex amplitude

and $\mathbb{ID}(x_1, x_2)$ is the unperturbed complex amplitude.

On page 31, no perturbation was assumed. In that case, $\mathbb{D}(x_1, x_2) = 0$ and consequently $\mathbb{D}(x_1, x_2) = \mathbb{ID}(x_1, x_2)$. The symbol $\mathbb{D}(x_1, x_2)$ was thus used on page 31 to represent the unperturbed complex amplitude in the object plane.

The aspects of the diffrimoscopic image which are as yet unexplained on the basis of the Fourier transform theory must in some way or another be explained in terms of the function $M_o(y_1)$ mentioned on page 19. The oddness characteristic of this function was derived essentially from the fact that the image presents a central minimum. This is the only part of the complex amplitude distribution in the mask plane which could possibly have any information concerning the perturbation and still be detected in the image plane. Consequently, only this part of the complex amplitude distribution in the mask plane, $M_o(y_1)$, will be used in the following calculations. It must be remembered that the complete form of $M_o(y_1)$ is as yet unknown and is not completely given by the second term of equation 20 on page 35.

a) In one dimension:

$$M_o(y_1) = \int_o^{K/2} \mathbb{D}(x_1)\, e^{-i 2\pi x_1 y_1}\, dx_1 \qquad (33)$$

where K is the diameter of the pupil in the object plane.

$$M_o(-y_1) = \int_o^{K/2} \mathbb{D}(x_1)\, e^{+i 2\pi x_1 y_1}\, dx_1 \qquad (34)$$

Since $M_o(y_1)$ is solely an odd function:

$$M_o(y_1) = -M_o(-y_1) \quad \text{or} \quad M_o(y_1) + M_o(-y_1) = 0 \qquad (35)$$

$$\therefore \int_0^{K/2} \mathbb{D}(x_i)\, e^{-i2\pi x_i y_i}\, dx_i + \int_0^{K/2} \mathbb{D}(x_i)\, e^{i2\pi x_i y_i}\, dx_i = 0 \qquad (36)$$

$$\therefore \int_0^{K/2} \mathbb{D}(x_i)\left[e^{-i2\pi x_i y_i} + e^{i2\pi x_i y_i} \right] dx_i = 0. \qquad (37)$$

$$2 \int_0^{K/2} \mathbb{D}(x_i) \cdot \cos(2\pi x_i y_i)\, dx_i = 0 \qquad (38)$$

This is true for all values of y_i. Therefore, $\int_0^{K/2} \mathbb{D}(x_i)\, dx_i = 0$ (39)

That is, the average value of the perturbed complex amplitude in the object plane is zero.

b) Using the notation introduced in equation 6 on page 18:

$$\mathbb{D}(x_i) = \int_{-L/2}^{L/2} M_o(y_i) \cos(2\pi x_i y_i)\, dy_i + i \int_{-L/2}^{L/2} M_o(y_i) \sin(2\pi x_i y_i)\, dy_i \qquad (40)$$

Since $M_o(y_i)$ is an odd function of y_i

$\cos(2\pi x_i y_i)$ is an even function of y_i

$\sin(2\pi x_i y_i)$ is an odd function of y_i

$$\therefore \mathbb{D}(x_i) = i \int_{-L/2}^{L/2} M_o(y_i) \sin(2\pi x_i y_i)\, dy_i \qquad (41)$$

The complex amplitude of the perturbation is thus 90° out of phase with the incident radiation.

c) At the edge $x_i = 0$

Thus

$$\mathbb{D}(x_i) = \int_{-L/2}^{L/2} M_o(y_i)\, e^{i2\pi x_i y_i}\, dy_i \qquad (42)$$

becomes

$$\mathbb{D}(x_i)\Big|_{x_i=0} = \int_{-L/2}^{L/2} M_o(y_i) \cdot dy_i \qquad (43)$$

Since $M_o(y_i)$ is an odd function of y_i,

$$\int_{-L/2}^{L/2} M_o(y_i)\, dy_i = 0 \qquad (44)$$

Thus $$\mathbb{D}(x_1)\Big|_{x_1=0} = 0 \qquad (4\text{-}5)$$

The complex amplitude of the perturbation at the edge is zero.